2007

Design, analysis and passive balance control of a 7-DOF biped robot

Li, Wenguang

Design, Analysis and Passive Balance Control of a 7-DOF Biped Robot

By: Wenguang Li

Supervised by: Dr. Xiaoping Liu

A thesis submitted to the faculty of graduate studies
Lakehead University
in partial fulfillment of the requirements for the degree of
Masters of Science in Control Engineering

Faculty of Engineering

Lakehead University

Thunder Bay, Ontario
P7B 5E1
September 2007

Your file Votre référence
ISBN: 978-0-494-31830-0
Our file Notre référence
ISBN: 978-0-494-31830-0

To my wife and my family

Abstract

Biped robots have many advantages than traditional wheeled or tracked robots. They have better mobility in rough terrain and can travel on discontinuous path. The legs can also provide an active suspension that decouples the path of the trunk from the paths of the feet. Furthermore, the legs are able to step over considerably bigger obstacles compared to wheeled robots. However, it is difficult to maintain the balance of biped robots because they can easily tip over or slide down. To be able to walk stably, it is necessary for the robot to walk through a proper trajectory, which is the goal of this research.

In this research, a complete 7-DOF biped walking trajectory is planned based on human walking trajectory by cubic Hermite interpolation method. The kinematics and dynamic model of the biped are derived by Denavit-Hartenberg (D-H) representation and Euler-Lagrange motion equations, respectively. The zero moment point of the robot is simulated to check the stability of the walking trajectory.

The setpoint sampling method and sampling rate for trajectory tracking control are investigated by studying sinusoidal curve tracking on a single link robot arm. Two control sampling time selection methods are introduced for digital controllers.

A 7-DOF biped is designed and built for experiments. Each joint has its own independent microcontroller-based control system. PD controllers are used to control the biped joints.

Simulations are performed for the walking trajectory and zero moment point. Simulation results show that the walking trajectory is stable for the 7-DOF biped. Experiment results indicate that the sampling time is proper and the PID controller works well in both setpoint control and trajectory tracking. The experiment for the marching in place shows the trajectory is stable and the biped can balance during the marching process.

Key Words: Biped, cubic Hermite interpolation, zero moment point, trajectory tracking, setpoint sampling time, control sampling time, PID, microcontroller

Acknowledgements

I wish to thank a number of people for their help and support during this research.

My supervisor, Dr. Xiaoping Liu, provided his endless guidance, invaluable insight and advice, encouragement, patience and financial support. He himself often took part in this research no matter weekdays or weekends. He is a valued supervisor and friend, I appreciate his work. I also appreciate my co-supervisor, Dr. Julian Cheng, for his financial support, even though we haven't met before he left Lakehead University. Dr. Abdelhamid Tayebi and Dr. Krishnamoorthy Natarajan gave me guidance in robotics and control theory.

Mr. Manfred Klein, Warren Paju and Kailash Bhatia helped me set up the experiment.

My fellow graduate students also provided valuable discussion and advice.

Finally, I must thank my wife, Peng, and my family, for their loving support throughout this research.

Contents

List of Figures

List of Tables

List of Acronym

CoG	**center of gravity**
CoM	**center of mass**
CoP	**center of pressure**
DFS	**double foot support**
D-H	**Denavit-Hartenberg**
FRL	**fuzzy reinforcement learning**
FS	**Fourier series**
GPS	**global positioning system**
I	**inertia**
LSB	**least significant bit**
M	**mass**
MCU	**micro controller unit**
PID	**proportional-integral-derivative**
RC	**radio control**
SFS	**single foot support**
ZMP	**zero moment point**

Chapter 1 Introduction

The aim of this thesis is to design a 7-DOF biped robot that is able to passively balanced walk with along a desired trajectory. The trajectory is based on human walking gait and has been modified such that the biped robot's zero moment point is always in the convex of support area, which is the key factor for balance.

This chapter describes some background knowledge about robots (robotics), the development of legged robots and the outline of this thesis.

1.1 Definition and History of Robots (Robotics)

The term 'Robot' originated around 1917 [10] in Karel Capek's science fiction, and later in 1921 the science fiction play, RUR (Rossum's Universal Robots), made this word well known. The word 'Robotics' was created by Isaac Asimov in about 1940. Instead of 'Robot' there are several other terms that describe robot, such as 'manipulator', 'telemanipulator', 'teleoperator', 'android' and 'cyborg' etc.

It is hard to define robot, but there are some basic characteristics in common:

1) A robot is made by manufacture rather than biology;

2) A robot has movable joints;

3) It must have a power or force source or amplifier;

4) It is able to accomplish some particular tasks independently;

5) It must have sensors to feel the environment, 'brain' to make decision and actuator to execute the task;

6) Its behavior is able to be modified by adjusting the 'brain'.

Robots evolved with the development of science and technology. The first true robot was 'born' after the computer emerged. In 1954, Devol invented the first programmable manipulator. The development of integrated circuits and microprocessors in 1960's to 1980's made cost-effective and reliable robots possible. They were frequently used in many industrial assembly lines because of the greater efficiency and accuracy. Nowadays, with higher and higher level of sensor technology, microprocessor technology and artificial intelligence, robots are getting smarter and smarter.

1.2 Robot Categories

Robots can be classified into different groups in many ways. For example, according to their work environment, there are surface robots, aerial robots and aquatic robots; according to their application area, there are commercial robots and industrial robots; according to the base's mobility, robots could be grouped into fixed-base robots and mobile robots, which could be further divided, into wheeled robots, tracked robots, pedrailed robots and legged robots, by how they move.

1.3 Legged Robot

Legged robots have many advantages than traditional wheeled or tracked robots. Firstly, legs provide better mobility in rough terrain, because the isolated feet can optimize support and traction. And they could travel on discontinuous path, like ladder. The legs also provide an active suspension that decouples the path of the trunk from the paths of the feet, such that the trunk could move smoothly despite pronounced variations in the support surface. Furthermore, the legs are able to step over considerably bigger obstacles compared with wheeled robots.

The study of legged machines began in about 1870. From then on, a lot of researches were done on single leg or multi-leg walking machines, employing both static balance (passive balance) and dynamic balance (active balance) technology. The passive balance strategy is based on well planned walking trajectory, while the active balance is based on the real time measurements to balance by adjusting the trajectory.

The first legged robot used a kinematic structure to support and move the body along a straight horizontal path while the feet moved vertically (up and down) during 'walking'. In 1893, Rygg patented a human-powered mechanical horse, which was powered by stepping motions on the stirrups and steered by pulling the rein to move the head and forelegs from side to side. By 1960, many legged machines were developed with poor performance due to lack of control.

In 1968, Liston and Mosher built a 4-legged truck [20], which was controlled by the rider. This truck was 11 feet tall, weighted 3000 lbs, powered hydraulically. The control handle or pedal for each leg of the walking truck was connected to the driver's limb. The driver depended on the force feedback to handle the obstacles.

This was a full human control walking machine.

After the computer came into use, the task of directly controlling the walking machine was assigned to the computer rather than human. In 1977, Robert McGhee's group at Ohio State University successfully built a computer-controlled insect-like six-leg robot [20]. It could walk with several designed gaits and step over obstacles.

With advancement of sensor technology, control theory, artificial intelligence theory and computer technology, many advanced legged robots have been built. The development of legged robots moves toward two main directions: non-biped robots and biped robots.

In non-biped field, researchers prefer multi-legged robots more, which are easier to be balanced compared to single-leg or biped ones. From the 1990s to present [14], Boston Dynamics produced three different advanced multi-leg robots, RHex, BigDog and RiSE. RHex is a six half-circle leg robot with extraordinary rough terrain mobility. RHex is able not only to travel in rocky fields, mud, sand, vegetation, railroad tracks and poles, but also to climb steep slopes and stairways. It has a sealed body, so it can also operate in rain or water. RHex is a remote controlled robot with onboard compass, global positioning system (GPS) and camera. BigDog is a dog-like robot, which is well dynamically balanced. This 'Dog' can walk or run in rock, snow, mud, up slope or stairs with heavy loads. It can be your load carrier when you climb. RiSE is a bug-like six-legged robot that can vertically climb trees, walls and fences. Its feet can be chosen from claws, micro-claws to sticky claws for different climbing tasks. Celaya and Porta [38] developed a robust controller for a six-legged robot that allows it to walk over difficult terrains in an autonomous way without any vision sensor. This controller can be driven by an upper level, which doesn't take care of the details of foot placement or leg movements, but takes care of only high level aspects such as global

speed and direction. Pongas, Mistry and Schaal [39] proposed a novel parameterization of the center of gravity (CoG) trajectory based on current position velocity, and acceleration of the four legs of the quadruped robot. This CoG trajectory guaranteed continuous velocity and acceleration profiles, which leads to continuous velocity and acceleration profiles of the leg movement. This method has been evaluated on Little-Dog quadruped robot.

In biped area, many research institutions and companies focused on humanoid robots. Great progresses were achieved in dynamic balance and artificial intelligence. In Japan, several humanoid biped robots were manufactured in recent years [12]. Qrio, presented by Sony in 2003 [13], is the world's first humanoid robot to run. It can walk and dance dynamically, detect and distinguish voice and faces. It is able to chat with people. Its maximum walking speed is 14m/min. It is able to walk on the ground with a slope up to 10 degrees. Asimo [7], by Honda in 2004, is able to walk and run with dynamic balancing. Its top walking speed is 3km/h. It can also recognize moving objects, follow movements and greet people.

Legged robots are more difficult to control than wheeled robots because dynamic balance is hard to maintain. The former studies of legged robots considered only static balance (passive balance), because of the limitation of not so well-developed sensor technology. After 1985, research gradually turned to the dynamic balance (active balance) of legged machines. In 1981, Miura and Shimoyama developed a dynamically balanced walking robot by an inverted pendulum model [20]. This robot had 3 degrees of freedom, each leg had one degree of freedom and trunk had one. In 1985, Marc H. Raibert [20] developed a 3-dimensional hopping machine with only one leg, which was actively balanced as well. This hopping machine had two parts: a body and a leg. The body had a weighted balance beam and the joints (hip and leg) were actuated by pneumatic actuators. The top recorded running speed of this machine was 2.2m/s.

In order to make the biped to walk, the first step is to plan a walking trajectory. Zerrugh and Radcliffe [4] developed a computer program to generate the motion variables of human gait from relative motions. Kinematic data during both free speed and forced speed were collected. Cunado [8] presented a new feature-based human gait model which exploited temporal behavior by gathering evidence over the entire sequence of images. By modelling the hip rotation by a Fourier series (FS), the gait signature could be generated directly from the evidence gathering process via the FS coefficients. Bharatkumar's group [6] derived a stick figure model of lower limb for free speed human walking and compared ordinary images of a walking person to this model. They obtained the kinematic data from 3D images of persons' walking with markers over the joints of their limbs. The average of these data was used to derive the stick figure model. Bekek and Erbatur [33] developed an online fuzzy adaptation scheme for one of the trajectory parameters in the offline generated walking pattern. Djoudi, Chevallereau and Aoustin [28] proposed a method to obtain optimal gaits for a biped without actuated ankle. In their research, the joints variables were assumed to be polynomial functions of a scalar path parameter. The coefficients of the polynomial functions are chosen to optimize a torque criterion and to ensure a cyclic motion for the biped. Rostami and Bessonnet [29] developed a method to generate optimal sagittal reference gaits for single foot support phase in biped walking. The approach is based on minimizing the integral of quadratic joint actuating torques. The impactless and non-sliding heel touch will ensure a more stable and easier controlled walking. Roussel and Goswami [30] proposed an approach to generate energy-optimal trajectory for a complete walking cycle (including single foot support state and double foot support state). Their study was based on a simplified robot dynamics without effects of centripetal forces. A generator of energy optimal gaits was proposed based on piecewise constant inputs. Like an inverted pendulum, the biped is easily to tip over, so it is required to take stability into consideration when planning walking trajectory. Huang [23] has proposed a method for formulating the walking trajectory with the largest stability

margin by adjusting only two parameters. Tang, Zhou and Sun [31] indroduced a trajectory planning method aiming to achieve smooth leg swing, by reducing the instant velocity change at the collision between the foot and ground. Zero moment point (ZMP) was considered in this method. Kajita's group [32] proposed a method of biped walking pattern generation by using a preview control of the ZMP.

The ZMP, indroduced in [5], [17], is defined as the point on the contact surface about which the sum of all the moments generated by the active forces equals to zero. It is a key issue in biped balance. If the ZMP of biped stays in the convex hull of all contact points between the feet and their support surface, the biped robot is able to balance. Sardain and Bessonnet [22] strictly defined the ZMP and center of pressure (CoP) and proved the coincidence of the CoP and the ZMP. This theory was investigated by an experiment [34]. In this experiment, the human walker wore rigid metallic shoes equipped with force sensors. The forces were measured to calculate the CoP and the ZMP during the walker walking.

Well planned walking trajectory can only guarantee static balance of biped robot. For the environment with disturbances, such as rough surface and undesired forces, dynamical balance method must be used to ensure the balance of the biped during walking. Wendlandt [11] described balancing controller based on a 3D multi-body model. The recursive techniques were used in the controller design. Simulation results of the human model reacting to a disturbance were presented. Baltes, McGrath and Anderson [19] have proposed a method in stabilizing the walking gait of a small humanoid robot. A feedback controller based on the rate information from two radio control (RC) hobby gyroscopes was designed to adjust the walking gait into the 'safe zone'. Shih and Gruver [35] developed an advanced control system for a 12-DOF biped robot in the double-support phase. A constrained dynamic model for the robot was formulated and a reduced order model for the double-support phase was derived. Control strategies based on feed forward compensation and linear state feedback were derived for tracking the specified joint trajectories. Zhou and Meng [37] indroduced a general fuzzy reinforcement learning

(FRL) method for biped dynamic balance control, based on neuro-fuzzy network architecture. The simulation results showed it is possible for a biped robot to start its walking with a priori knowledge and then learn to improve its behavior with FRL agents.

1.4 Thesis Outline

Chapter 2 introduces the expression of robot frame rotation and orientation, homogeneous transformations, Denavit-Hartenberg (D-H) representation and inverse kinematics. The D-H representation of a 7-DOF biped is derived.

Chapter 3 discusses dynamics of a 7-DOF biped. Velocity Jacobians and dynamics equations for the 7-DOF biped are derived for both single support phase and double support phase. The formula for calculating CoM and ZMP are given as well.

Chapter 4 designs the walking trajectory for each joint of the biped robot by cubic Hermite interpolation based on record of human walking postures.

Simulation results on the position, speed and acceleration of the center of mass for the links of the biped are provided in Chapter 5. The trajectory for the zero moment point is also given in this chapter. Finally, the toque and power required for each joint are simulated as well.

Proportional-integral-derivative (PID) control of a single link robot arm is discussed in Chapter 6. Sampled setpoint trajectory tracking methods and sampling rate are studied with sinusoidal wave tracking. The PID controller is designed for the position control of a single joint. Experiment on a single joint is carried for both setpoint and trajectory tracking control.

Chapter 7 provides mechanical design, electrical hardware design and control software programming for the biped robot.

Chapter 8 provides experiment results.

Conclusions and the future work are given in Chapter 9.

Chapter 2 Kinematics of a 7-DOF Biped Robot

Cartesian coordinate systems are very important in robot kinematics. To represent the position and orientation of a rigid robot link, it is necessary to establish the frame Cartesian coordinate systems for each link and the relationship between them. This chapter gives the background knowledge of robot kinematics, D-H representation of the 7-DOF robot, inverse kinematics and singularities.

2.1 Frame Rotation and Its Representations

In Figure 2-1, the Cartesian frame $OX_1Y_1Z_1$ is obtained by several rotations of frame $OX_0Y_0Z_0$. Let p_0 and p_1 denote the vector OP expressed in frame $OX_0Y_0Z_0$ and $OX_1Y_1Z_1$, respectively [18]. Then p_0 and p_1 can be expressed as:

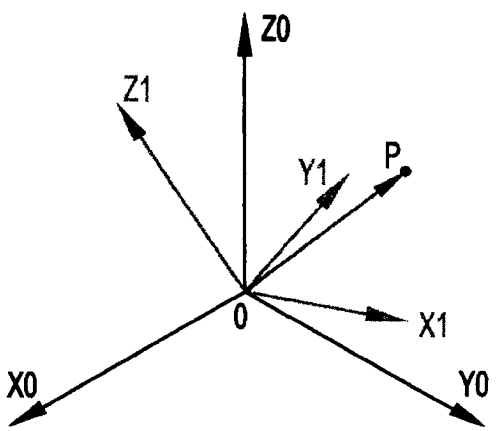

Figure 2-1 Frame Rotation

$$\mathbf{p}_0 = p_{0x}\mathbf{i}_0 + p_{0y}\mathbf{j}_0 + p_{0z}\mathbf{k}_0 \quad \text{.....(2.1.1)}$$

$$\mathbf{p}_1 = p_{1x}\mathbf{i}_1 + p_{1y}\mathbf{j}_1 + p_{1z}\mathbf{k}_1 \quad \text{.....(2.1.2)}$$

where $\{\mathbf{i}_0, \mathbf{j}_0, \mathbf{k}_0\}$ and $\{\mathbf{i}_1, \mathbf{j}_1, \mathbf{k}_1\}$ denote the standard orthonormal basis unit vector on frame $OX_0Y_0Z_0$ and $OX_1Y_1Z_1$, respectively.

Since $\mathbf{p}_0$ and $\mathbf{p}_1$ are representations of the same vector, the relationship between the components of this vector in these two frames can be derived as follows [18].

$$\begin{aligned}
p_{0x} &= \mathbf{p}_0 \cdot \mathbf{i}_0 = \mathbf{p}_1 \cdot \mathbf{i}_0 \\
&= p_{1x}\mathbf{i}_1 \cdot \mathbf{i}_0 + p_{1y}\mathbf{j}_1 \cdot \mathbf{i}_0 + p_{1z}\mathbf{k}_1 \cdot \mathbf{i}_0 \\
p_{0y} &= \mathbf{p}_0 \cdot \mathbf{j}_0 = \mathbf{p}_1 \cdot \mathbf{j}_0 \\
&= p_{1x}\mathbf{i}_1 \cdot \mathbf{j}_0 + p_{1y}\mathbf{j}_1 \cdot \mathbf{j}_0 + p_{1z}\mathbf{k}_1 \cdot \mathbf{j}_0 \\
p_{0z} &= \mathbf{p}_0 \cdot \mathbf{k}_0 = \mathbf{p}_1 \cdot \mathbf{k}_0 \\
&= p_{1x}\mathbf{i}_1 \cdot \mathbf{k}_0 + p_{1y}\mathbf{j}_1 \cdot \mathbf{k}_0 + p_{1z}\mathbf{k}_1 \cdot \mathbf{k}_0
\end{aligned} \quad \text{.....(2.1.3)}$$

The equations (2.1.3) can be rewritten as:

$$\mathbf{p}_0 = R_0^1 \mathbf{p}_1 \quad \text{.....(2.1.4)}$$

where

$$R_0^1 = \begin{bmatrix} \mathbf{i}_1 \cdot \mathbf{i}_0 & \mathbf{j}_1 \cdot \mathbf{i}_0 & \mathbf{k}_1 \cdot \mathbf{i}_0 \\ \mathbf{i}_1 \cdot \mathbf{j}_0 & \mathbf{j}_1 \cdot \mathbf{j}_0 & \mathbf{k}_1 \cdot \mathbf{j}_0 \\ \mathbf{i}_1 \cdot \mathbf{k}_0 & \mathbf{j}_1 \cdot \mathbf{k}_0 & \mathbf{k}_1 \cdot \mathbf{k}_0 \end{bmatrix}$$

The matrix R_0^1 is the transformation matrix which transforms the same vector *OP's* coordinates expressed in frame $OX_1Y_1Z_1$ into the coordinates expressed in frame $OX_0Y_0Z_0$. It is the general expression of rotation matrix. The first column, second column and third column of the rotation matrix specify the direction of x-axis, y-axis and z-axis of the rotated frame with respect to the original frame, respectively.

Equation (2.1.5) provides three special rotation matrices, $R_{z,\theta}$, $R_{x,\theta}$, $R_{y,\theta}$ obtained by rotating frame $OX_0Y_0Z_0$ by an angle θ about axis *Z*, *X*, and *Y*, respectively.

$$R_{z,\theta}=\begin{bmatrix} cos\theta & -sin\theta & 0 \\ sin\theta & cos\theta & 0 \\ 0 & 0 & 1 \end{bmatrix}$$

$$R_{x,\theta}=\begin{bmatrix} 1 & 0 & 0 \\ 0 & cos\theta & -sin\theta \\ 0 & sin\theta & cos\theta \end{bmatrix} \quad \text{.....(2.1.5)}$$

$$R_{y,\theta}=\begin{bmatrix} cos\theta & 0 & sin\theta \\ 0 & 1 & 0 \\ -sin\theta & 0 & cos\theta \end{bmatrix}$$

For some successive rotations about the original axis the resultant rotation matrix is the multiplication of all the rotation matrices in the *reverse order.* But for the successive rotations about the successive current axis the resultant rotation matrix is the multiplication of all the rotation matrices in the forward order.

There are three ways to represent rotations. The first way is the *axis-angle representation*, the second way is the *Euler Angle representation* and the third way is the *roll-pitch-yaw representation.*

In the *axis-angle representation*, any rotation matrix can be represented by a single rotation about a suitable axis k in space by a suitable angle θ as

$$R = R_{k,\theta} = \begin{bmatrix} r_{11} & r_{12} & r_{13} \\ r_{21} & r_{22} & r_{23} \\ r_{31} & r_{32} & r_{33} \end{bmatrix} \quad \text{.....(2.1.6)}$$

where

$$\theta = cos^{-1}\left(\frac{r_{11}+r_{22}+r_{33}-1}{2}\right), \mathbf{k} = \frac{1}{2sin\theta}\begin{bmatrix} r_{32}-r_{23} \\ r_{13}-r_{31} \\ r_{21}-r_{12} \end{bmatrix}$$

if $\sin\theta \neq 0$ and when $\sin\theta = 0$, k is undefined.

In the *Euler Angle representation*, the orientation of the rotated frame can be specified relative to the original frame by three angles (θ, ϕ, ψ). The rotation is obtained by three successive rotations: rotation about the original z-axis by an angle ϕ, rotation about the current y-axis by an angle θ and rotation about the current z-axis by an angle ψ. The rotation matrix is represented as:

$$R = R_{z,\phi}R_{y,\theta}R_{z,\psi} = \begin{bmatrix} \cos\phi & -\sin\phi & 0 \\ \sin\phi & \cos\phi & 0 \\ 0 & 0 & 1 \end{bmatrix}\begin{bmatrix} \cos\theta & 0 & \sin\theta \\ 0 & 1 & 0 \\ -\sin\theta & 0 & \cos\theta \end{bmatrix}\begin{bmatrix} \cos\psi & -\sin\psi & 0 \\ \sin\psi & \cos\psi & 0 \\ 0 & 0 & 1 \end{bmatrix} \quad \text{.....(2.1.7)}$$

$$= \begin{bmatrix} \cos\phi\cos\theta\cos\psi - \sin\phi\sin\psi & -\cos\phi\cos\theta\sin\psi - \sin\phi\cos\psi & \cos\phi\sin\theta \\ \sin\phi\cos\theta\cos\psi + \cos\phi\sin\psi & -\sin\phi\cos\theta\sin\psi + \cos\phi\cos\psi & \sin\phi\sin\theta \\ -\sin\theta\cos\psi & \sin\theta\sin\psi & \cos\theta \end{bmatrix}$$

In the *roll-pitch-yaw representation*, the rotation can be specified as a product of successive rotations about the original frame axes by *roll*, *pitch* and *yaw* angles (θ, ϕ, ψ). The rotation is obtained by three successive rotations. First *roll* about the original x-axis by an angle ψ. Then *pitch* about the original y-axis by an angle θ. Finally *yaw* about the original z-axis by an angle ϕ. The rotation matrix is represented as:

$$R = R_{z,\phi}R_{y,\theta}R_{x,\psi} = \begin{bmatrix} \cos\phi & -\sin\phi & 0 \\ \sin\phi & \cos\phi & 0 \\ 0 & 0 & 1 \end{bmatrix}\begin{bmatrix} \cos\theta & 0 & \sin\theta \\ 0 & 1 & 0 \\ -\sin\theta & 0 & \cos\theta \end{bmatrix}\begin{bmatrix} 1 & 0 & 0 \\ 0 & \cos\psi & -\sin\psi \\ 0 & \sin\psi & \cos\psi \end{bmatrix} \quad \text{.....(2.1.8)}$$

$$= \begin{bmatrix} \cos\phi\cos\theta & \cos\phi\sin\theta\sin\psi - \sin\phi\cos\psi & \cos\phi\sin\theta\cos\psi + \sin\phi\sin\psi \\ \sin\phi\cos\theta & \sin\phi\sin\theta\sin\psi + \cos\phi\cos\psi & \sin\phi\sin\theta\cos\psi - \cos\phi\sin\psi \\ -\sin\theta & \cos\theta\sin\psi & \cos\theta\cos\psi \end{bmatrix}$$

2.2 Homogeneous Transformations and Denavit-Hartenberg Representation

The form of homogeneous transformation matrix [18] is given by:

$$T=\begin{bmatrix}\mathbf{R} & \mathbf{d}\\ 0 & 1\end{bmatrix}=\begin{bmatrix}n_x & s_x & a_x & d_x\\ n_y & s_y & a_y & d_y\\ n_z & s_z & a_z & d_z\\ 0 & 0 & 0 & 1\end{bmatrix}=\begin{bmatrix}\mathbf{n} & \mathbf{s} & \mathbf{a} & \mathbf{d}\\ 0 & 0 & 0 & 1\end{bmatrix} \quad \text{.....(2.2.1)}$$

In the above equation $\mathbf{n}=[n_x\ n_y\ n_z]^T$ is a vector representing the direction of the O_1X_1 axis in frame $O_0X_0Y_0Z_0$, $\mathbf{s}=[s_x\ s_y\ s_z]^T$ represents the direction of the O_1Y_1 axis, and $\mathbf{a}=[a_x\ a_y\ a_z]^T$ represents the direction of the O_1Z_1 axis. The matrix R=[n s a] is the rotation matrix representing the rotation of the frame $O_0X_0Y_0Z_0$ to frame $O_1X_1Y_1Z_1$. The vector $\mathbf{d}=[d_x\ d_y\ d_z]^T$ represents the vector from the origin O_0 to the origin O_1 expressed in the $O_0X_0Y_0Z_0$ frame.

If p_0 and p_1 are the vectors representing the same point p in frame 0 and frame 1, respectively, then the augmented vectors P_0 and P_1 by adding a fourth component of 1 are known as homogenous representations of the vector p_0 and p_1, respectively.

$$\mathbf{P}_0=\begin{bmatrix}\mathbf{p}_0\\ 1\end{bmatrix} \quad \mathbf{P}_1=\begin{bmatrix}\mathbf{p}_1\\ 1\end{bmatrix} \quad \text{.....(2.2.2)}$$

Then the homogenous representations of point p in frame 0 can be calculated with the homogenous representations of point p in frame 1 by using the following equation:

.....(2.2.3)

It is very helpful to be systematic in the choice of the frames, which are attached to the rigid links, when describing the orientation and position of links.

D-H representation is a commonly used convention for selecting frames of reference in robotic applications. In this convention, each homogeneous transformation A_i is represented as a product of four "basic" transformations.

$$A_i = Rot_{z,\theta_i} Trans_{z,d_i} Trans_{x,a_i} Rot_{x,\alpha_i}$$

$$= \begin{bmatrix} \cos\theta_i & -\sin\theta_i & 0 & 0 \\ \sin\theta_i & \cos\theta_i & 0 & 0 \\ 0 & 0 & 1 & 0 \\ 0 & 0 & 0 & 1 \end{bmatrix} \begin{bmatrix} 1 & 0 & 0 & 0 \\ 0 & 1 & 0 & 0 \\ 0 & 0 & 1 & d_i \\ 0 & 0 & 0 & 1 \end{bmatrix} \begin{bmatrix} 1 & 0 & 0 & a_i \\ 0 & 1 & 0 & 0 \\ 0 & 0 & 1 & 0 \\ 0 & 0 & 0 & 1 \end{bmatrix} \begin{bmatrix} 1 & 0 & 0 & 0 \\ 0 & \cos\alpha_i & -\sin\alpha_i & 0 \\ 0 & \sin\alpha_i & \cos\alpha_i & 0 \\ 0 & 0 & 0 & 1 \end{bmatrix}$$

$$= \begin{bmatrix} \cos\theta_i & -\sin\theta_i\cos\alpha_i & \sin\theta_i\sin\alpha_i & a_i\cos\theta_i \\ \sin\theta_i & \cos\theta_i\cos\alpha_i & -\cos\theta_i\sin\alpha_i & a_i\sin\theta_i \\ 0 & \sin\alpha_i & \cos\alpha_i & d_i \\ 0 & 0 & 0 & 1 \end{bmatrix}$$

.....(2.2.4)

where the four quantities θ_i, a_i, d_i, α_i are parameters of link i and joint i. These parameters are generally given the following names: a_i is called the length, α_i is called the twist, d_i is called the offset, and θ_i is called the angle.

Then the homogeneous matrix A_i , which transforms the coordinates of a point from frame i to frame $i-1$, is a function of only a single joint variable, namely q_i (for revolute joint q_i is θ_i and for prismatic joint q_i is d_i).

Now the homogeneous matrix that transforms the coordinates of a point from frame j to frame i is called a transformation matrix, and is usually denoted by T_i^j:

$$T_i^j = A_{i+1}A_{i+2}\cdots A_{j-1}A_j \quad if\ i < j$$
$$T_i^j = I \quad if\ i = j$$
$$T_i^j = (T_j^i)^{-1} \quad if\ i > j$$

.....(2.2.5)

The transformation matrices that are commonly used are the ones that transform coordinates from frame i to frame 0.

$$T_0^i = A_1A_2\cdots A_{i-1}A_i \quad i \le n$$

.....(2.2.6)

2.3 Structure of the 7-DOF Biped Robot

Figure 2-2 shows the structure of the 7-DOF biped robot. There are 3 DOF at each leg for back and forth movement, and 1 DOF at trunk for side to side movement.

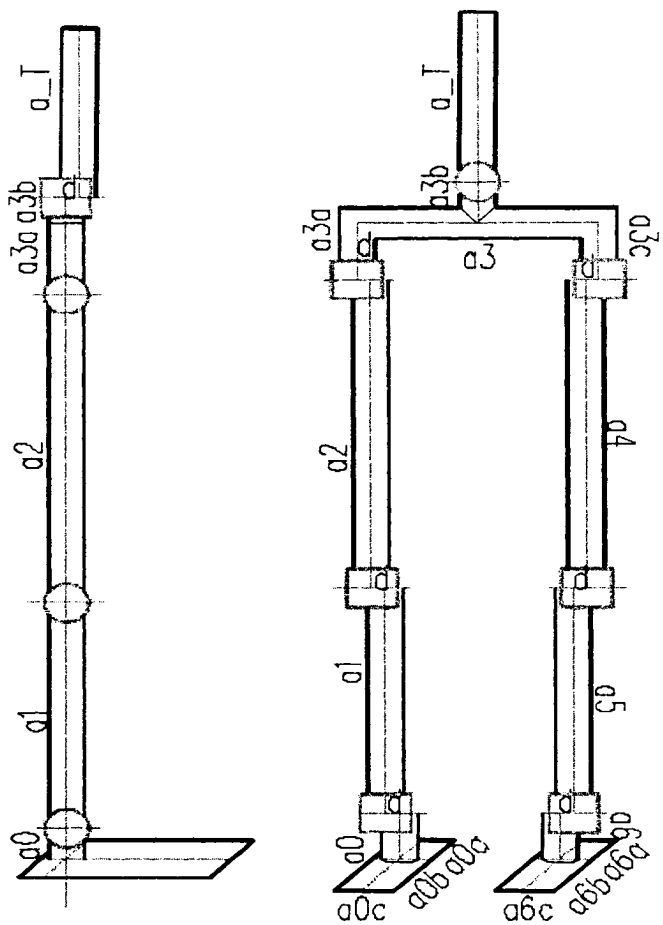

Figure 2-2 7-DOF Biped Robot Structure

2.4 D-H Representation of the 7-DOF Biped Robot

Unlike fixed base manipulators, the walking robot doesn't have a fixed reference frame on itself. The walking of a biped contains mainly two states: single foot support state and double foot support state. In single support state there are two

situations: right foot support state and left foot support state. If we choose the frame of the foot which supports the body in the single foot support state as the reference frame (frame *0* is for right foot support and frame *0'* is for left foot support) we could establish the D-H representation for the walking robot. Suppose there is a fixed reference frame *r* and the transformation matrix from frame *0* (or *0'*) to frame *r* is given by T_r^0 ($T_r^{0'}$). Then the coordinates of a point in frame *i* of the walking robot can be transformed to frame r by:

$$T_r^i = T_r^0 T_0^i = T_r^0 A_1 A_2 \cdots A_{i-1} A_i \quad i \le n \qquad \text{.....(2.4.1)}$$

for the right foot support and

$$T_r^{i'} = T_r^{0'} T_{0'}^{i'} = T_r^{0'} A_{1'} A_{2'} \cdots A_{(i-1)'} A_{i'} \quad i' \le n \qquad \text{.....(2.4.2)}$$

for the right foot support.

We should be very careful in using equations (2.4.1) and (2.4.2) because T_r^0 and $T_r^{0'}$ are changing in every step, and the joint variable q_i and $q_{i'}$ are from different joints.

Figure 2-3 and Figure 2-4 show the frames of the links of the 7-DOF robot in single foot support phase, according to the D-H representation procedures. Figure 2-3 is for right foot on the ground while Figure 2-4 is for left foot on the ground. Table 2-1 shows the D-H parameters in single foot support phase.

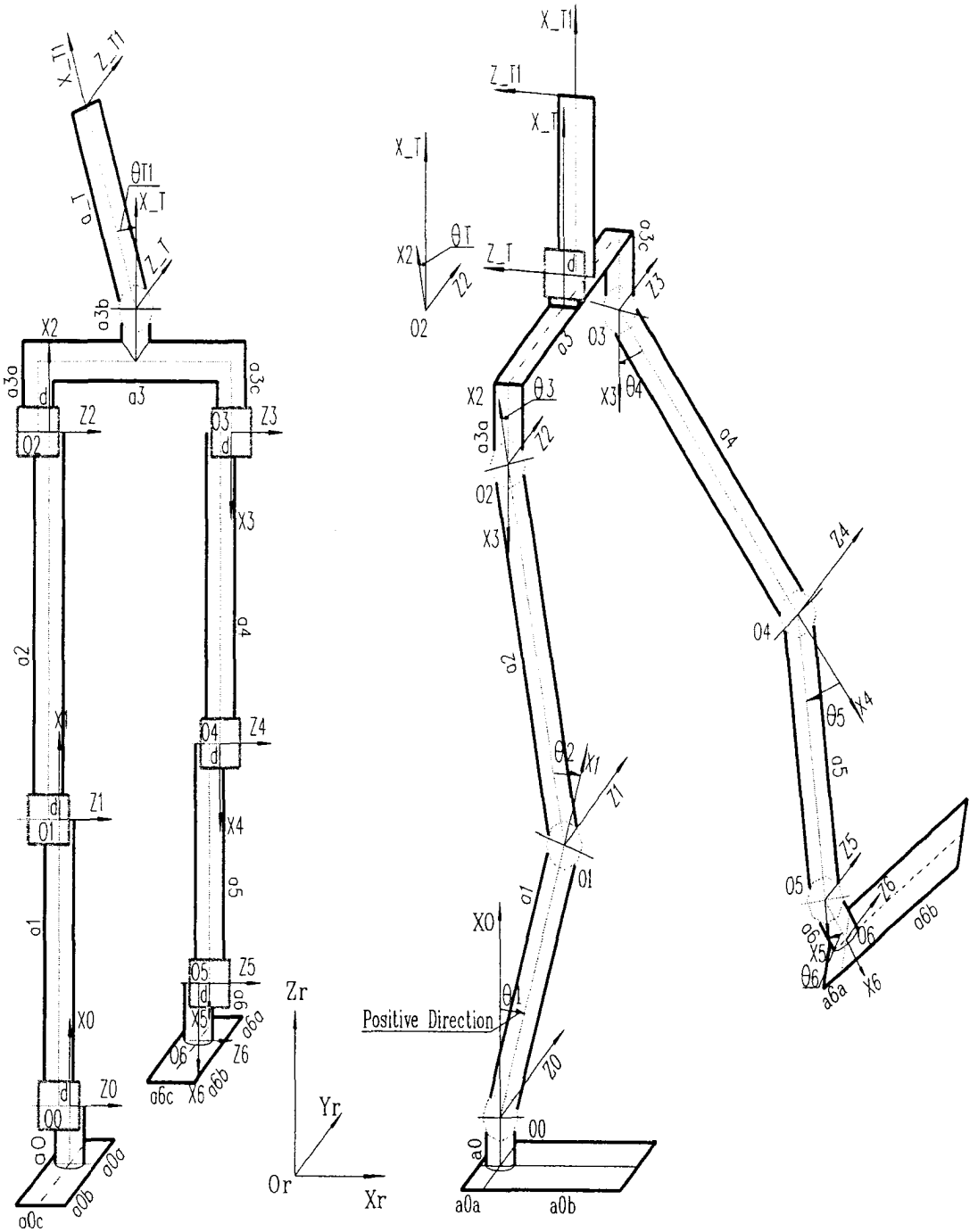

Figure 2-3 D-H Frames for Right Foot on Ground

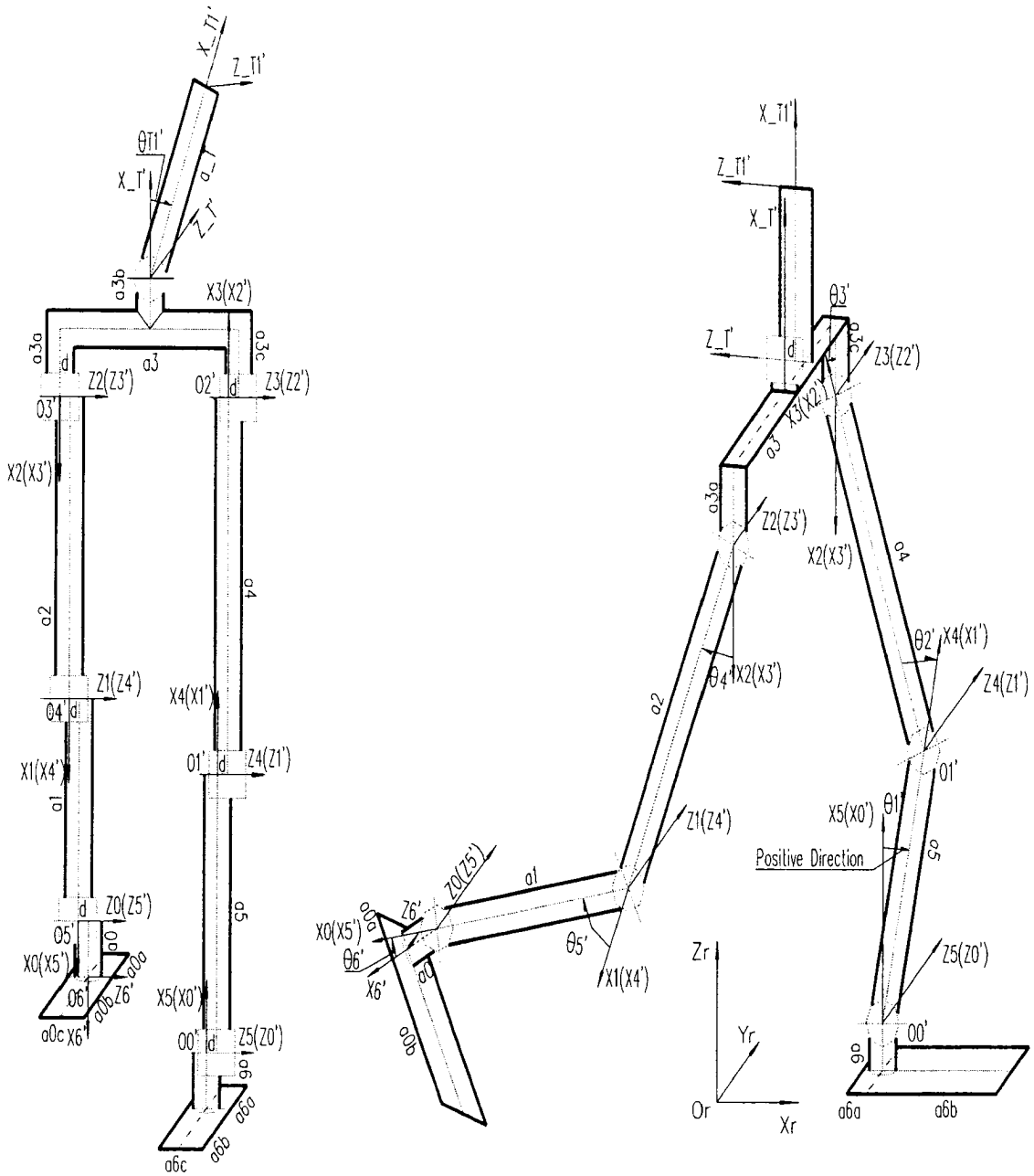

Figure 2-4 D-H Frames for Left Foot on Ground

Table 2-1 D-H Representation Joint Parameters (Single Support)

D-H Representation Table (For Right Foot on Ground)								
Link	a_i	d_i	α_i	θ_i	Joint No.	Initial θi	A_i	Right foot on Ground
1	a1	-d	0	θ_1	0	0	A_1	
2	a2	-d	0	θ_2	1	0	A_2	
3	0	a3-d	0	$\theta_3-\pi$	2	0	A_3	
4	a4	-d	0	θ_4	3	0	A_4	
5	a5	-d	0	θ_5	4	0	A_5	
6	a6	-d	0	θ_6	5	0	A_6	
T	a3a+a3b	a3/2-d	90	θ_T	2	0	A_T	
T1	a_T	-d	0	θ_{T1}	T	0	A_{T1}	
Robot base joint: Jiont 0, Coordinates (X0, Y0, Z0)								
D-H Representation Table (For Left Foot on Ground)								
Link	$a_{i'}$	$d_{i'}$	$\alpha_{i'}$	$\theta_{i'}$	Joint No.	Initial θi	$A_{i'}$	Left foot on Ground
1'	a5	d	0	θ_1'	5	0	$A_{1'}$	
2'	a4	d	0	θ_2'	4	0	$A_{2'}$	
3'	0	-a3+d	0	$\theta_3'-\pi$	3	0	$A_{3'}$	
4'	a2	d	0	θ_4'	2	0	$A_{4'}$	
5'	a1	d	0	θ_5'	1	0	$A_{5'}$	
6'	a0	d	0	θ_6'	0	0	$A_{6'}$	
T'	a3c+a3b	-a3/2+d	90	θ_T'	3	0	$A_{T'}$	
T1'	a_T	-d	0	θ_{T1}'	T	0	$A_{T1'}$	
Robot base joint: Jiont 0', Coordinates (X0', Y0', Z0')								

Figure 2-5 and Figure 2-6 show the frames of the links of the 7-DOF robot in double foot support phase, according to the D-H representation procedures. Figure 2-5 is for double support at start or stop while Figure 2-6 is for double support at walking. Table 2-2 shows the D-H parameters in double support phase.

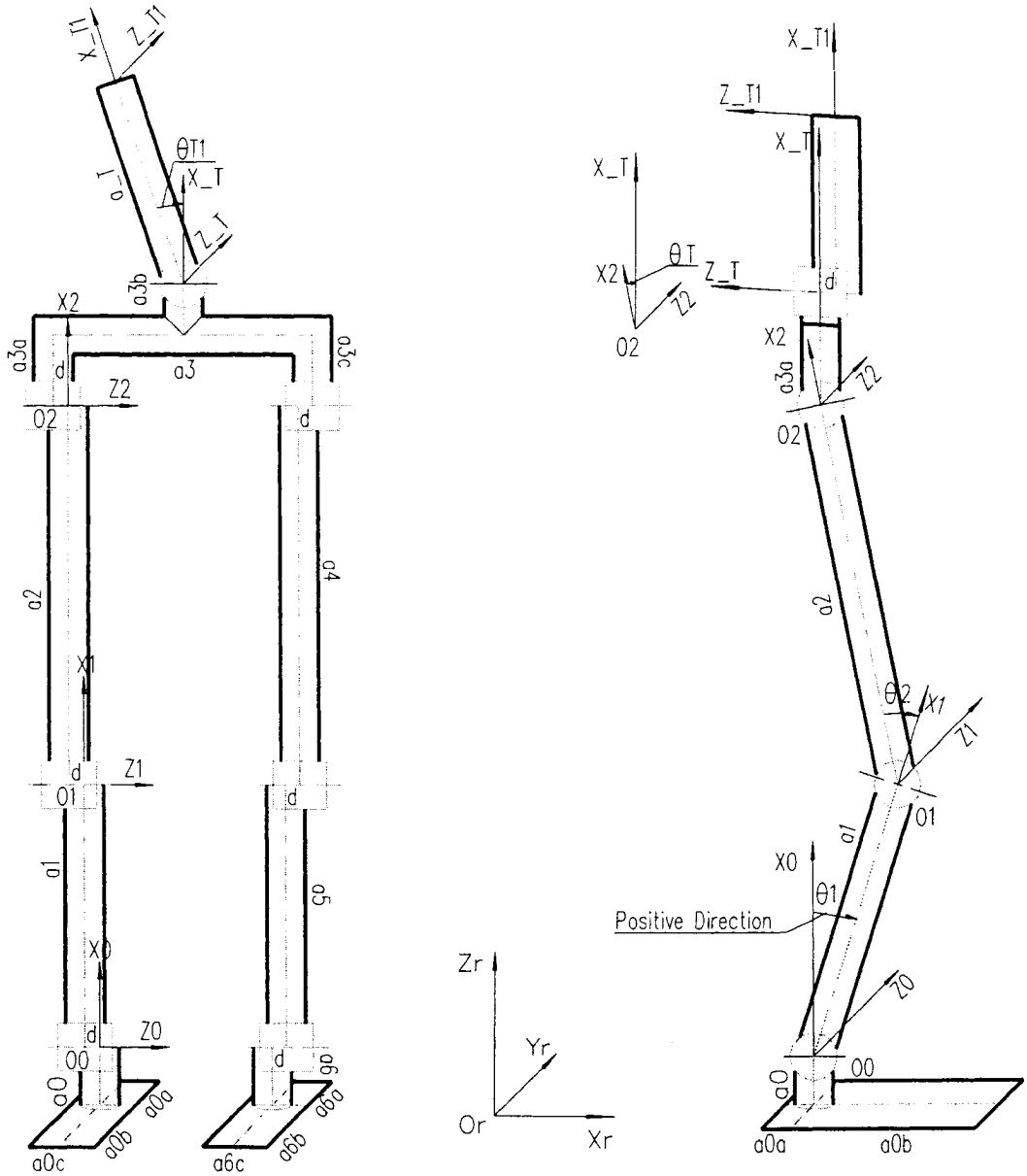

Figure 2-5 D-H Frames for Double Support Phase at Stop or Start

To simplify the leg movement, during the double support phase at stop or start, let two legs have the same movement, and then the D-H frames are simplified as well.

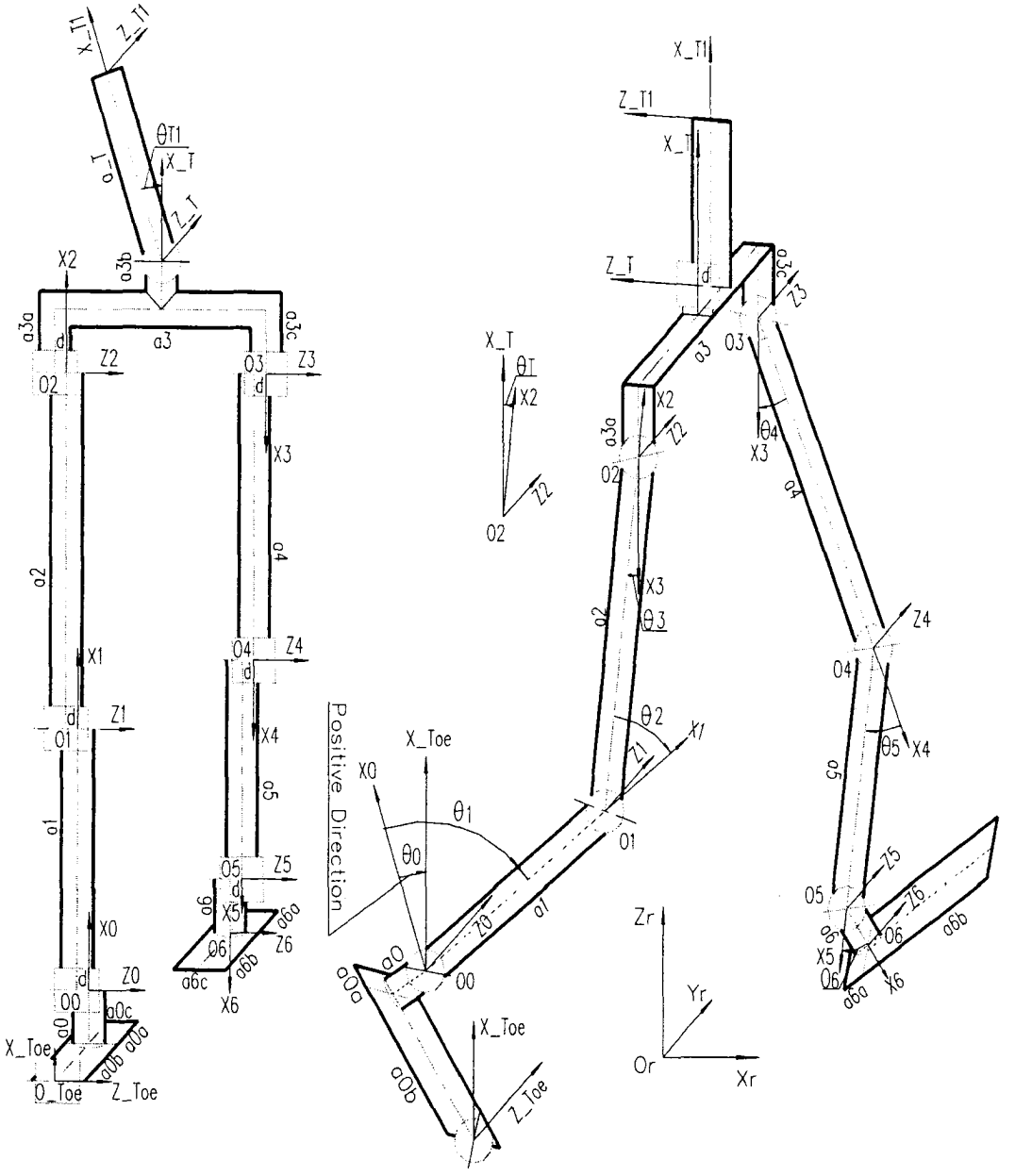

Figure 2-6 D-H Frames for Double Support Phase in Walking

At double support phase in walking, there is additional virtual joint frame 'Toe' (shown in Figure 2-6). This joint is a passive joint, because its movement is formed by friction, inertial and/or gravity force.

Table 2-2 D-H Representation Joint Parameters (Double Support)

D-H Representation Table (Double Support at Start or Stop)							
Link	**a_i**	**d_i**	**α_i**	**θ_i**	**Joint No.**	**Initial θi**	**A_i**
1	a1	-d	0	θ_1	0	0	A_1
2	a2	-d	0	θ_2	1	0	A_2
T	a3a+a3b	a3/2+d	90	θ_T	2	0	A_T
T1	a_T	-d	0	θ_{T1}	T	0	A_{T1}
Robot base joint: Joint 0,Coordinates(X0,Y0,Z0)							

D-H Representation Table (Double Support at Walking)							
Link	**a_i**	**d_i**	**α_i**	**θ_i**	**Joint No.**	**Initial θi**	**A_i**
0	$(a0b^2+a0^2)^{0.5}$	0	0	θ_0	Toe	$-tg^{-1}$ (a0b/a0)	A_0
1	a1	-d	0	θ_1	0	0	A_1
2	a2	-d	0	θ_2	1	0	A_2
3	0	a3+d	0	$\theta_3-\pi$	2	0	A_3
4	a4	-d	0	θ_4	3	0	A_4
5	a5	-d	0	θ_5	4	0	A_5
6	a6	-d	0	θ_6	5	0	A_6
T	a3a+a3b	a3/2+d	90	θ_T	2	0	A_T
T1	a_T	-d	0	θ_{T1}	T	0	A_{T1}
Robot base joint: Joint Toe, Coordinates(X0,Y0,Z0)							

2.5 Inverse Kinematics

When programming the task for a robot manipulator, both the orientation and the position of the end effector should be taken into consideration. Figure 2-7 shows

the end effector *P* at the same orientation but different position, which is expressed in the base frame [21].

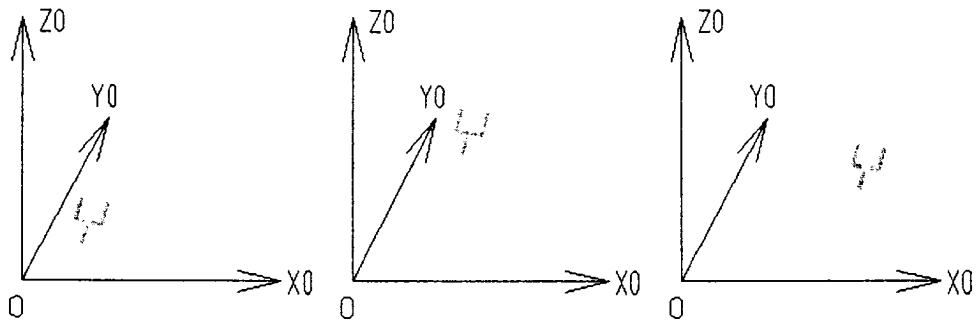

Figure 2-7 End Effector has Same Orientation but Different Positions

Figure 2-8 shows the end effector *P* at the same position but different orientation, which is expressed in the base frame.

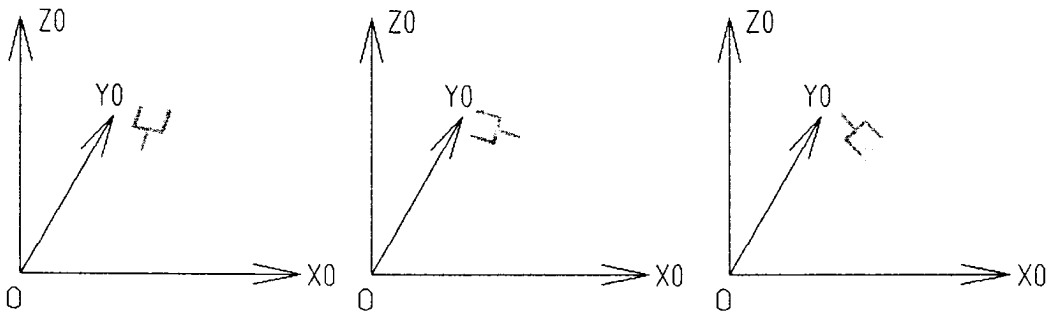

Figure 2-8 End Effector with the Same Position but Different Orientations

The problem to find the joint variables for a given end effector's orientation and position is an inverse kinematics problem. Recall equation (2.2.1), the end effector's orientation expressed in frame *0* gives the rotation matrix in the

homogeneous transformation matrix from the end effector frame to frame *0* and the position gives the translation vector. Both the rotation matrix and the translation vector are function of all the joint variables, therefore the variables can be found mathematically. Sometimes there are multiple solutions, sometimes there is only one single solution and sometimes there is no solution.

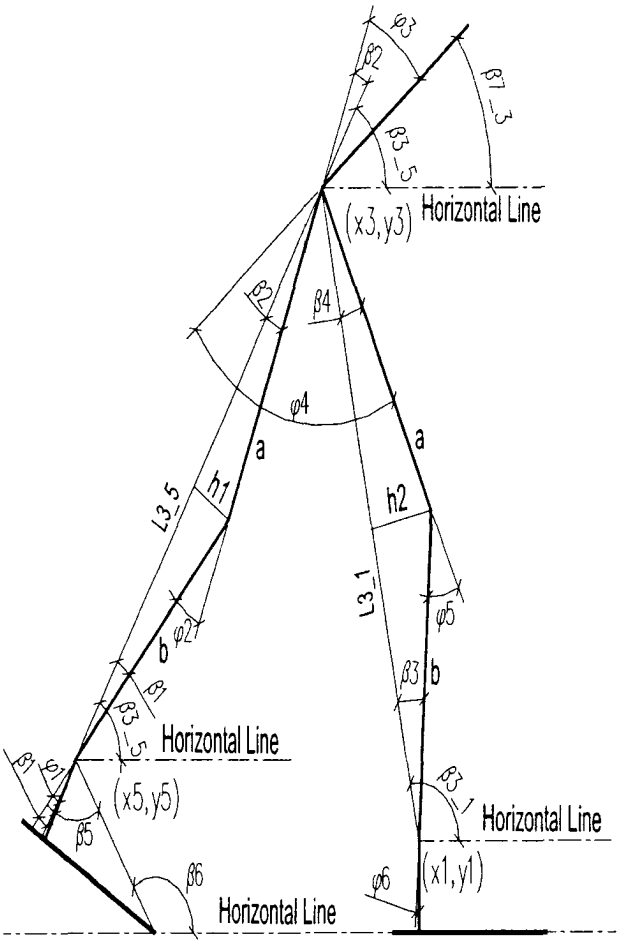

Figure 2-9 Inverse Kinematics

In this thesis, the joint angles in double foot support phase are calculated by inverse kinematics. To simplify the calculation, coordinates of the waist and ankles and $\beta 6$ are given first by trajectory planning, and then joint D-H angles in Figure 2-9 can be calculated geometrically by the following equations.

$$
\begin{aligned}
\varphi_1 &= \beta_1 + \beta_6 - \beta_{3\_5} - \beta_5 \\
\varphi_2 &= -\beta_1 - \beta_2 \\
\varphi_3 &= \beta_2 + \beta_{3\_5} - \beta_{7\_3} \\
\varphi_4 &= \beta_{7\_3} - \beta_{3\_1} - \beta_4 \\
\varphi_5 &= \beta_3 + \beta_4 \\
\varphi_6 &= \beta_{3\_1} - \beta_3 - \pi/2
\end{aligned}
\qquad \text{.....(2.5.1)}
$$

where

$$\beta_1 = arcsin\left(\frac{h_1}{b}\right);\ \beta_2 = arcsin\left(\frac{h_1}{a}\right);\ \beta_3 = arcsin\left(\frac{h_2}{b}\right);\ \beta_2 = arcsin\left(\frac{h_2}{a}\right);$$

$$h_1 = \frac{2\times\sqrt{\Delta_1(\Delta_1-a)(\Delta_1-b)(\Delta_1-L_{3\_5})}}{L_{3\_5}};\ \Delta_1 = \frac{1}{2}(a+b+L_{3\_5});$$

$$L_{3\_5} = \sqrt{(y_3-y_5)^2+(x_3-x_5)^2};\ \beta_{3\_5} = arctan\left(\frac{y_3-y_5}{x_3-x_5}\right); \qquad \text{.....(2.5.2)}$$

$$h_2 = \frac{2\times\sqrt{\Delta_2(\Delta_2-a)(\Delta_2-b)(\Delta_1-L_{3\_1})}}{L_{3\_1}};\ \Delta_2 = \frac{1}{2}(a+b+L_{3\_1});$$

$$L_{3\_1} = \sqrt{(y_3-y_1)^2+(x_3-x_1)^2};\ \beta_{3\_1} = arctan\left(\frac{y_3-y_1}{x_3-x_1}\right);$$

$$L_{3\_1} \le (a+b);\ L_{3\_5} \le (a+b);$$

2.6 Singular Configurations for the 7-DOF Biped

Singular configurations satisfy the condition [18]:

$$rank(J(q)) < max(rank(J(q))) \qquad \text{.....(2.6.1)}$$

where: J(q) is the velocity Jacobian of the end effector.

At singular configuration, the joint angle may have infinite solutions for inverse kinematics. For this 7-DOF biped, if the foot in the air is considered as its end effector, and all z-axes of the related joints (joint 0-5) are in parallel, then the maximum rank of Jacobian is 3. For this structure, the two leg joints connected to the waist are always singularly configured, because the z-axes of these two joints are in line. In addition, the related joint angles at 0 or π, or the z-axes of any two related joints in line are also singular. Figure 2-10 shows one example of singularity configurations. In this example all joint angles are zero.

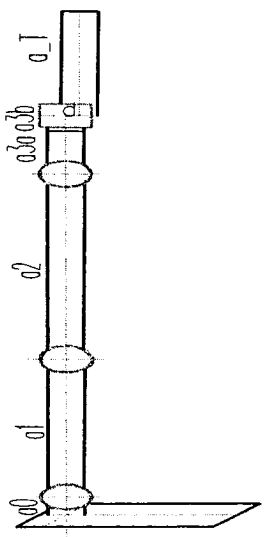

Figure 2-10 Singularities

Chapter 3 Dynamics of the 7-DOF Biped Robot

3.1 Velocity Jacobian

The linear and angular velocity of the end-effector of a robot [18] can be expressed as:

$$\mathbf{v}_0^n = J_v \dot{\mathbf{q}}$$
$$\omega_0^n = J_\omega \dot{\mathbf{q}} \qquad \text{.....(3.1.1)}$$

J_v **and** J_ω **are** $3 \times n$ **matrices, where n is the joint number of the robot. Equations (3.1.1) can be written together:**

$$\begin{bmatrix} \mathbf{v}_0^n \\ \omega_0^n \end{bmatrix} = \begin{bmatrix} J_v \\ J_\omega \end{bmatrix} \dot{\mathbf{q}} = \begin{bmatrix} J_{v1} \cdots J_{vn} \\ J_{\omega 1} \cdots J_{\omega n} \end{bmatrix} \dot{\mathbf{q}} = \begin{bmatrix} J_1 \; J_2 \cdots J_n \end{bmatrix} \dot{\mathbf{q}} = J_0^n \dot{\mathbf{q}} \qquad \text{.....(3.1.2)}$$

J_0^n **is the velocity Jacobian matrix of the end-effector. By several derivations, the** *i*-**th column** J_i **is worked out as:**

$$\begin{cases} J_i = \begin{bmatrix} z_{i-1} \times (o_n - o_{i-1}) \\ z_{i-1} \end{bmatrix} & \text{if joint } i \text{ is revolute} \\ J_i = \begin{bmatrix} z_{i-1} \\ 0 \end{bmatrix} & \text{if joint } i \text{ is prismatic} \end{cases} \qquad \text{.....(3.1.3)}$$

where z_i **is given by the first three elements in the third column of homogeneous transformation matrix** T_0^i**, while** o_i **is given by the first three elements in the fourth column of** T_0^i**.**

The equation (3.1.2) is not only used for computing the velocity of the end-effector but also for computing the velocity of any point on the robot by

changing equation accordingly.

If the point p is in the frame *j* , and the coordinates of point *p* expressed in frame *0* is o_p, then the velocity Jacobian for this point is given by:

$$J_0^j = \begin{bmatrix} J_1 & J_2 & \cdots & J_j \end{bmatrix} \quad \text{.....(3.1.4)}$$

where

$$\begin{cases} J_i = \begin{bmatrix} z_{i-1} \times (o_p - o_{i-1}) \\ z_{i-1} \end{bmatrix} & \text{if joint } i \text{ is revolute} \\ J_i = \begin{bmatrix} z_{i-1} \\ 0 \end{bmatrix} & \text{if joint } i \text{ is prismatic} \end{cases}$$

for i=1, ... , j

The velocity of this point can be calculated by:

$$\begin{bmatrix} \mathbf{v}_0^j \\ \omega_0^j \end{bmatrix} = \begin{bmatrix} J_v \\ J_\omega \end{bmatrix} \dot{\mathbf{q}} = \begin{bmatrix} J_{v1} & \cdots & J_{vj} \\ J_{\omega 1} & \cdots & J_{\omega j} \end{bmatrix} \dot{\mathbf{q}} = \begin{bmatrix} J_1 & J_2 & \cdots & J_j \end{bmatrix} \dot{\mathbf{q}} = J_0^j \begin{bmatrix} \dot{q}_1, \dot{q}_2, \cdots, \dot{q}_j \end{bmatrix}^T \quad \text{.....(3.1.5)}$$

3.1.1 Velocity Jacobian for the Biped Robot in Single Support Phase

For the 7-DOF biped robot, the Jacobian can be derived by equation (3.1.4) and (3.1.5). Let p_i denote the coordinate of the point expressed in frame *i*, and $z_2 = \{A\}_{(1:m,n)}$ represent the sub-matrix of the matrix A, composed of the first m elements in the n-th column of the matrix A. In the following, the velocity Jacobian for this point in the single support phase will be determined.

For points in frame 1, $q=\theta_1$,

$$J_0^1 = \begin{bmatrix} z_0 \times (p_0^1 - o_0) \\ z_0 \end{bmatrix} \quad \text{.....(3.1.6)}$$

where

$$z_0 = \begin{bmatrix} 0 \\ 0 \\ 1 \end{bmatrix}; o_0 = \begin{bmatrix} 0 \\ 0 \\ 0 \end{bmatrix}; \; p_0^1 = \left\{ A_1 \begin{bmatrix} p_1 \\ 1 \end{bmatrix} \right\}_{(1:3,1)} ;$$

For points in frame 2, $q=[\theta_1 \; \theta_2]^T$,

$$J_0^2 = \begin{bmatrix} z_0 \times (p_0^2 - o_0) & z_1 \times (p_0^2 - o_1) \\ z_0 & z_1 \end{bmatrix} \quad \text{.....(3.1.7)}$$

where

$$z_1 = \{A_1\}_{(1:3,3)}; \; o_1 = \{A_1\}_{(1:3,4)}; \; p_0^2 = \left\{ A_1 A_2 \begin{bmatrix} p_2 \\ 1 \end{bmatrix} \right\}_{(1:3,1)} ;$$

For points in frame 3, $q=[\theta_1 \; \theta_2 \; \theta_3]^T$,

$$J_0^3 = \begin{bmatrix} z_0 \times (p_0^3 - o_0) & z_1 \times (p_0^3 - o_1) & z_2 \times (p_0^3 - o_2) \\ z_0 & z_1 & z_2 \end{bmatrix} \quad \text{.....(3.1.8)}$$

where

$$z_2 = \{A_1 A_2\}_{(1:3,3)}; \; o_2 = \{A_1 A_2\}_{(1:3,4)}; \; p_0^3 = \left\{ A_1 A_2 A_3 \begin{bmatrix} p_3 \\ 1 \end{bmatrix} \right\}_{(1:3,1)} ;$$

For points in frame 4, $q=[\theta_1 \; \theta_2 \; \theta_3 \; \theta_4]^T$,

$$J_0^4 = \begin{bmatrix} z_0 \times (p_0^4 - o_0) & z_1 \times (p_0^4 - o_1) & z_2 \times (p_0^4 - o_2) & z_3 \times (p_0^4 - o_3) \\ z_0 & z_1 & z_2 & z_3 \end{bmatrix} \quad \text{.....(3.1.9)}$$

where

$$z_3 = \{A_1 A_2 A_3\}_{(1:3,3)}; \; o_3 = \{A_1 A_2 A_3\}_{(1:3,4)}; \; p_0^4 = \left\{ A_1 A_2 A_3 A_4 \begin{bmatrix} p_4 \\ 1 \end{bmatrix} \right\}_{(1:3,1)} ;$$

For points in frame 5, $q=[\theta_1 \; \theta_2 \; \theta_3 \; \theta_4 \; \theta_5]^T$,

$$J_0^5 = \begin{bmatrix} z_0 \times (p_0^5 - o_0) & z_1 \times (p_0^5 - o_1) & z_2 \times (p_0^5 - o_2) & z_3 \times (p_0^5 - o_3) & z_4 \times (p_0^5 - o_4) \\ z_0 & z_1 & z_2 & z_3 & z_4 \end{bmatrix} \quad \text{.....(3.1.10)}$$

where

$$z_4 = \{A_1 A_2 A_3 A_4\}_{(1:3,3)}; \; o_4 = \{A_1 A_2 A_3 A_4\}_{(1:3,4)}; \; p_0^5 = \left\{ A_1 A_2 A_3 A_4 A_5 \begin{bmatrix} p_5 \\ 1 \end{bmatrix} \right\}_{(1:3,1)} ;$$

For points in frame 6, $q=[\theta_1 \; \theta_2 \; \theta_3 \; \theta_4 \; \theta_5 \; \theta_6]^T$,

$$J_0^5 = \begin{bmatrix} z_0 \times (p_0^6 - o_0) & z_1 \times (p_0^6 - o_1) & z_2 \times (p_0^6 - o_2) & z_3 \times (p_0^6 - o_3) & z_4 \times (p_0^6 - o_4) & z_5 \times (p_0^6 - o_5) \\ z_0 & z_1 & z_2 & z_3 & z_4 & z_5 \end{bmatrix} \quad \text{.....(3.1.11)}$$

where

$$z_5 = \{A_1A_2A_3A_4A_5\}_{(1:3,3)};\ o_5 = \{A_1A_2A_3A_4A_5\}_{(1:3,4)};\ p_0^6 = \left\{A_1A_2A_3A_4A_5A_6\begin{bmatrix} p_6 \\ 1 \end{bmatrix}\right\}_{(1:3,1)};$$

For points in frame T, $q=[\theta_1\ \theta_2\ \theta_T]^T$ with $\theta_T=\theta_3$,

$$J_0^T = \begin{bmatrix} z_0\times(p_0^T - o_0) & z_1\times(p_0^T - o_1) & z_2\times(p_0^T - o_2) \\ z_0 & z_1 & z_2 \end{bmatrix} \quad \text{(3.1.12)}$$

where

$$z_2 = \{A_1A_2\}_{(1:3,3)};\ o_2 = \{A_1A_2\}_{(1:3,4)};\ p_0^T = \left\{A_1A_2A_T\begin{bmatrix} p_T \\ 1 \end{bmatrix}\right\}_{(1:3,1)};$$

For points in frame T1, $q=[\theta_1\ \theta_2\ \theta_T\ \theta_{T1}]^T$ with $\theta_T=\theta_3$,

$$J_0^{T1} = \begin{bmatrix} z_0\times(p_0^{T1} - o_0) & z_1\times(p_0^{T1} - o_1) & z_2\times(p_0^{T1} - o_2) & z_3\times(p_0^{T1} - o_T) \\ z_0 & z_1 & z_2 & z_T \end{bmatrix} \quad \text{(3.1.13)}$$

where

$$z_T = \{A_1A_2A_T\}_{(1:3,3)};\ o_T = \{A_1A_2A_T\}_{(1:3,4)};\ p_0^{T1} = \left\{A_1A_2A_TA_{T1}\begin{bmatrix} p_{T1} \\ 1 \end{bmatrix}\right\}_{(1:3,1)}.$$

3.1.2 Velocity Jacobian for the Biped Robot in Double Support Phase at Start or Stop

For simplification, let two legs have the same movement during the double support phase at start or stop. Then the biped robot is reduced to 4-DOF. The velocity Jacobians for frames 1-3 have the same expressions as in (3.1.6)- (3.1.8), and the velocity Jacobians for frames *T* and *T1* are the same as (3.1.12)- (3.1.13).

3.1.3 Velocity Jacobian for the Biped Robot in Double Support Phase at Walking

During the double support phase at walking, there is a virtual joint at the toe of one foot (the 'joint' at the heel of the other foot could also be considered as the

virtual joint). The angle of this virtual joint is passive, because this angle depends on the friction force and balance status. The velocity Jacobians for the points in each frame can be calculated by the following equations.

For points in frame 0, $q=\theta_0$,

$$J_{Toe}^{0}=\begin{bmatrix} z_{Toe}\times(p_{Toe}^{0}-o_{Toe}) \\ z_0 \end{bmatrix} \quad \text{(3.1.14)}$$

where

$$z_{Toe}=\begin{bmatrix}0\\0\\1\end{bmatrix};\ o_{Toe}=\begin{bmatrix}0\\0\\0\end{bmatrix};\ p_{Toe}^{0}=\left\{A_0\begin{bmatrix}p_0\\1\end{bmatrix}\right\}_{(1:3,1)};$$

For points in frame 1, $q=[\theta_0\ \theta_1]^T$,

$$J_{Toe}^{1}=\begin{bmatrix} z_{Toe}\times(p_{Toe}^{1}-o_{Toe}) & z_0\times(p_{Toe}^{1}-o_0) \\ z_{Toe} & z_0 \end{bmatrix} \quad \text{(3.1.15)}$$

where

$$z_0=\{A_0\}_{(1:3,3)};\ o_0=\{A_0\}_{(1:3,4)};\ p_{Toe}^{1}=\left\{A_0A_1\begin{bmatrix}p_1\\1\end{bmatrix}\right\}_{(1:3,1)};$$

For points in frame 2, $q=[\theta_0\ \theta_1\ \theta_2]^T$,

$$J_{Toe}^{2}=\begin{bmatrix} z_{Toe}\times(p_{Toe}^{2}-o_{Toe}) & z_0\times(p_{Toe}^{2}-o_0) & z_1\times(p_{Toe}^{2}-o_1) \\ z_{Toe} & z_0 & z_1 \end{bmatrix} \quad \text{(3.1.16)}$$

where

$$z_1=\{A_0A_1\}_{(1:3,3)};\ o_1=\{A_0A_1\}_{(1:3,4)};\ p_{Toe}^{2}=\left\{A_0A_1A_2\begin{bmatrix}p_2\\1\end{bmatrix}\right\}_{(1:3,1)};$$

For points in frame 3, $q=[\theta_0\ \theta_1\ \theta_2\ \theta_3]^T$,

$$J_{Toe}^{3}=\begin{bmatrix} z_{Toe}\times(p_{Toe}^{3}-o_{Toe}) & z_0\times(p_{Toe}^{3}-o_0) & z_1\times(p_{Toe}^{3}-o_1) & z_2\times(p_{Toe}^{3}-o_2) \\ z_{Toe} & z_0 & z_1 & z_2 \end{bmatrix} \quad \text{(3.1.17)}$$

where

$$z_2=\{A_0A_1A_2\}_{(1:3,3)};\ o_2=\{A_0A_1A_2\}_{(1:3,4)};\ p_{Toe}^{3}=\left\{A_0A_1A_2A_3\begin{bmatrix}p_3\\1\end{bmatrix}\right\}_{(1:3,1)};$$

For points in frame 4, $q=[\theta_0\ \theta_1\ \theta_2\ \theta_3\ \theta_4]^T$,

$$J_{Toe}^{4}=\begin{bmatrix} z_{Toe}\times\left(p_{Toe}^{4}-o_{Toe}\right) & z_0\times\left(p_{Toe}^{4}-o_0\right) & z_1\times\left(p_{Toe}^{4}-o_1\right) & z_2\times\left(p_{Toe}^{4}-o_2\right) & z_3\times\left(p_{Toe}^{4}-o_3\right) \\ z_{Toe} & z_0 & z_1 & z_2 & z_3 \end{bmatrix} \quad \text{.....(3.1.18)}$$

where

$$z_3=\left\{A_0A_1A_2A_3\right\}_{(1:3,3)};\ o_3=\left\{A_0A_1A_2A_3\right\}_{(1:3,4)};\ p_{Toe}^{4}=\left\{A_0A_1A_2A_3A_4\begin{bmatrix}p_4\\1\end{bmatrix}\right\}_{(1:3,1)};$$

For points in frame 5, q=[θ_0 θ_1 θ_2 θ_3 θ_4 θ_5]^T ,

$$J_{Toe}^{5}=\begin{bmatrix} z_{Toe}\times\left(p_{Toe}^{5}-o_{Toe}\right) & z_0\times\left(p_{Toe}^{5}-o_0\right) & z_1\times\left(p_{Toe}^{5}-o_1\right) & z_2\times\left(p_{Toe}^{5}-o_2\right) & z_3\times\left(p_{Toe}^{5}-o_3\right) & z_4\times\left(p_{Toe}^{5}-o_4\right) \\ z_{Toe} & z_0 & z_1 & z_2 & z_3 & z_4 \end{bmatrix} \quad \text{.....(3.1.19)}$$

where

$$z_4=\left\{A_0A_1A_2A_3A_4\right\}_{(1:3,3)};\ o_4=\left\{A_0A_1A_2A_3A_4\right\}_{(1:3,4)};\ p_{Toe}^{5}=\left\{A_0A_1A_2A_3A_4A_5\begin{bmatrix}p_5\\1\end{bmatrix}\right\}_{(1:3,1)};$$

For points in frame 6, q=[θ_0 θ_1 θ_2 θ_3 θ_4 θ_5 θ_6]^T ,

$$J_{Toe}^{6}=\begin{bmatrix} z_{Toe}\times\left(p_{Toe}^{6}-o_{Toe}\right) & z_0\times\left(p_{Toe}^{6}-o_0\right) & z_1\times\left(p_{Toe}^{6}-o_1\right) & z_2\times\left(p_{Toe}^{6}-o_2\right) & z_3\times\left(p_{Toe}^{6}-o_3\right) & z_4\times\left(p_{Toe}^{6}-o_4\right) & z_5\times\left(p_{Toe}^{6}-o_5\right) \\ z_{Toe} & z_0 & z_1 & z_2 & z_3 & z_4 & z_5 \end{bmatrix}$$

.....(3.1.20)

where

$$z_5=\left\{A_0A_1A_2A_3A_4A_5\right\}_{(1:3,3)};\ o_5=\left\{A_0A_1A_2A_3A_4A_5\right\}_{(1:3,4)};\ p_{Toe}^{6}=\left\{A_0A_1A_2A_3A_4A_5A_6\begin{bmatrix}p_6\\1\end{bmatrix}\right\}_{(1:3,1)};$$

For points in frame T, q=[θ_0 θ_1 θ_2 θ_T]^T with $\theta_T=\theta_3$,

$$J_{Toe}^{T}=\begin{bmatrix} z_{Toe}\times\left(p_{Toe}^{T}-o_{Toe}\right) & z_0\times\left(p_{Toe}^{T}-o_0\right) & z_1\times\left(p_{Toe}^{T}-o_1\right) & z_2\times\left(p_{Toe}^{T}-o_2\right) \\ z_{Toe} & z_0 & z_1 & z_2 \end{bmatrix} \quad \text{.....(3.1.21)}$$

where

$$z_2=\left\{A_0A_1A_2\right\}_{(1:3,3)};\ o_2=\left\{A_0A_1A_2\right\}_{(1:3,4)};\ p_{Toe}^{T}=\left\{A_0A_1A_2A_T\begin{bmatrix}p_T\\1\end{bmatrix}\right\}_{(1:3,1)};$$

For points in frame T1, q=[θ_0 θ_1 θ_2 θ_T θ_{T1}]^T and $\theta_T=\theta_3$,

$$J_{Toe}^{T1}=\begin{bmatrix} z_{Toe}\times\left(p_{Toe}^{T1}-o_{Toe}\right) & z_0\times\left(p_{Toe}^{T1}-o_0\right) & z_1\times\left(p_{Toe}^{T1}-o_1\right) & z_2\times\left(p_{Toe}^{T1}-o_2\right) & z_3\times\left(p_{Toe}^{T1}-o_3\right) \\ z_{Toe} & z_0 & z_1 & z_2 & z_3 \end{bmatrix} \quad \text{.....(3.1.22)}$$

where

$$z_T=\left\{A_1A_2A_T\right\}_{(1:3,3)};\ o_T=\left\{A_0A_1A_2A_T\right\}_{(1:3,4)};\ p_{Toe}^{T1}=\left\{A_0A_1A_2A_TA_{T1}\begin{bmatrix}p_{T1}\\1\end{bmatrix}\right\}_{(1:3,1)}.$$

3.2 Dynamical Equations of Motion

Two methods [18] can be used to calculate the robot dynamics, known as Euler-Lagrange equations and Newton-Euler formulation. We will use the Euler-Lagrange equations to calculate the dynamics of the biped robot.

The Lagrangian is:

$$L = K - V \qquad \text{.....(3.2.1)}$$

where K is called the kinetic energy and V is called the potential energy.

The Euler-Lagrange equations of motion are:

$$\frac{d}{dt}\frac{\partial L}{\partial \dot{q}_j} - \frac{\partial L}{\partial q_j} = \tau_j \qquad j = 1 \cdots n \qquad \text{.....(3.2.2)}$$

The overall kinetic energy of the robot is:

$$K = \frac{1}{2}\dot{\mathbf{q}}^T \underbrace{\sum_{i=1}^{n}\left[m_i J_{v_{ci}}(\mathbf{q})^T J_{v_{ci}}(\mathbf{q}) + J_{\omega_i}(\mathbf{q})^T R_i(\mathbf{q}) I_i R_i(\mathbf{q})^T J_{\omega_i}(\mathbf{q})\right]}_{D(\mathbf{q})}\dot{\mathbf{q}} = \frac{1}{2}\dot{\mathbf{q}}^T D(\mathbf{q})\dot{\mathbf{q}} \qquad \text{.....(3.2.3)}$$

where m_i and I_i are the mass and inertia of link *i*, respectively, $J_{v_{ci}}(\mathbf{q}), J_{\omega_i}(\mathbf{q})$ are linear and angular velocity Jacobians for the center of mass of link *i*, $R_i(\mathbf{q})$ is the rotation matrix transformation from frame *i* to frame *0*. Thus $D(\mathbf{q})$ is a symmetric positive definite matrix.

The overall potential energy [18] of the robot is:

$$V = \int_B \mathbf{g}^T \mathbf{r}\, dm = \mathbf{g}^T \int_B \mathbf{r}\, dm = \mathbf{g}^T \mathbf{r}_c m \qquad \text{.....(3.2.4)}$$

where $\mathbf{g} \in \Re^{3\times 1}$ is the gravity vector; B is the body of the mass; $\mathbf{r} \in \Re^{3\times 1}$ is the vector from the reference frame origin to the point mass dm; $\mathbf{r}_c \in \Re^{3\times 1}$ is the vector from the reference frame origin to the center of mass m.

By several derivations, the Euler-Lagrange equations can be written as:

$$\sum_{j=1}^{n} d_{kj}(\mathbf{q})\ddot{q}_j + \sum_{i=1}^{n}(\sum_{j=1}^{n} c_{ijk}(\mathbf{q})\dot{q}_j)\dot{q}_i + \phi_k(\mathbf{q}) = \tau_k \,, \qquad k = 1,\cdots,n \quad \text{.....(3.2.5)}$$

where d_{kj} is the k-th element of j-th column of matrix D, c_{ijk} are known as Christoffel symbols, defined by

$$c_{ijk}(\mathbf{q}) \stackrel{def}{=} \frac{1}{2}\left(\frac{\partial d_{kj}}{\partial q_i} + \frac{\partial d_{ki}}{\partial q_j} - \frac{\partial d_{ij}}{\partial q_k}\right);$$

and ϕ_k is given by

$$\phi_k(\mathbf{q}) = \frac{\partial V}{\partial q_k} = \frac{\partial \sum_i^n V_i}{\partial q_k}$$

It is a common practice to write the equations (3.2.5) in matrix form:

$$D(\mathbf{q})\ddot{\mathbf{q}} + C(\mathbf{q},\dot{\mathbf{q}})\dot{\mathbf{q}} + G(\mathbf{q}) = \tau \quad \text{.....(3.2.6)}$$

where D(q) is defined in equation (3.2.3); the *k*, *j*-th element of the matrix $C(\mathbf{q},\dot{\mathbf{q}})$ is defined by

$$c_{kj} = \sum_{i=1}^{n} \frac{1}{2}\left(\frac{\partial d_{kj}}{\partial q_i} + \frac{\partial d_{ki}}{\partial q_j} - \frac{\partial d_{ij}}{\partial q_k}\right)\dot{q}_i \quad \text{.....(3.2.7)}$$

and

$$G(\mathbf{q}) = [\phi_1(\mathbf{q}), \phi_2(\mathbf{q}), \cdots, \phi_n(\mathbf{q})]^T$$

With the given mass and center of mass coordinates of each link, it is quite straightforward to get the $D(\mathbf{q})$. Now we need to derive the $C(\mathbf{q},\dot{\mathbf{q}})$. It follows from the definition of c_{kj} in equation (3.2.7). To get $C(\mathbf{q},\dot{\mathbf{q}})$, it is useful to calculate the partial derivatives of $D(\mathbf{q})$ with respect to $\mathbf{q}_m$, $m \in [1, n]$.

$$\frac{\partial dD(\mathbf{q})}{\partial q_m} = \frac{\partial \sum_{i=1}^{n} \left[m_i J_{v_{ci}}(\mathbf{q})^T J_{v_{ci}}(\mathbf{q}) + J_{\omega_i}(\mathbf{q})^T R_i(\mathbf{q}) I_i R_i(\mathbf{q})^T J_{\omega_i}(\mathbf{q}) \right]}{\partial q_m}$$

$$= \sum_{i=1}^{n} \left[m_i \frac{\partial J_{v_{ci}}(\mathbf{q})^T}{\partial q_m} J_{v_{ci}}(\mathbf{q}) + m_i J_{v_{ci}}(\mathbf{q})^T \frac{\partial J_{v_{ci}}(\mathbf{q})}{\partial q_m} + \frac{\partial J_{\omega_i}(\mathbf{q})^T}{\partial q_m} R_i(\mathbf{q}) I_i R_i(\mathbf{q})^T J_{\omega_i}(\mathbf{q}) + J_{\omega_i}(\mathbf{q})^T \frac{R_i(\mathbf{q})}{\partial q_m} I_i R_i(\mathbf{q})^T J_{\omega_i}(\mathbf{q}) \right.$$

$$\left. + J_{\omega_i}(\mathbf{q})^T R_i(\mathbf{q}) I_i \frac{\partial R_i(\mathbf{q})^T}{\partial q_m} J_{\omega_i}(\mathbf{q}) + J_{\omega_i}(\mathbf{q})^T R_i(\mathbf{q}) I_i R_i(\mathbf{q})^T \frac{\partial J_{\omega_i}(\mathbf{q})}{\partial q_m} \right]$$

.....(3.2.8)

The dynamical equations for single support phase and double support phase at start or stop can be derived by above equation. But for the double support phase in walking, we should consider the constraints that the heel of the other foot is on ground.

3.2.1 Dynamic Equations in Double Support Phase at Walking

With both orientation and position, the end effector can be expressed by a complete external coordinates' vector $X = [x \quad y \quad z \quad \psi \quad \theta \quad \phi]$, **where** $[x \quad y \quad z]$ **denotes the Cartesian coordinates of the end effector and** $[\psi \quad \theta \quad \phi]$ **denotes the orientation by yaw, pitch, and roll angles. Then X can be expressed by S [21]**

$$\mathbf{S} = [s_1 \quad s_2 \quad s_3 \quad s_4 \quad s_5 \quad s_6]^T \qquad \text{.....(3.2.9)}$$

The second derivative of S is:

$$\ddot{\mathbf{s}} = J(\mathbf{q})\ddot{\mathbf{q}} + A(\mathbf{q}, \dot{\mathbf{q}}) \qquad \text{.....(3.2.10)}$$

where $J = \frac{\partial \mathbf{s}}{\partial \mathbf{q}} \in \Re^{6 \times n}$ **is the Jacobian matrix and** $A(\mathbf{q}, \dot{\mathbf{q}}) = \frac{\partial^2 \mathbf{s}}{\partial \mathbf{q}^2} \dot{\mathbf{q}}\dot{\mathbf{q}} \in \Re^{6 \times 1}$ **is the adjoint vector.**

In a constrained situation, it is useful to partition the vector S into two subsets, $\mathbf{s}^f \in \Re^{(6-m)\times 1}$ and $\mathbf{s}^c \in \Re^{m\times 1}$ for the *free* elements and *constrained* elements in the position vectors, respectively. Then the equation (3.2.10) becomes [21]:

$$\begin{aligned} \ddot{\mathbf{s}}^f &= J^f(\mathbf{q})\ddot{\mathbf{q}} + A^f(\mathbf{q},\dot{\mathbf{q}}) \\ \ddot{\mathbf{s}}^c &= J^c(\mathbf{q})\ddot{\mathbf{q}} + A^c(\mathbf{q},\dot{\mathbf{q}}) \end{aligned} \qquad \text{.....(3.2.11)}$$

The restriction of motion results in the reaction forces. Reactions will appear in the directions of the constrained coordinates s^c. Thus, there will be m independent components of the reaction. Let these components form the vector $\lambda \in \Re^{m\times 1}$. The reaction components may be in the form of forces if translation is constrained, or in the form of torque if rotation is constrained.

With the constrained situation, the dynamical model becomes:

$$D(\mathbf{q})\ddot{\mathbf{q}} + C(\mathbf{q},\dot{\mathbf{q}})\dot{\mathbf{q}} + g(\mathbf{q}) = \tau + J^{c^T}(\mathbf{q})\lambda \qquad \text{.....(3.2.12)}$$

where $J^c = \dfrac{\partial \mathbf{s}^c}{\partial \mathbf{q}}$

Equations (3.2.11) and (3.2.12) are the dynamical equations for the robot in the double support phase and they contain n+m scalar equations. They can be solved for τ and λ, respectively.

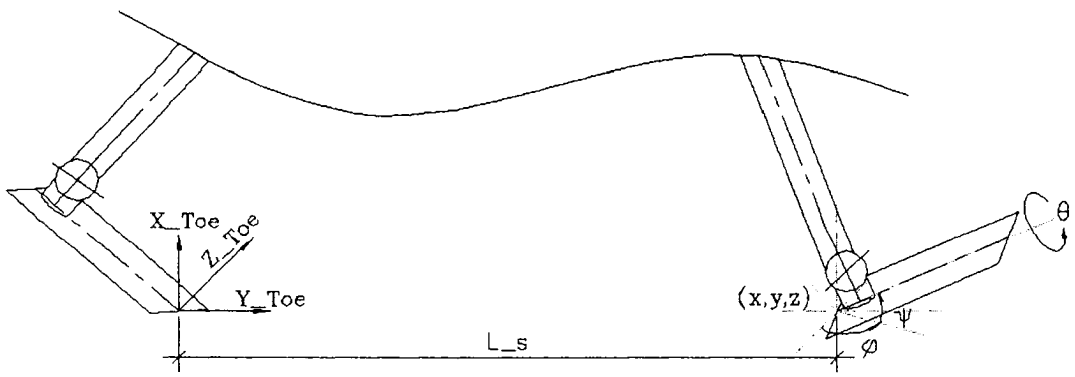

Figure 3-1 Constraints for Double Support Phase

In double support phase, the constrained situation could be expressed as in Figure 3-1. To simplify the expression, we take the frame of the back foot toe as the reference frame. Then the constrained coordinate vector becomes:

$$s^c = [x \quad y \quad z \quad \theta \quad \phi]^T = [0 \quad L\_s \quad a3 \quad 0 \quad 0]^T \qquad \text{.....(3.2.13)}$$

3.3 Center of Mass of the Link

Center of mass calculation: **For robot links, the mass distributes over the links. However, the mass can be lumped to several parts. Hence the center of the mass (CoM) can be calculated by equation (3.3.1) [27].**

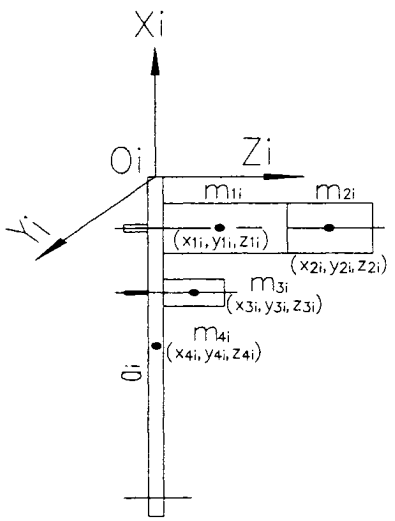

Figure 3-2 Link Structure

$$\mathbf{R} = \frac{1}{M}\sum m_i \mathbf{r}_i \qquad \text{.....(3.3.1)}$$

where m_i and r_i are mass and center of mass position of part i, respectively. $M=\sum m_i$.

For example, if the robot link *i* contains 4 parts (in Figure 3-2) with mass m_{1i}, m_{2i}, m_{3i} and m_{4i}, and the center of mass of each part expressed in frame *i* are (x_{1i}, y_{1i}, z_{1i}), (x_{2i}, y_{2i}, z_{2i}), (x_{3i}, y_{3i}, z_{3i}) and (x_{4i}, y_{4i}, z_{4i}), respectively. Then the resultant center of mass expressed in frame *i* can be calculated as follows:

$$x_{Ci} = \frac{m_{1i}x_{1i} + m_{2i}x_{2i} + m_{3i}x_{3i} + m_{4i}x_{4i}}{m_{1i} + m_{2i} + m_{3i} + m_{4i}} \qquad \text{.....(3.3.2)}$$

$$y_{Ci} = \frac{m_{1i}y_{1i} + m_{2i}y_{2i} + m_{3i}y_{3i} + m_{4i}y_{4i}}{m_{1i} + m_{2i} + m_{3i} + m_{4i}} \qquad \text{.....(3.3.3)}$$

$$z_{Ci} = \frac{m_{1i}z_{1i} + m_{2i}z_{2i} + m_{3i}z_{3i} + m_{4i}z_{4i}}{m_{1i} + m_{2i} + m_{3i} + m_{4i}} \quad \text{.....(3.3.4)}$$

3.4 Zero Moment Point

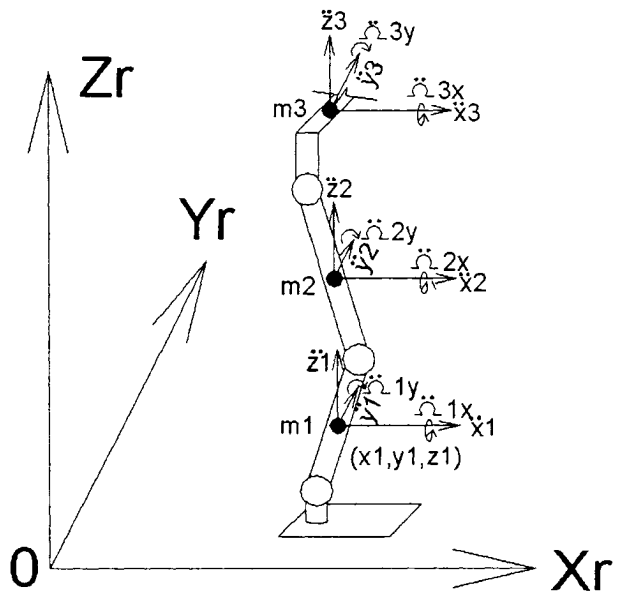

Figure 3-3 Zero Moment Point

The zero moment point (ZMP) is defined as the point on the support surface where the resultant tipping moment acting on the biped, due to gravity and inertial forces, etc., equals to zero. The ZMP does not always falls in the convex hull of the contact area. When the ZMP lays out of the convex hull of the contact area, the biped robot can not be balanced or it will tip over. Therefore the task of dynamically balancing is to control the ZMP in the contact area.

The ZMP can be calculated by the following equations [22]:

$$x_{ZMP} = \frac{\sum_{i=1}^{n} m_i(\ddot{z}_i - g)x_i - \sum_{i=1}^{n} m_i\ddot{x}_i z_i - \sum_{i=1}^{n} I_{iy}\ddot{\Omega}_{iy}}{\sum_{i=1}^{n} m_i(\ddot{z}_i - g)} \quad \text{.....(3.4.1)}$$

$$y_{ZMP} = \frac{\sum_{i=1}^{n} m_i(\ddot{z}_i - g)y_i - \sum_{i=1}^{n} m_i\ddot{y}_i z_i - \sum_{i=1}^{n} I_{ix}\ddot{\Omega}_{ix}}{\sum_{i=1}^{n} m_i(\ddot{z}_i - g)} \quad \text{.....(3.4.2)}$$

where m_i is the mass of link i (Figure 3-3). I_{ix} and I_{iy} are the inertia of link i about axes from the center of mass of link i and parallel to the x-axis and y-axis in reference frame, respectively. $\ddot{\Omega}_{ix}$ and $\ddot{\Omega}_{iy}$ are the angular acceleration about the axes from the center of mass of link i and parallel to the x-axis and y-axis in

reference frame, respectively. g is the gravitational acceleration, and $(x_{ZMP}, y_{ZMP}, 0)$ are the ZMP coordinates expressed in the reference frame. (x_i, y_i, z_i) are the coordinates of the center of mass of link i expressed in the reference frame.

Chapter 4 Walking Trajectory Planning

The passively balanced walk of biped robots depends on good trajectory planning. In our research, we plan the walking trajectory based on human walking pattern record. The human walking pattern data are collected for some critical points in the walking cycle. Then the cubic Hermite interpolation is used to generate intermediate values between the critical points to generate continuous trajectories. The successful trajectory planning guarantees that zero moment point is in the stable area so that the robot will not tip over. The process flow chart is shown in Figure 4-1.

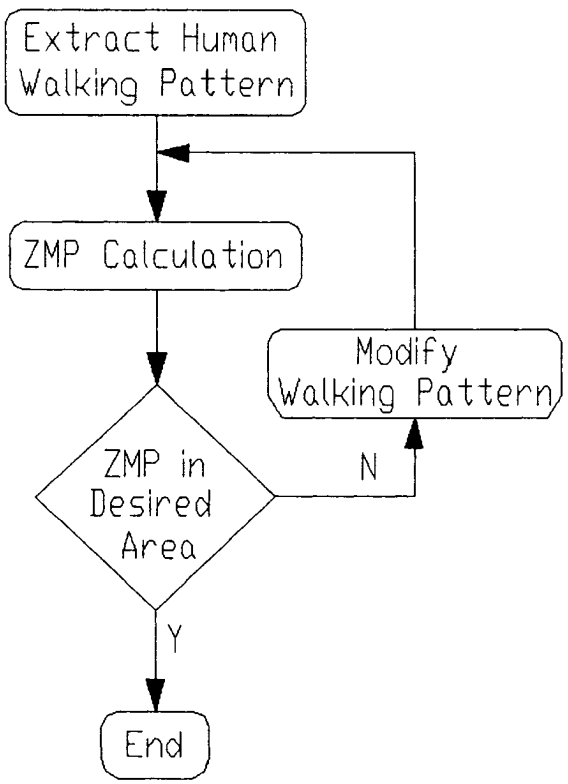

Figure 4-1 Flow Chart for Walking Pattern Planning

4.1 Record of Human Walking Trajectory

The whole walking pattern is shown in Figure 4-2, which is composed of 13 critical points. This pattern was derived by the record of human walking with a video camera, which can record 25 frames per second. The critical point is the point where the coordinates of the hip and ankle joints are specified by measuring the captured pictures. In this figure, the periods for start, walking and stop are normalized to 1, 2 and 1, respectively. The t in this figure is the normalized time for the critical point. The walking pattern is divided into 12 sub intervals. The first two subintervals are considered as the start phase. During the start phase, the robot shifts its CoM forward and to the left side, then lifts the right foot to a certain height. The subintervals from the third to the 10^{th} are considered as the walking phase. The walking phase is partitioned into two parts. The first part consists of the 3^{rd}, 4^{th}, 5^{th} and 6^{th} subintervals. In this part, the right foot lands on the ground; the robot shifts its CoM; and the left foot takes off the ground. The second part mirrors the movements of the first part. The left foot lands on the ground; the robot shifts its CoM; and the right foot takes off the ground. The robot can continuously walk by repeating the walking phase. The last two subintervals are defined as the stop phase. In this phase, the right foot lands on the ground and the robot returns to its initial status.

In this trajectory planning, the recorded walking patterns are modified to fit the 7 DOF parameters and satisfy the criteria that the center of mass of the robot is close to the center of the support convex area at every critical point. Recall equations (3.4.1) and (3.4.2), if the acceleration of the robot is not big then the ZMP position of the robot is close to its CoM position and the robot is able to balance. Figure 4-3 shows the walking pattern of start and stop phases. Figure 4-4 shows the walking pattern of the first part of walking phases. In Figure 4-3 and Figure 4-4, both side view and back view are shown. The bottom of these figures shows the desired CoM positions in the area of two feet projected to the ground. The shadowed area is the contacted area, also known as stable region for ZMP.

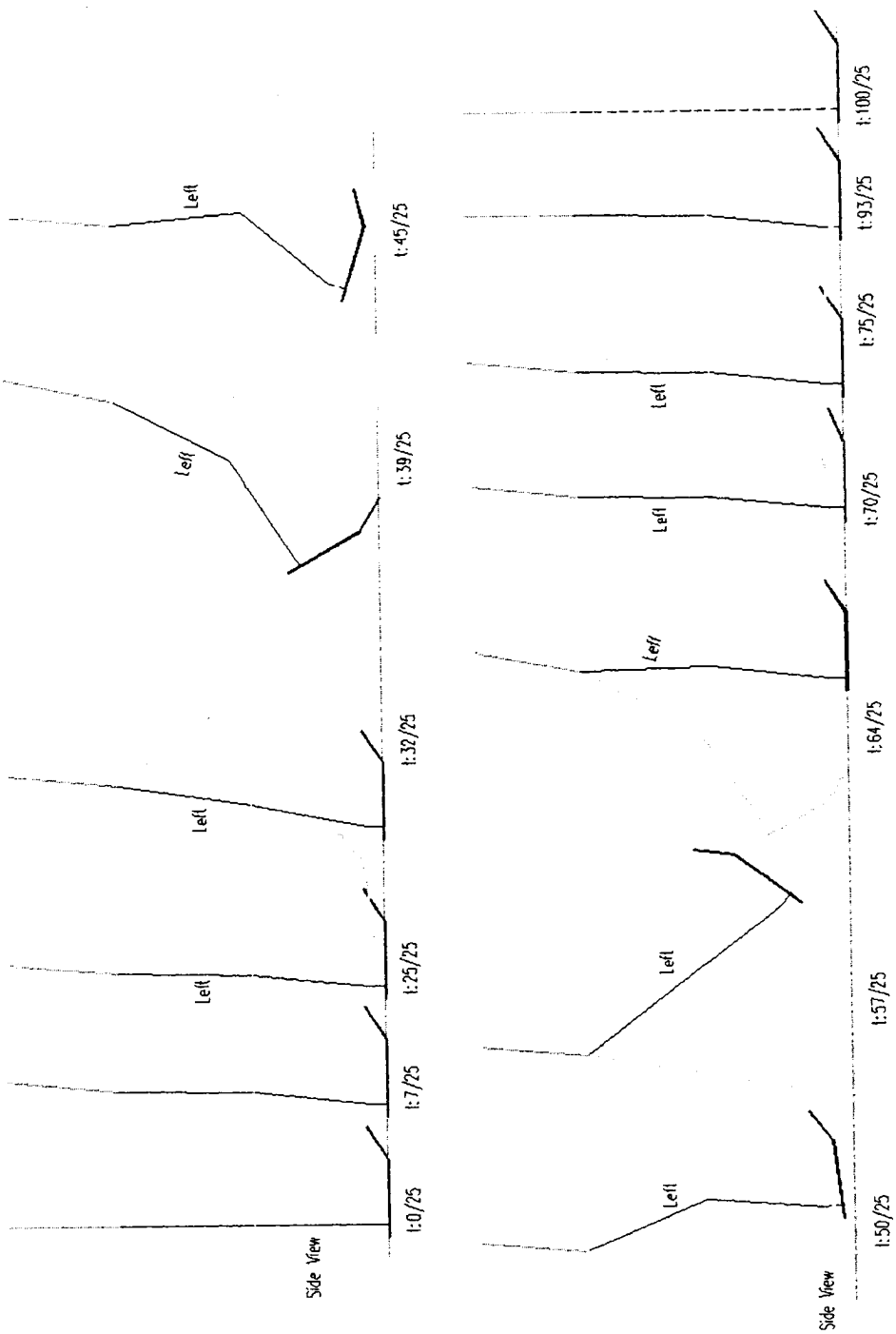

Figure 4-2 Critical Points in a Complete Walking Cycle

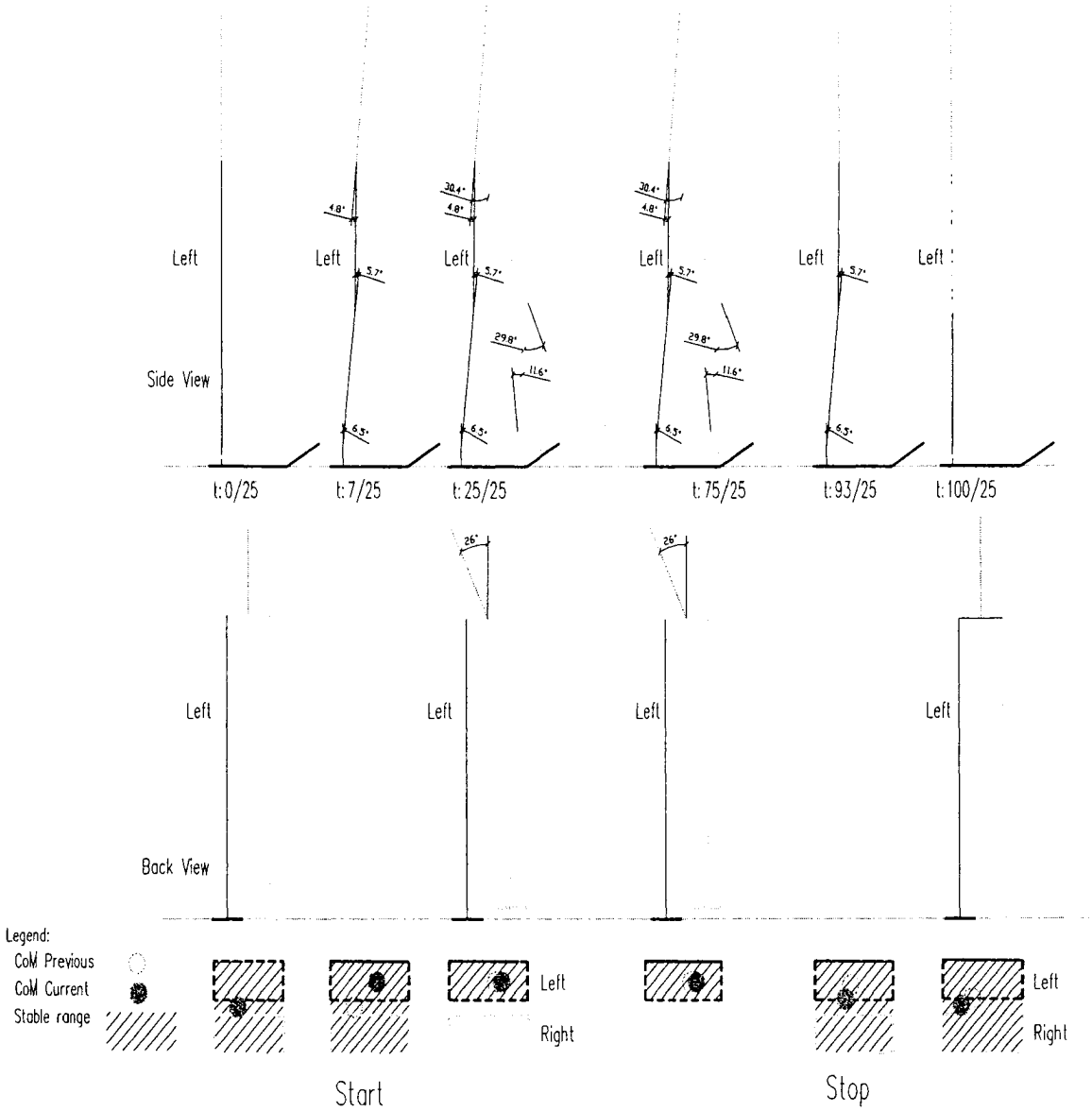

Figure 4-3 Walking Pattern at Stop and Start

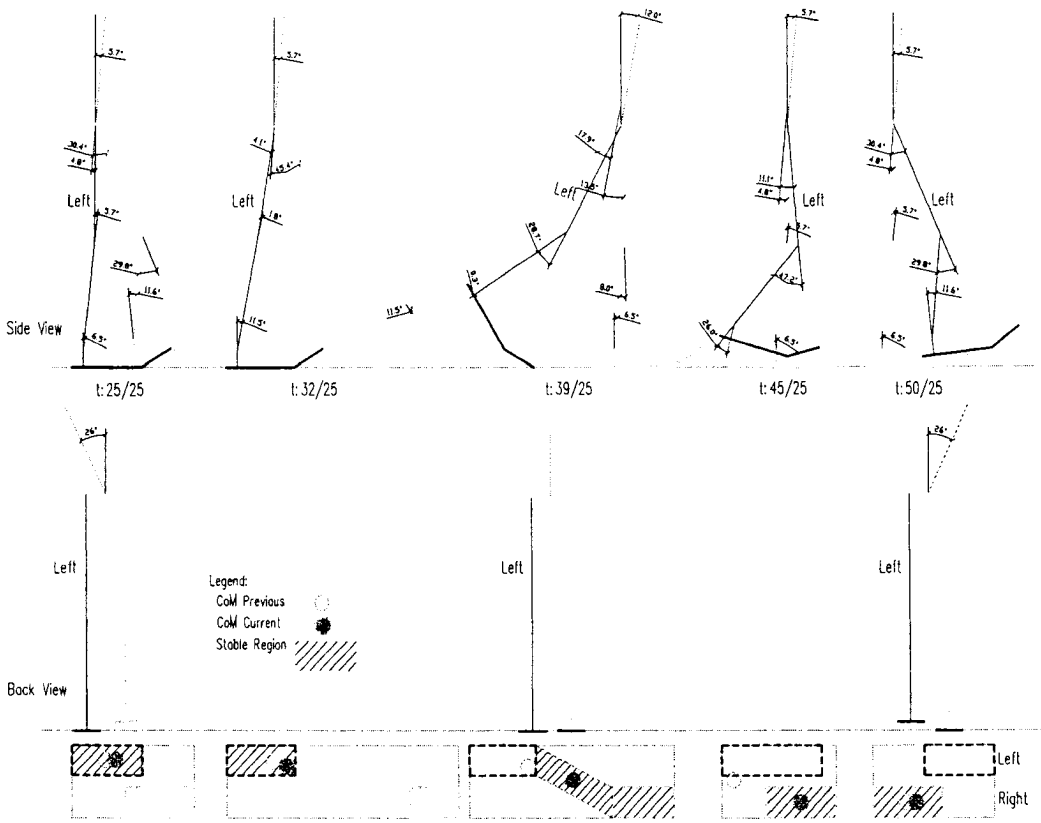

Figure 4-4 Walking Pattern at Walking

Table 4-1 Values of Joint Angles at Critical Points

	Start			Walking Phase									Stop		
T	0/25	7/25	25/25	25/25	32/25	39/25	45/25	50/25	57/25	64/25	70/25	75/25	75/25	93/25	100/25
θ_1	0	6.5	6.5	6.5	11.5	-0.3	26	11.5	11.5	6.5	6.5	6.5	6.5	6.5	0
θ_2	0	-5.7	-5.7	-5.7	-1.8	-28.7	-47.2	-29.8	0	-8	-5.7	-5.7	-5.7	-5.7	0
θ_3	0	4.8	4.8	4.8	-4.1	-17.9	11.1	30.4	45.4	13.5	4.8	4.8	4.8	0.9	0
θ_4	0	-4.8	-30.4	-30.4	-45.4	-13.5	-4.8	-4.8	-4.1	17.9	-11.1	-30.4	-30.4	-0.9	0
θ_5	0	5.7	29.8	29.8	0	8	5.7	5.7	1.8	28.7	47.2	29.8	29.8	5.7	0
θ_6	0	-6.5	-11.5	-11.5	-11.5	-6.5	-6.5	-6.5	-11.5	0.3	-26	-11.6	-11.6	-6.5	0
θ_T															
θ_{T1}	0	26				0		-26		0				26	0

Note: All angles are measured in 'Left Foot on Ground Fran

Legend:

Left Foot On Ground | Both Foot On Groun

Right Foot On Ground | Intersection

Table 4-1 lists values of joint angles at critical points in the walking pattern and these angles are measured based on the configuration of the left foot on ground. The continuous curves can be generated for joint angles based on these points by the cubic Hermite interpolation.

4.2 Cubic Hermite Interpolation

Cubic Hermite interpolation [9] is a method to generate a continuous curve based on 3 or more discrete values by piecing together third order polynomial functions. This method is suitable for non-smooth break points to avoid minima and maxima that do not exist and may destroy monotonicity of the curve. The Hermite form consists of two control tangents for each polynomial. For interpolation on a grid with points x_k for k = 1,...,n, interpolation is performed on one subinterval $[x_k, x_{k+1}]$ at a time (given that tangent values are predetermined). The subinterval $[x_k, x_{k+1}]$ is normalized to [0,1] via $t = (x - x_k) / (x_{k+1} - x_k)$.

On each normalized subinterval, given a starting point p_0 at t = 0 and an ending point p_1 at t = 1 with starting tangent m_0 at t = 0 and ending tangent m_1 at t = 1, the polynomial can be defined by

$$\mathbf{p}(t) = (2t^3 - 3t^2 + 1)\mathbf{p}_0 + (t^3 - 2t^2 + t)\mathbf{m}_0 + (-2t^3 + 3t^2)\mathbf{p}_1 + (t^3 - t^2)\mathbf{m}_1 \quad \text{.....(4.2.1)}$$

where $0 \le t \le 1$.

Define

$$\begin{aligned} h_{00}(t) &= 2t^3 - 3t^2 + 1 \\ h_{10}(t) &= t^3 - 2t^2 + t \\ h_{01}(t) &= -2t^3 + 3t^2 \\ h_{11}(t) &= t^3 - t^2 \end{aligned} \quad \text{.....(4.2.2)}$$

Then, (4.2.1) can be expressed as

$$\mathbf{p}(t) = h_{00}(t)\mathbf{p}_0 + h_{10}(t)\mathbf{m}_0 + h_{01}(t)\mathbf{p}_1 + h_{11}(t)\mathbf{m}_1 \quad \text{.....(4.2.3)}$$

Given n+1 points $p_0, \ldots, p_n$, n cubic Hermite curve segments are required to generate a continuous curve. Each curve segment starts at point p_i and ends at point p_{i+1} with starting tangent m_i and ending tangent m_{i+1} defined by

$$\mathbf{m}_i = \frac{1}{2}(1-c)(\mathbf{p}_{i+1} - \mathbf{p}_{i-1}) \quad c \in [0,1] \qquad \text{.....(4.2.4)}$$

where the first and last tangents, m_0 and m_n, are given and c is a constant that modifies the length of the tangent (the tension parameter).

With the joint angles at critical points in Table 4-1, Cubic Hermite interpolation can be used to generate a continuous curve for each joint angle in the walking period, excluding the double support phase in walking. Because the joint angles of double support phase in walking are constrained, they can only be calculated with inverse kinematics. The curves for coordinates of the waist and two ankles, and the angle between the foot and ground are generated first by Cubic Hermite interpolation. Then the trajectories for the joint angles are calculated by inverse kinematics.

The angular velocity and angular acceleration for each joint can be generated by using equations (4.2.5) and (4.2.6) numerically.

$$\begin{cases} \dfrac{d\mathbf{p}}{dt}(i) = \dfrac{\mathbf{p}_i - \mathbf{p}_{i-1}}{\Delta T}, & i \in [2, n+1] \\ \dfrac{d\mathbf{p}}{dt}(1) = 0 \end{cases} \qquad \text{.....(4.2.5)}$$

$$\begin{cases} \dfrac{d^2\mathbf{p}}{dt^2}(i) = \dfrac{\dfrac{d\mathbf{p}}{dt}(i) - \dfrac{d\mathbf{p}}{dt}(i-1)}{\Delta T}, & i \in [2, n+1] \\ \dfrac{d^2\mathbf{p}}{dt^2}(1) = 0 \end{cases} \qquad \text{.....(4.2.6)}$$

4.3 Joint Angle, Angular Velocity and Angular Acceleration

The simulation results for the joint angle, velocity and acceleration are shown

in Figure 4-5 ~ Figure 4-11. In these figures, 'DFS' and 'SFS' denote 'Double Foot Support Phase' and 'Single Foot Support Phase', respectively. In the simulation, the walking period is 16 seconds, both start and stop period are 8 seconds.

The angle curves for the leg joints in 'Start Phase', 'Stop Phase' and single foot support phase in walking are generated by Cubic Hermite interpolation with angles at critical points. The angle curve for the joint of the trunk is generated by Cubic Hermite interpolation with angles at critical points as well. While angle curves for the leg joints in double foot support phase in walking are calculated by inverse kinematics for the constrained foot position.

The following observations can be made on the walking trajectories for the biped joints. First, there are some symmetries between the trajectories for joint n and joint 7-n with n=1, 2, ..., 6, during the walking phase. For example, the trajectory for joint 5 from t=16 to 24 can be obtained by multiplying -1 to the trajectory for joint 2 from t=8 to 16. This kind of symmetries can also be observed from the human walking patterns. Second, the maximum acceleration for joint 1 to 6 is less than 0.8 rad/s^2, while the maximum acceleration for the trunk is about 1.8 rad/s^2. The maximum speed for joint 1 to 6 is less than 0.4 rad/s, while the maximum speed for the trunk is about 0.6 rad/s. Third, Figure 4-11 shows that the trunk tilts toward the support foot to shift the CoM or ZMP so that the biped will not slide down.

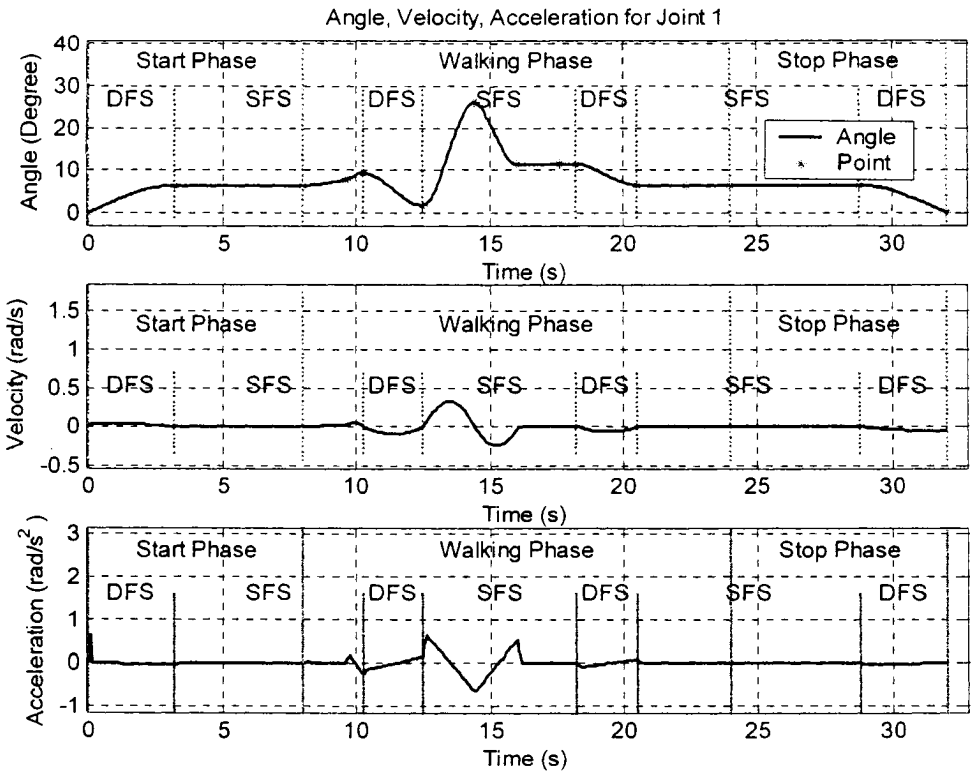

Figure 4-5 Angle, Velocity and Acceleration for Joint 1

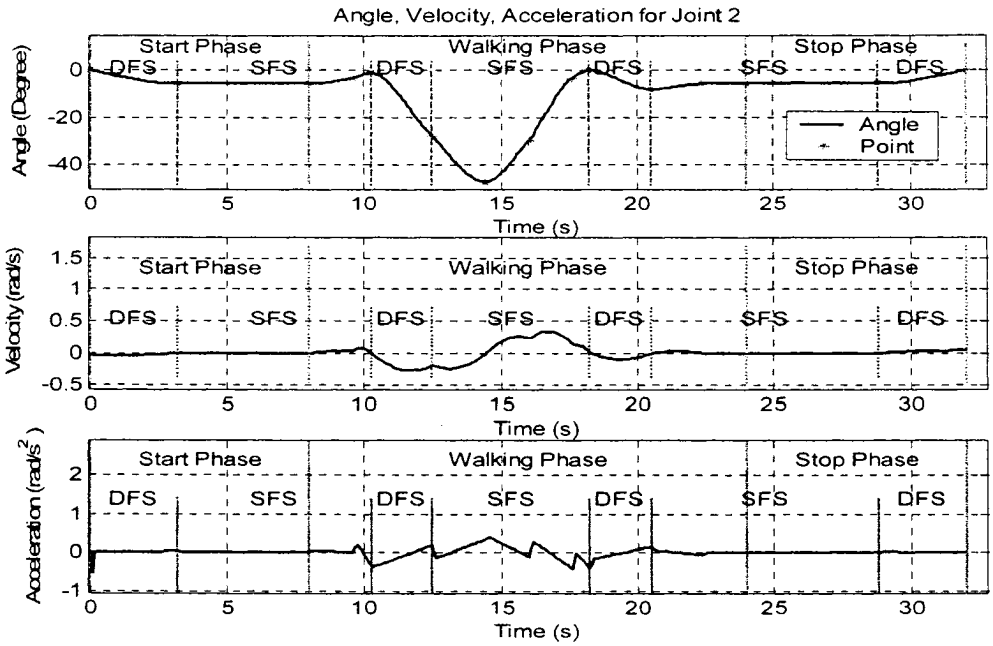

Figure 4-6 Angle, Velocity and Acceleration for Joint 2

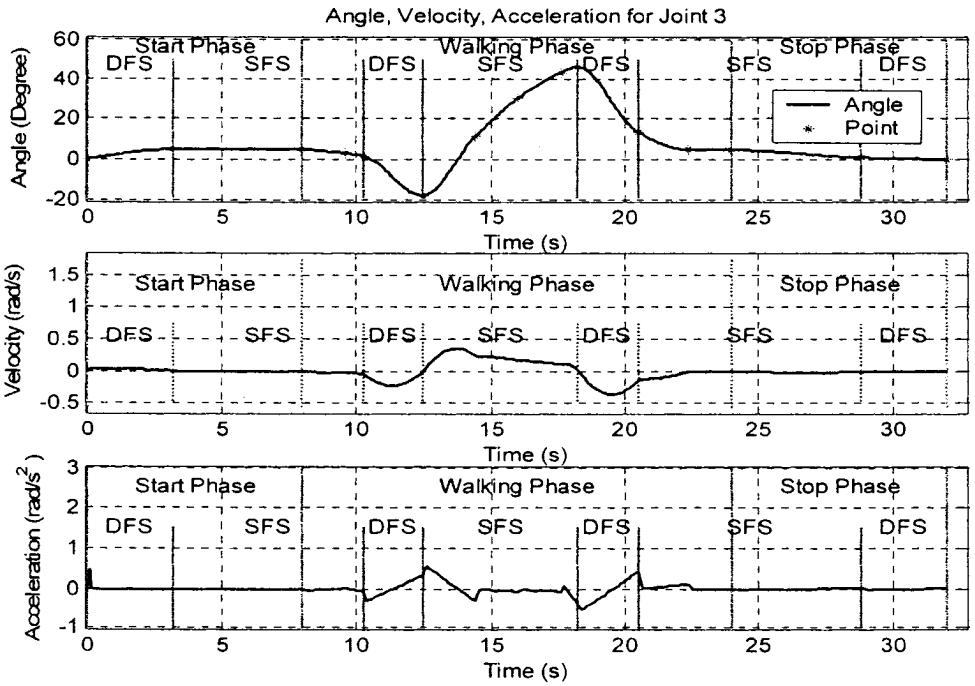

Figure 4-7 Angle, Velocity and Acceleration for Joint 3

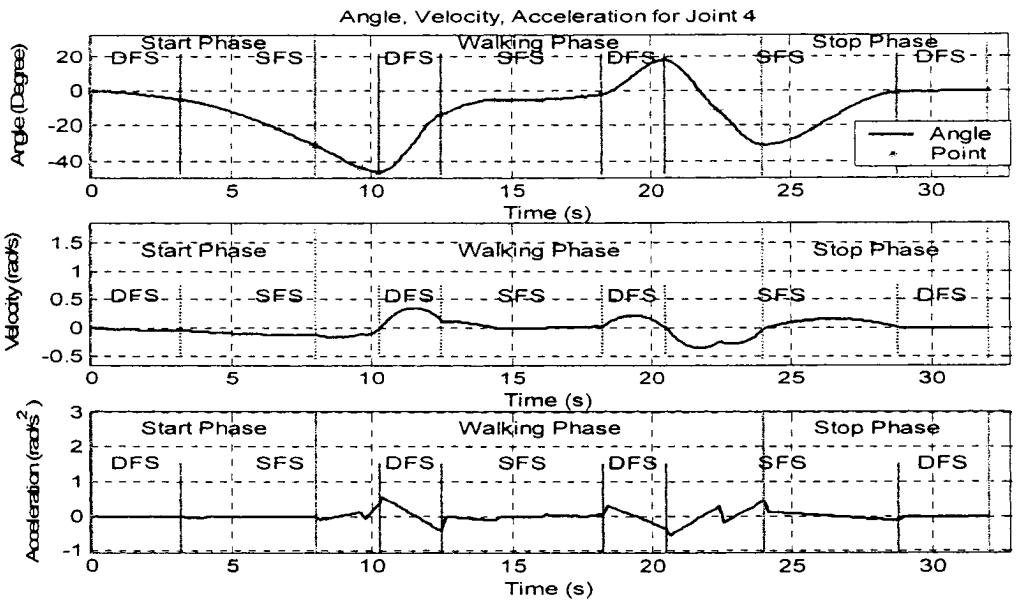

Figure 4-8 Angle, Velocity and Acceleration for Joint 4

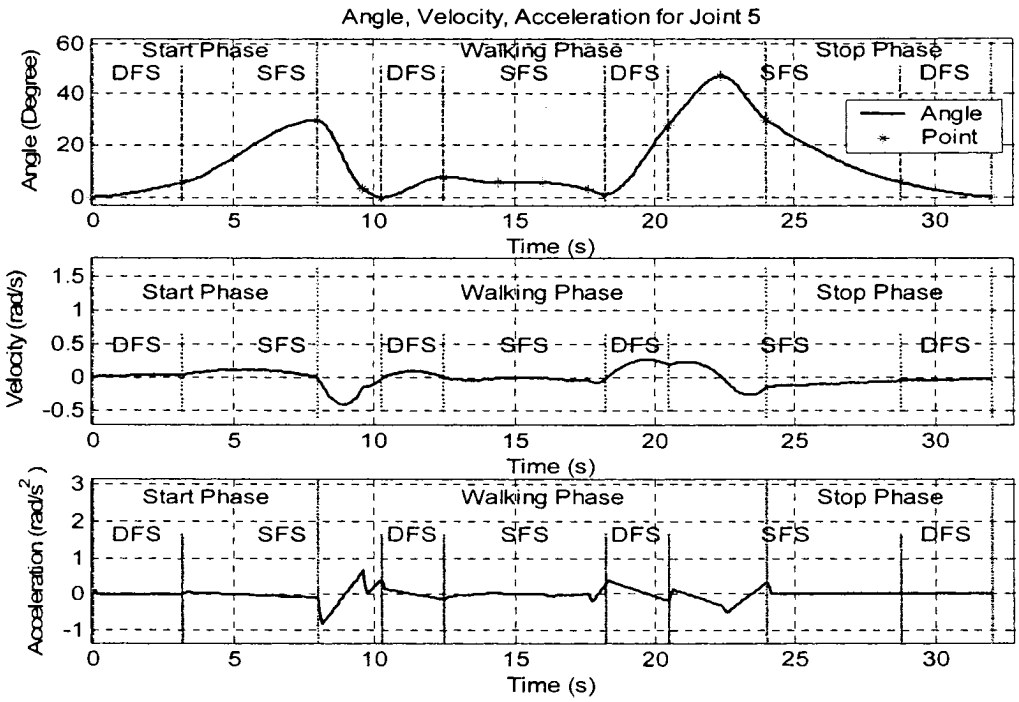

Figure 4-9 Angle, Velocity and Acceleration for Joint 5

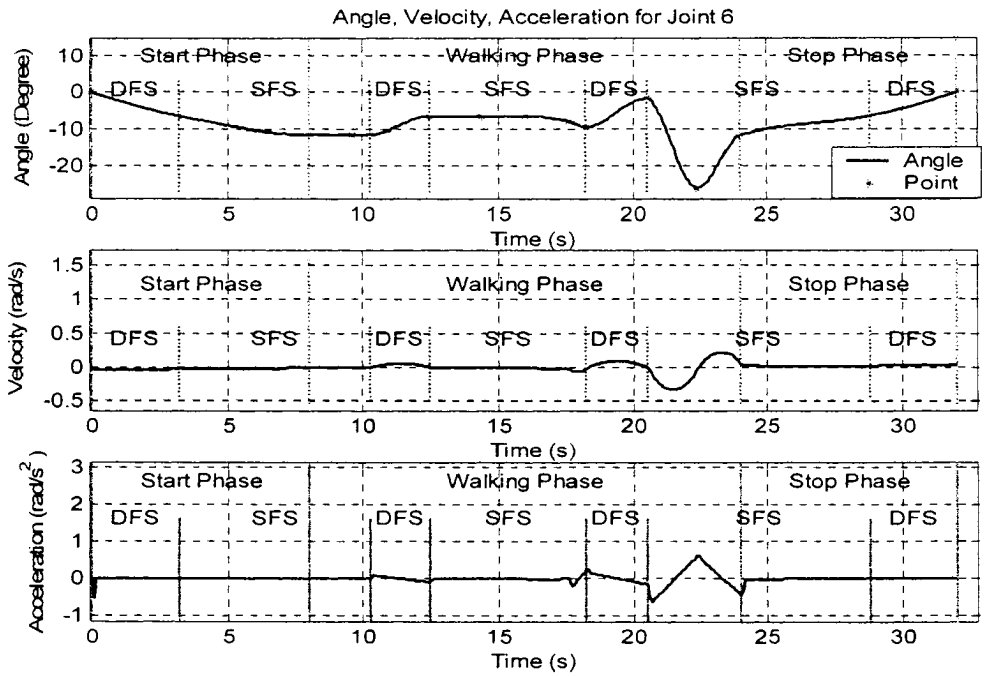

Figure 4-10 Angle, Velocity and Acceleration for Joint 6

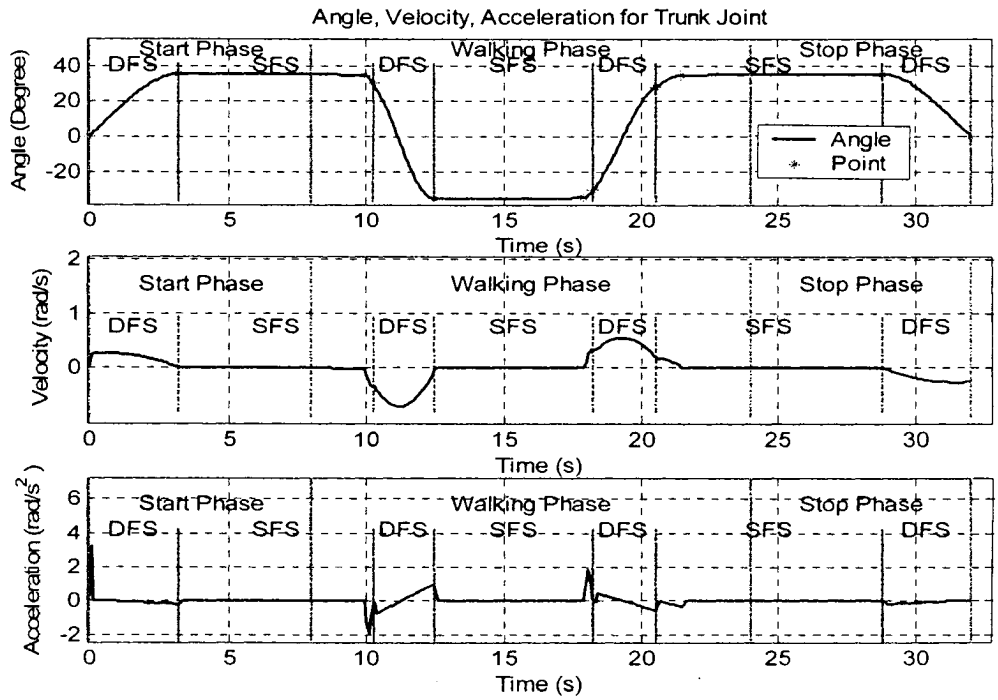

Figure 4-11 Angle, Velocity and Acceleration for Trunk Joint

Chapter 5 Simulation Results on Biped Kinematics and Dynamics

The dynamical characteristics (for single support phase) of the biped are simulated in this chapter. Some simulations are performed on the links' positions, velocities and accelerations based on the proposed walking trajectories. The simulation results provide references for the mechanical design of the biped. The robot's zero moment point is calculated as well, which provides guidance for the balance of the biped robot.

5.1 Parameters of the 7-DOF Biped

Moment of inertia: The moment of inertia of a point mass rotating about a known axis is defined by [27]:

$$I = mr^2 \quad \text{.....(5.1.1)}$$

where m is the mass and r is the perpendicular distance of the mass from the axis of rotation.

For a rigid body consisting of N point masses m_i with distances r_i to the rotation axis, the total moment of inertia equals to the sum of the point-mass moments of inertia.

$$I = \sum_{i=1}^{N} m_i r_i^2 \quad \text{.....(5.1.2)}$$

To simplify the robot link inertia calculation, the parts of the link can be considered as point masses. Then equation (5.1.2) can be used for this calculation. It should be noted that the inertia of the link calculated by (5.1.2) is smaller than the actual value. To accurately calculate the inertia of mass *i*, equation (5.1.3) will be

used.

$$I_i = I_{i\,Centroid} + m_i r_i^2 \qquad \text{.....(5.1.3)}$$

where $I_{i\,Centroid}$ is the inertia of mass *i* about the axis passing through the center of mass i and parallel to the rotation axis. m_i is its mass; r_i is the distance from its center of mass to the rotation axis.

For the link in Figure 5-1, the approximate moment of inertia can be calculated by

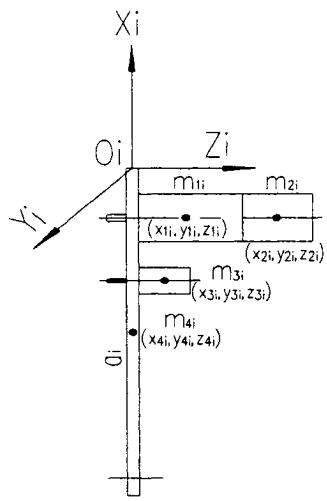

Figure 5-1 Link Structure

$$I_i \approx \sum_{k=1}^{4} m_{ki}\left((a_i + x_{ki})^2 + y_{ki}^2\right) \qquad \text{.....(5.1.4)}$$

Table 5-1 is the list of the biped robot parameters, including link D-H parameters, link masses, inertias and links' center of mass. The CoMs of links are expressed in the frame attached.

Table 5-1 Parameters for the Biped Robot

Simulation Joint Parameters Table (For Right Foot on Ground)							
Link	a_i (m)	d_i (m)	α_i (deg)	CoM in Frame i	$mass_i$ (kg)	Inertia I_i(kg.m^2)	A_i
1	0.185	0.014	0	[-1.67e-2 0 -3.61e-2]	0.481	1.36E-02	A_1
2	0.2	0.014	0	[-1.90e-2 0 -3.56e-2]	0.487	1.60E-02	A_2
3	0	0.114	0	[-2.27e-2 -3.75e-2 -5.28e-2]	0.97	1.90E-03	A_3
4	0.2	0.014	0	[-1.81e-1 0 3.56e-2]	0.487	1.77E-04	A_4
5	0.185	0.014	0	[-1.68e-1 0 3.61e-2]	0.481	1.34E-04	A_5
6	0.035	0.014	0	[-2.34e-2 -2.03e-2 3.63e-2]	0.612	3.00E-04	A_6
T	0.08	0.064	90	[-5.84e-2 -3.1e-3 -4.86e-2]	0.97	2.70E-03	A_T
T1	0.3	-0.014	0	[-7.00e-2 0 -3.36e-2]	2.046	1.08E-01	A_{T1}
Robot base joint: Jiont 0, Coordinates(X0, Y0, Z0)							
Simulation Joint Parameters Table (For Left Foot on Ground)							
Link	a_i' (m)	d_i' (m)	α_i' (deg)	CoM in Frame i'	$mass_i'$ (kg)	Inertia I_i' (kg.m^2)	A_i'
1'	0.185	-0.014	0	[-1.67e-2 0 3.61e-2]	0.481	1.36E-02	A_1'
2'	0.2	-0.014	0	[-1.90e-2 0 3.56e-2]	0.487	1.60E-02	A_2'
3'	0	-0.114	0	[-2.27e-2 -3.75e-2 4.88e-2]	0.97	1.90E-03	A_3'
4'	0.2	-0.014	0	[-1.81e-1 0 -3.56e-2]	0.487	1.77E-04	A_4'
5'	0.185	-0.014	0	[-1.68e-1 0 -3.61e-2]	0.481	1.34E-04	A_5'
6'	0.035	-0.014	0	[-2.34e-2 -2.03e-2 2.04e-2]	0.612	3.00E-04	A_6'
T'	0.08	-0.064	90	[-5.84e-2 -3.1e-3 -4.86e-2]	0.97	2.70E-03	A_T'
T1'	0.3	-0.014	0	[-7.00e-2 0 -3.36e-2]	2.046	1.08E-01	A_{T1}'
Robot base joint: Jiont 0', Coordinates(X0', Y0', Z0')							

5.2 Simulation Results of Position, Velocity and Acceleration of CoM of Links

In figures 5-2 to 5-29, words "DFS" and "SFS" denote "Double Foot Support" and "Single Foot Support", respectively. The walking period is 16 seconds, and the start period and stop period are 8 seconds. The position, velocity and acceleration of the CoM of links are expressed in the reference frame.

The positions of the CoM of links expressed in the reference frame are calculated by forward kinematics equations (5.1.5) and (5.1.6).

$$P_r^{ci} = T_r^i P_i^{ci} = T_r^0 A_1 A_2 \cdots A_{i-1} A_i P_i^{ci} \quad i \le n \qquad \text{(5.1.5)}$$

for the right foot on the ground, and

$$P_r^{ci'} = T_r^{i'} P_{i'}^{ci'} = T_r^{0'} A_{1'} A_{2'} \cdots A_{i-1'} A_{i'} P_{i'}^{ci'} \quad i' \le n \qquad \text{(5.1.6)}$$

for the left foot on the ground, where $P_r^{ci} \in \Re^{4\times 1}$ and $P_r^{ci'} \in \Re^{4\times 1}$ are the augmented vector for the coordinates of CoM of links i and i' expressed in the reference frame, respectively. T_r^i and $T_r^{i'}$ are the homogeneous transformation matrices from frames i and i' to the reference frame, respectively. $P_i^{ci} \in \Re^{4\times 1}$ and $P_{i'}^{ci'} \in \Re^{4\times 1}$ are the augmented vectors for the coordinates of CoM of links i and i' expressed in frames i and i', respectively.

The velocities of the CoM of links expressed in reference frame are calculated by velocity Jacobians with equation (5.1.7) and (5.1.8).

$$\begin{bmatrix} \mathbf{v}_r^i \\ \omega_r^i \end{bmatrix} = \begin{bmatrix} R_r^0 & \mathbf{0} \\ \mathbf{0} & R_r^0 \end{bmatrix} J_0^i [\dot{q}_1, \dot{q}_2, \cdots, \dot{q}_i]^T \quad i \le n \qquad \text{(5.1.7)}$$

for the right foot on the ground, and

$$\begin{bmatrix} \mathbf{v}_r^{i'} \\ \omega_r^{i'} \end{bmatrix} = \begin{bmatrix} R_r^{0'} & \mathbf{0} \\ \mathbf{0} & R_r^{0'} \end{bmatrix} J_{0'}^{i'} [\dot{q}_{1'}, \dot{q}_{2'}, \cdots, \dot{q}_{i'}]^T \quad i' \le n \qquad \text{(5.1.8)}$$

for the left foot on the ground, where $\begin{bmatrix} \mathbf{v}_r^i \\ \omega_r^i \end{bmatrix}$ and $\begin{bmatrix} \mathbf{v}_r^{i'} \\ \omega_r^{i'} \end{bmatrix}$ are the velocity vectors for the coordinates of CoM of links i and i' expressed in the reference frame, respectively. R_r^0 and $R_r^{0'}$ are rotation matrices from frames 0 and 0' to the reference frame, respectively. J_0^i and $J_{0'}^{i'}$ are the velocity Jocobians for the coordinates of CoM of links i and i' expressed in frames 0 and 0', respectively.

The acceleration of the CoM of links is obtained from equations (5.1.9) and (5.1.10).

$$\begin{bmatrix} \mathbf{a}_r^i \\ \alpha_r^i \end{bmatrix} = \begin{bmatrix} R_r^0 & \mathbf{0} \\ \mathbf{0} & R_r^0 \end{bmatrix} \left[J_0^i [\ddot{q}_1, \ddot{q}_2, \cdots, \ddot{q}_i]^T + \dot{J}_0^i [\dot{q}_1, \dot{q}_2, \cdots, \dot{q}_i]^T \right] \quad i \le n \quad \text{.....(5.1.9)}$$

for the right foot on the ground, and

$$\begin{bmatrix} \mathbf{a}_r^{i'} \\ \alpha_r^{i'} \end{bmatrix} = \begin{bmatrix} R_r^{0'} & \mathbf{0} \\ \mathbf{0} & R_r^{0'} \end{bmatrix} \left[J_{0'}^{i'} [\ddot{q}_{1'}, \ddot{q}_{2'}, \cdots, \ddot{q}_{i'}]^T + \dot{J}_{0'}^{i'} [\dot{q}_{1'}, \dot{q}_{2'}, \cdots, \dot{q}_{i'}]^T \right] \quad i' \le n \quad \text{.....(5.1.10)}$$

for the left foot on the ground, where $\begin{bmatrix} \mathbf{a}_r^i \\ \alpha_r^i \end{bmatrix}$ **and** $\begin{bmatrix} \mathbf{a}_r^{i'} \\ \alpha_r^{i'} \end{bmatrix}$ **are the acceleration vectors for the coordinates of CoM of links i and i' expressed in the reference frame, respectively.** $\dot{J}_0^i$ **and** $\dot{J}_{0'}^{i'}$ **are derivatives of velocity Jocobians with respect to joint angles, for the coordinates of CoM of links i and i', respectively.**

For simplicity, the frame of the support foot is chosen as the base frame. In the first double foot support (DFS) phase and first single foot support (SFS) phase, the right ankle frame is used as the base frame and the origin of this frame is chosen as (0, 0, 0). For the second DFS, the second SFS phase and the third DFS phase, the left ankle frame is chosen as the base frame and the origin of this frame is set to (step-length, waist-width, 0). In the last SFS and the last DFS, the right ankle frame is considered as the base frame and the origin of this frame is (2step-length, 0, 0).

Simulation results shown in Figure 5-2 to Figure 5-22 provide the displacements, velocities and accelerations for the CoM of each link of the biped. These results are mainly used to calculate the ZMP. It can be observed that the trajectory for link 1 is similar to the trajectory for link 5 during the walking phase. The same goes to link 2 and link 4. Notice that the y-coordinates for links 1-6 do not change because the mechanical structure of the biped legs can only move in the x-z plane , however the y-coordinate for the trunk shifts from side to side to prevent the biped from sliding down. The simulation results for the linear and angular acceleration are not smooth because the joint angle trajectory is generated with the cubic interpolation method, the second derivative of the cubic interpolation function is not smooth.

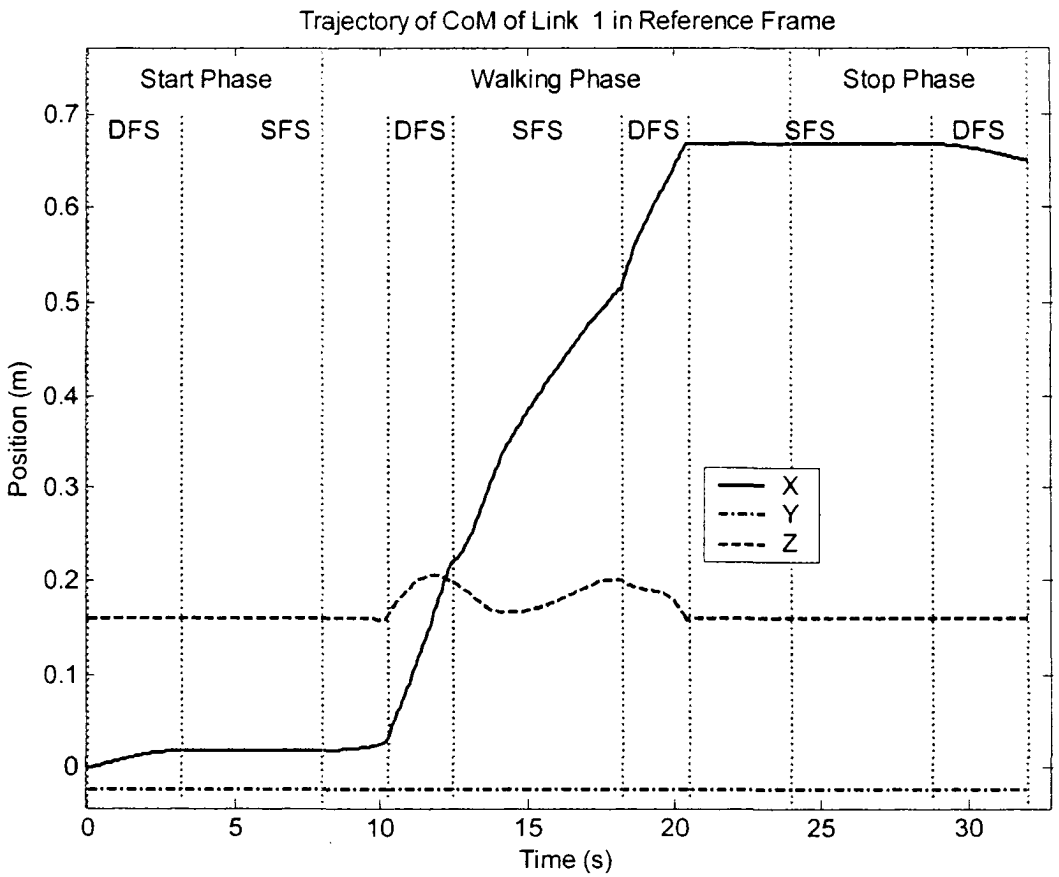

Figure 5-2 Trajectory of CoM of Link 1 in Reference Frame

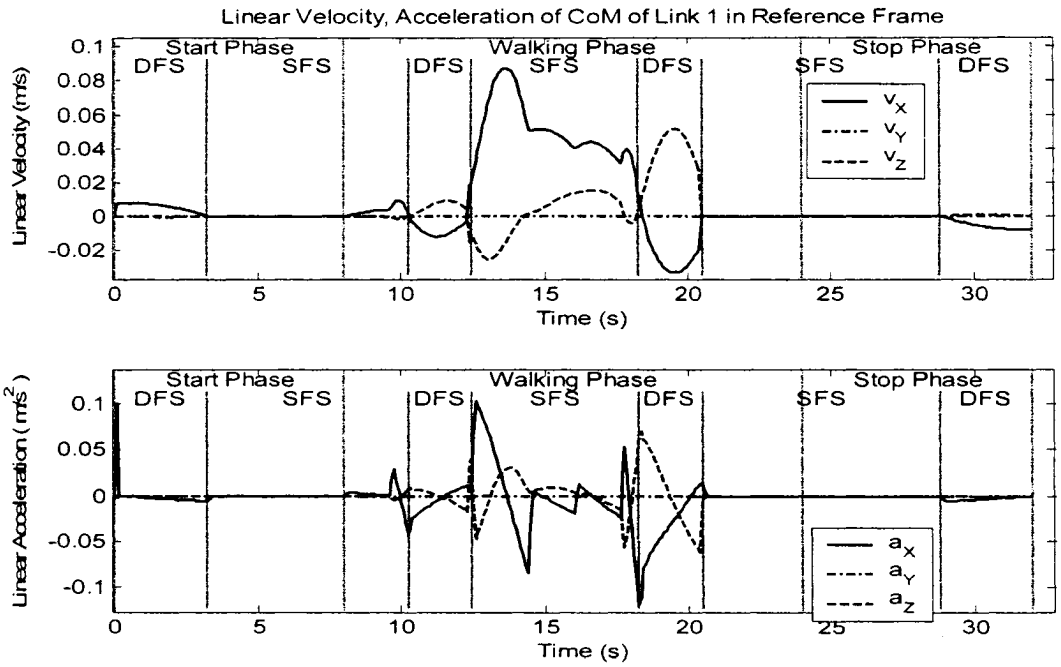

Figure 5-3 Linear Velocity and Acceleration of CoM of Link 1 in Reference Frame

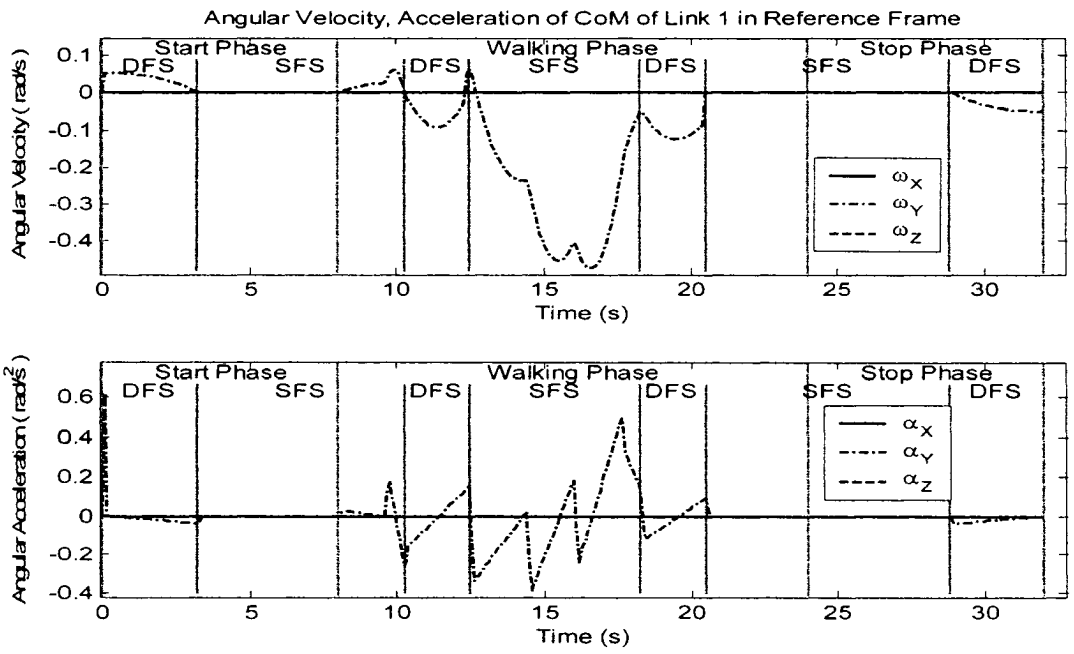

Figure 5-4 Angular Velocity and Acceleration of CoM of Link 1 in Reference Frame

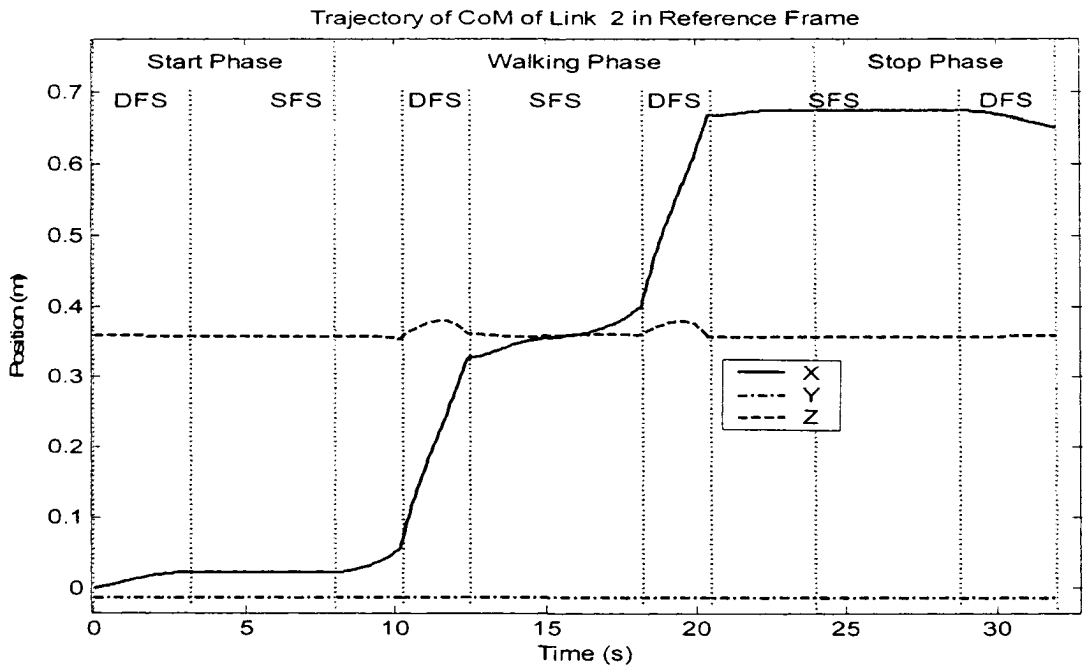

Figure 5-5 Trajectory of CoM of Link 2 in Reference Frame

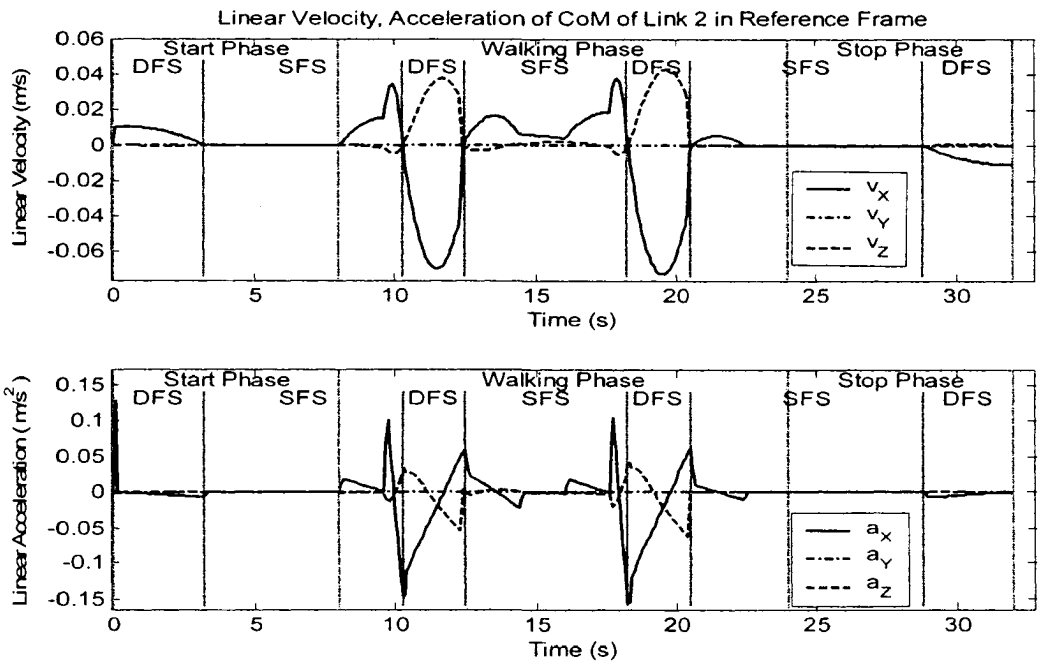

Figure 5-6 Linear Velocity and Acceleration of CoM of Link 2 in Reference Frame

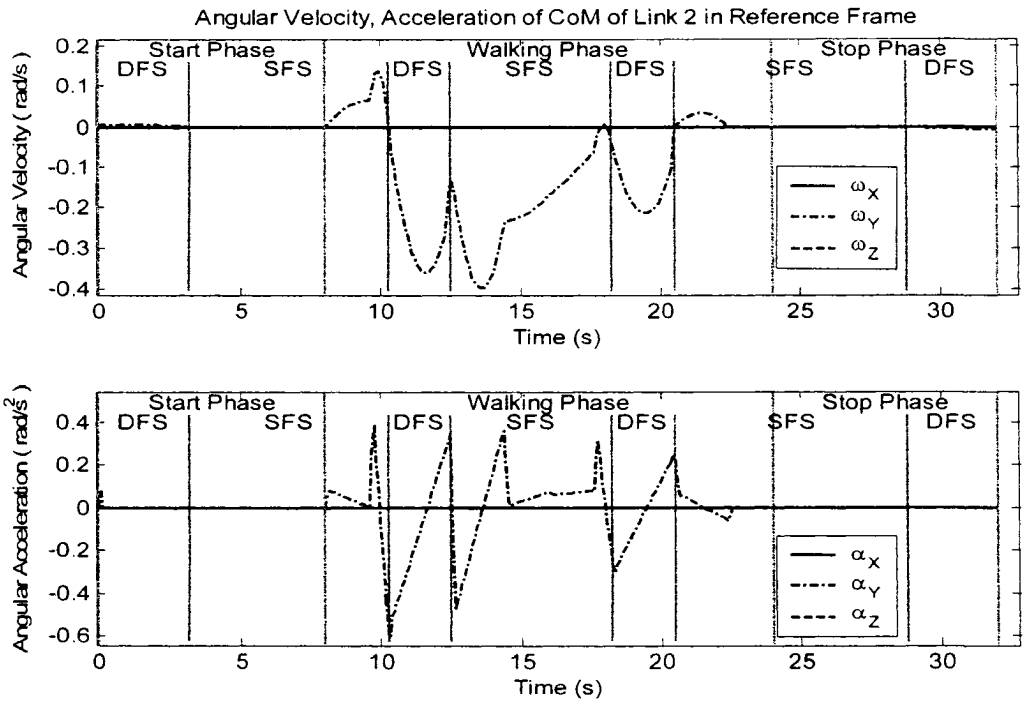

Figure 5-7 Angular Velocity and Acceleration of CoM of Link 2 in Reference Frame

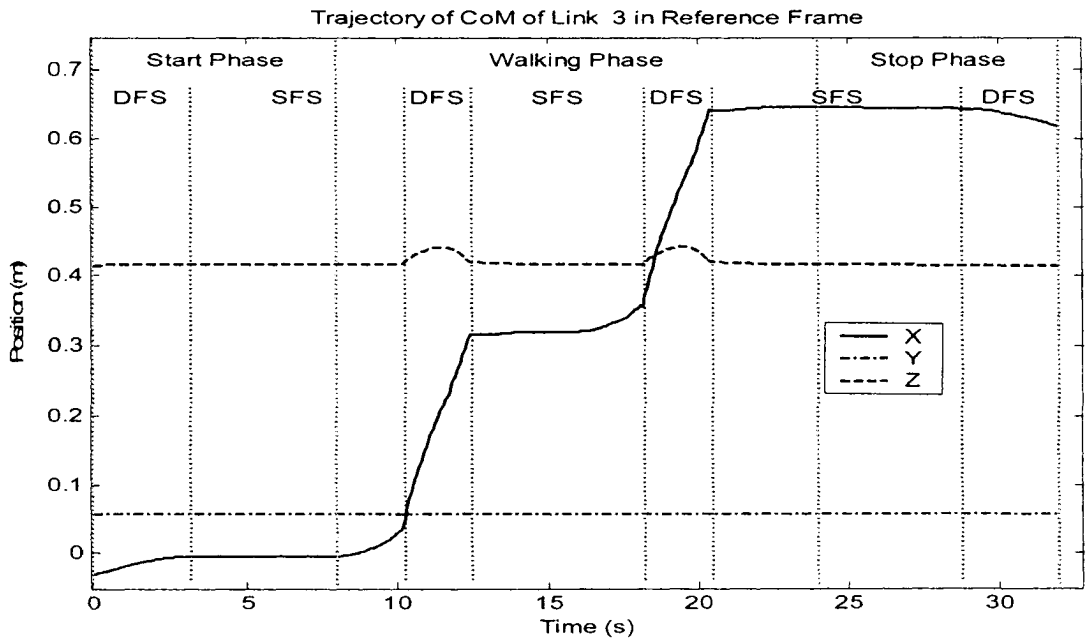

Figure 5-8 Trajectory of CoM of Link 3 in Reference Frame

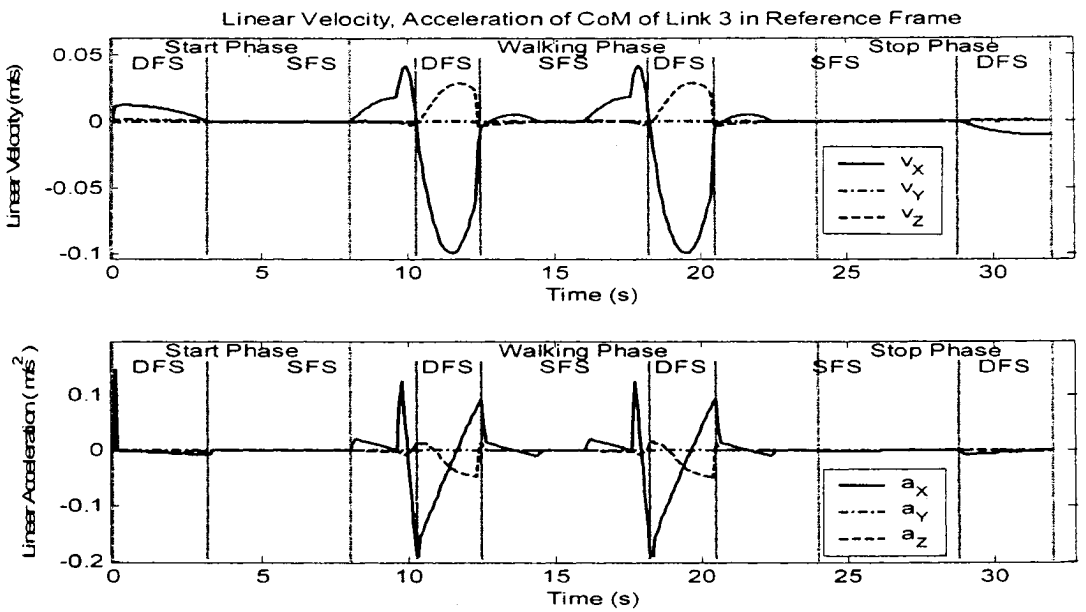

Figure 5-9 Linear Velocity and Acceleration of CoM of Link 3 in Reference Frame

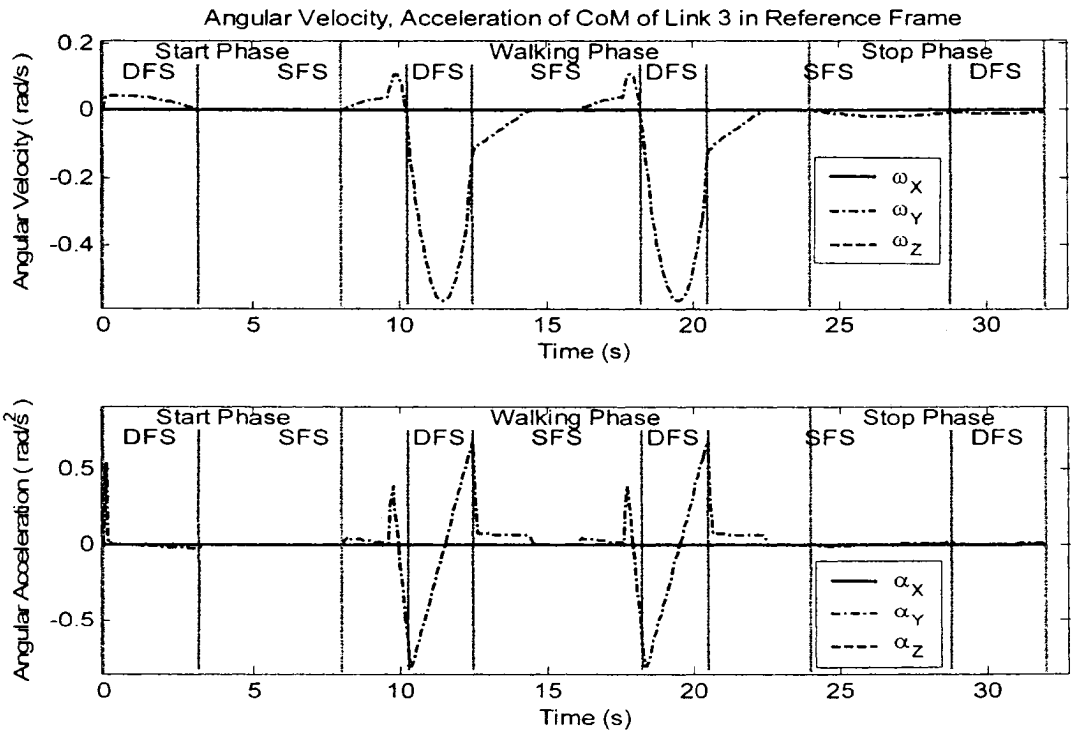

Figure 5-10 Angular Velocity and Acceleration of CoM of Link 3 in Reference Frame

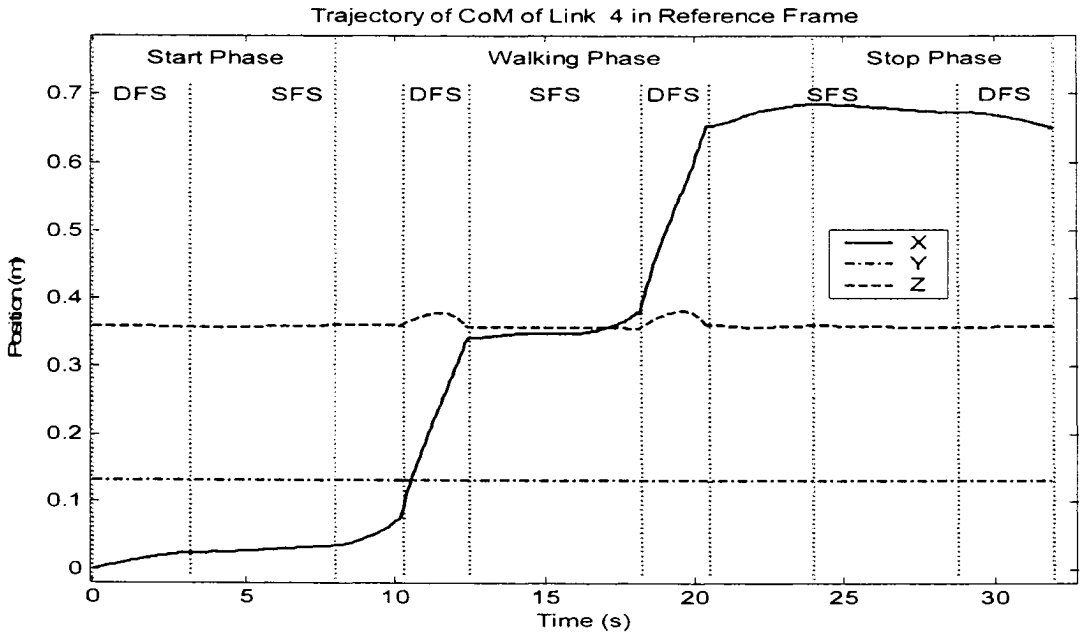

Figure 5-11 Trajectory of CoM of Link 4 in Reference Frame

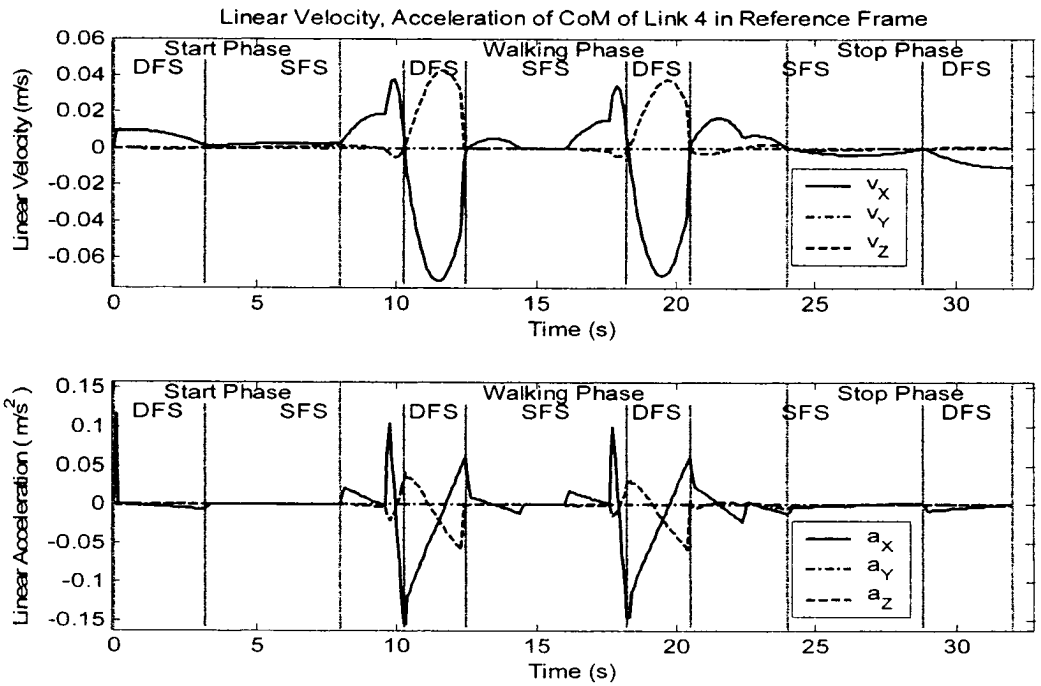

Figure 5-12 Linear Velocity and Acceleration of CoM of Link 4 in Reference Frame

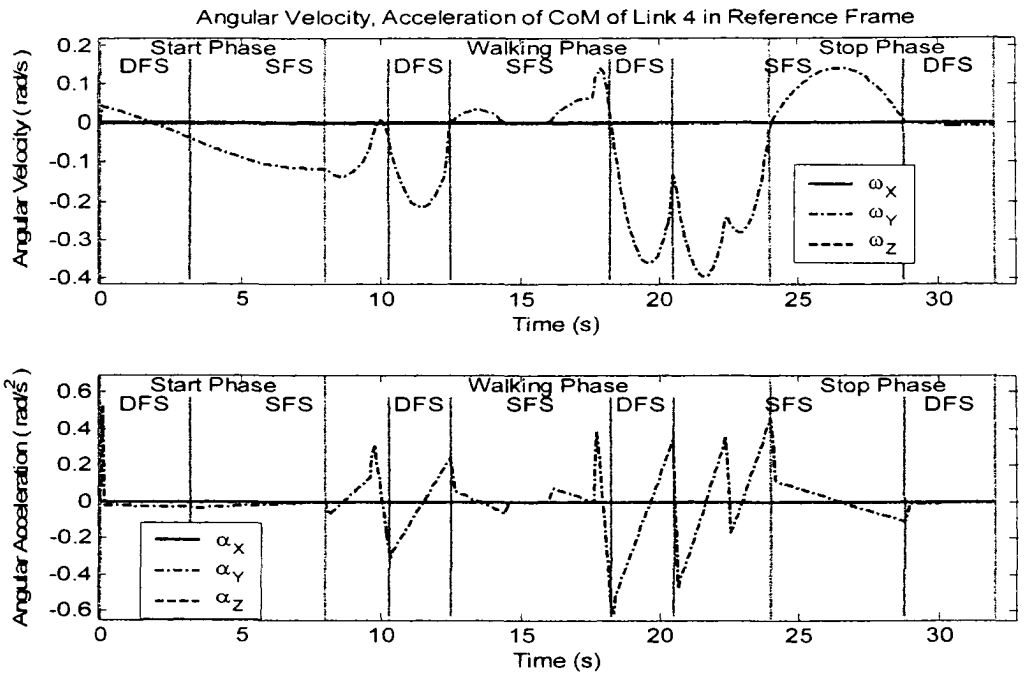

Figure 5-13 Angular Velocity and Acceleration of CoM of Link 4 in Reference Frame

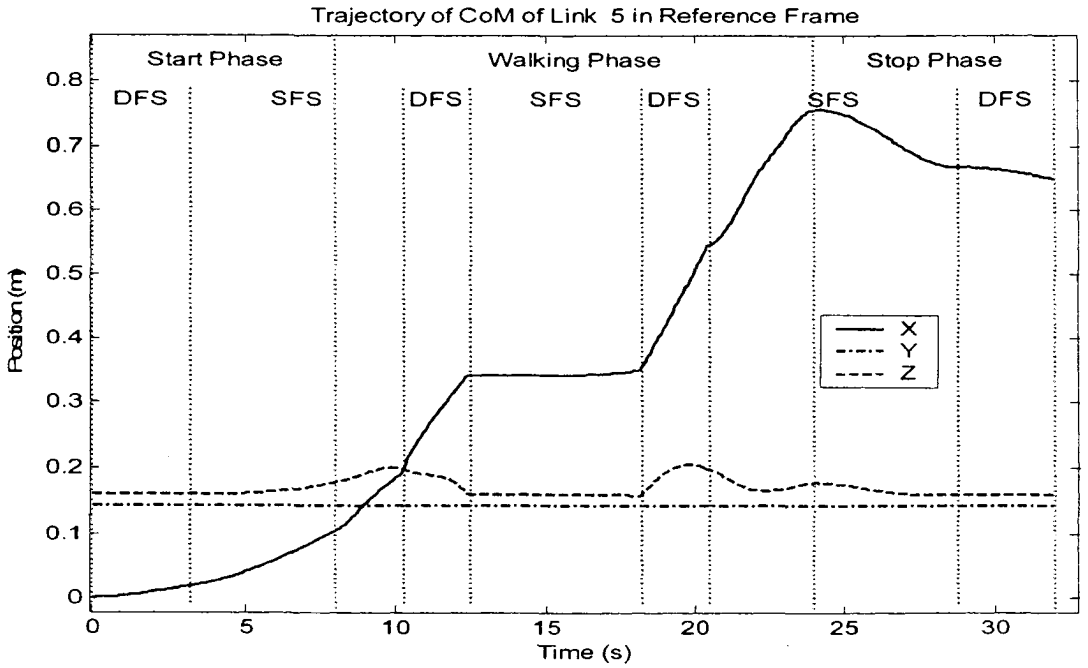

Figure 5-14 Trajectory of CoM of Link 5 in Reference Frame

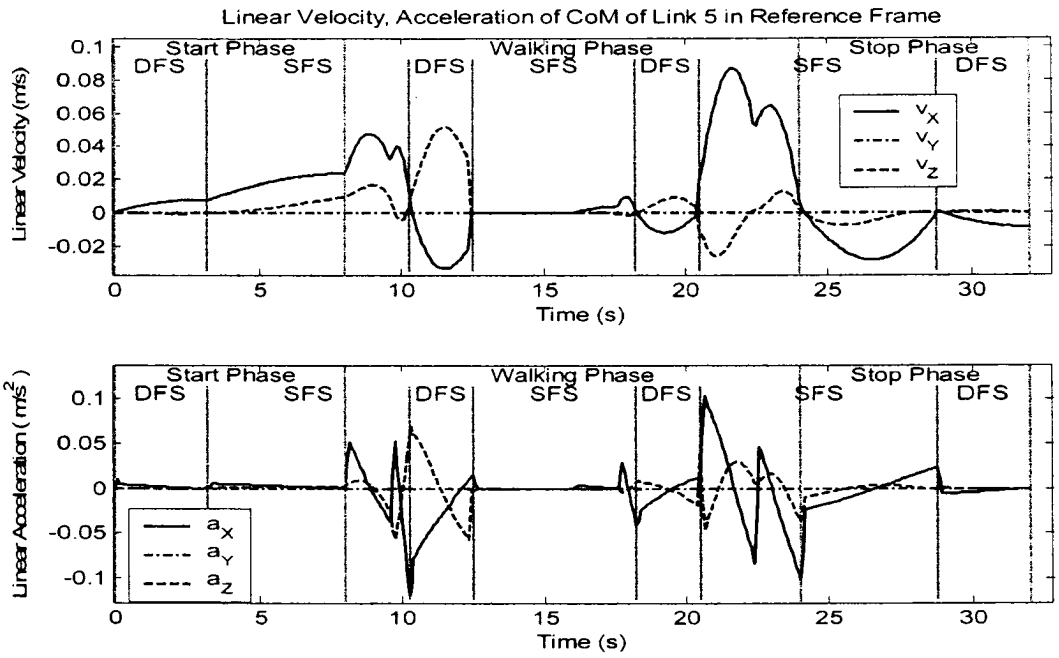

Figure 5-15 Linear Velocity and Acceleration of CoM of Link 5 in Reference Frame

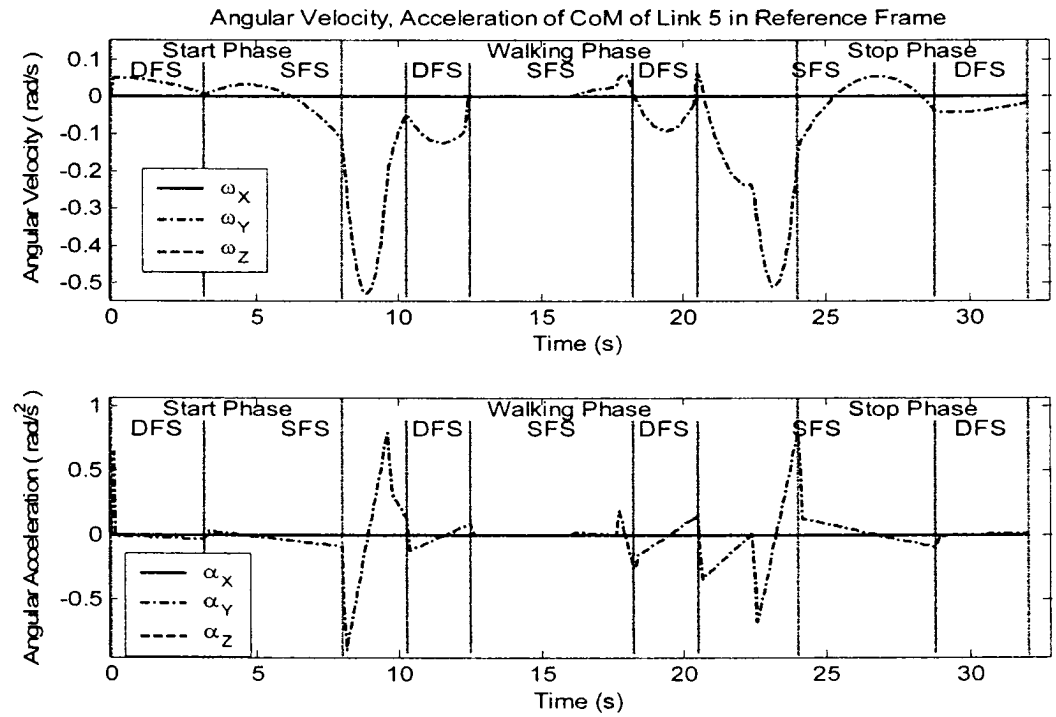

Figure 5-16 Angular Velocity and Acceleration of CoM of Link 5 in Reference Frame

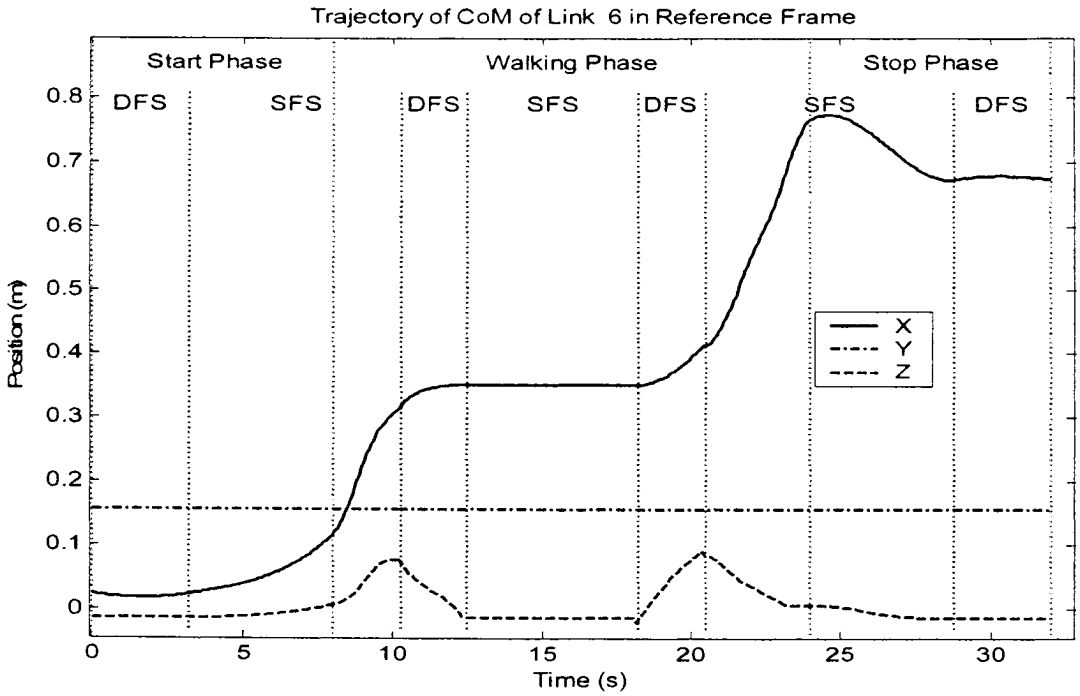

Figure 5-17 Trajectory of CoM of Link 6 in Reference Frame

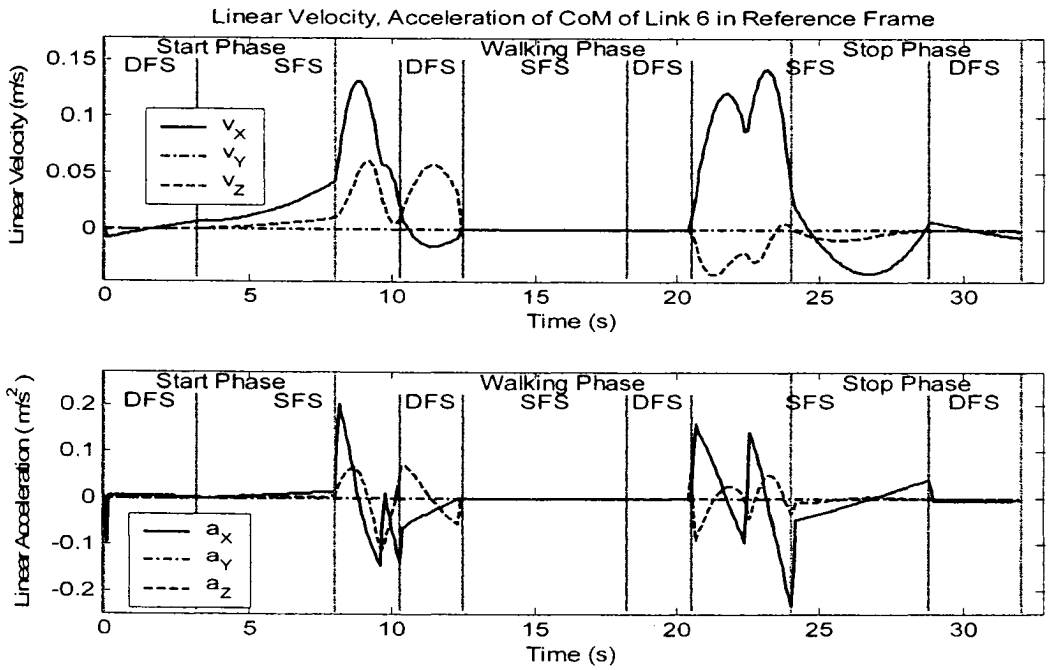

Figure 5-18 Linear Velocity and Acceleration of CoM of Link 6 in Reference Frame

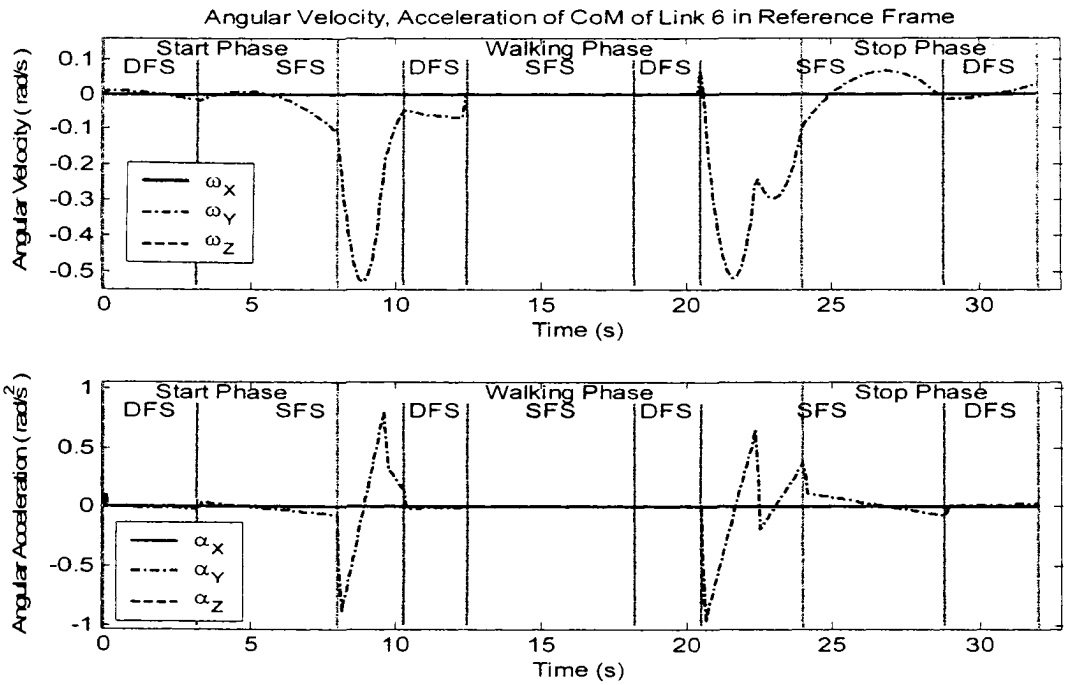

Figure 5-19 Angular Velocity and Acceleration of CoM of Link 6 in Reference Frame

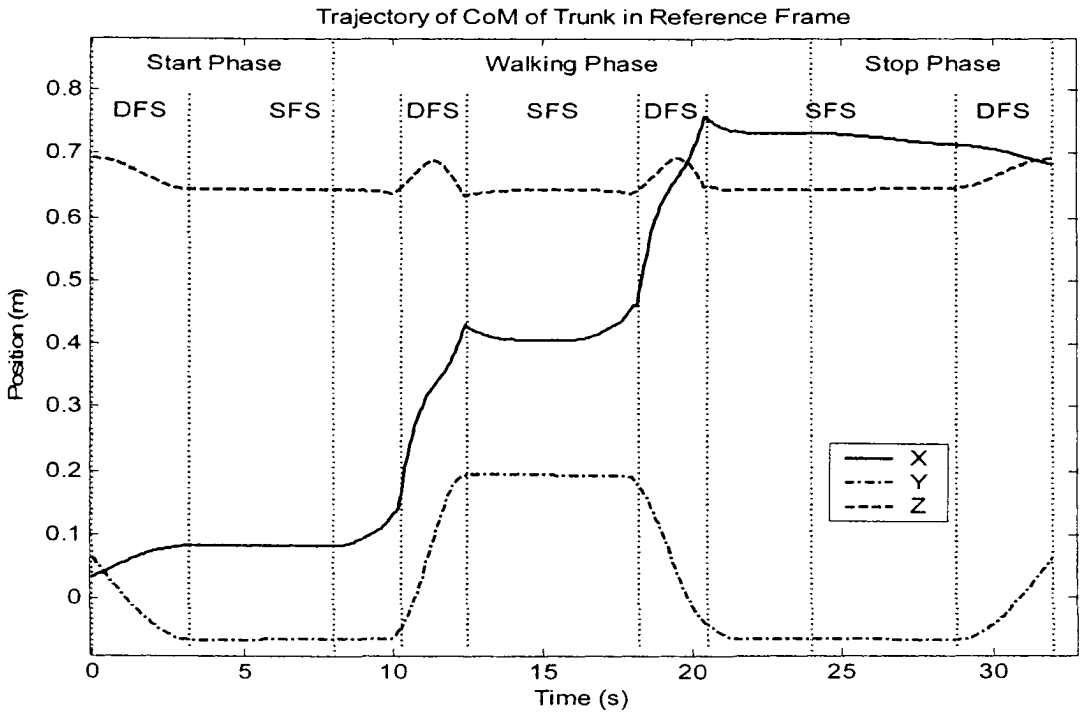

Figure 5-20 Trajectory of CoM of Trunk in Reference Frame

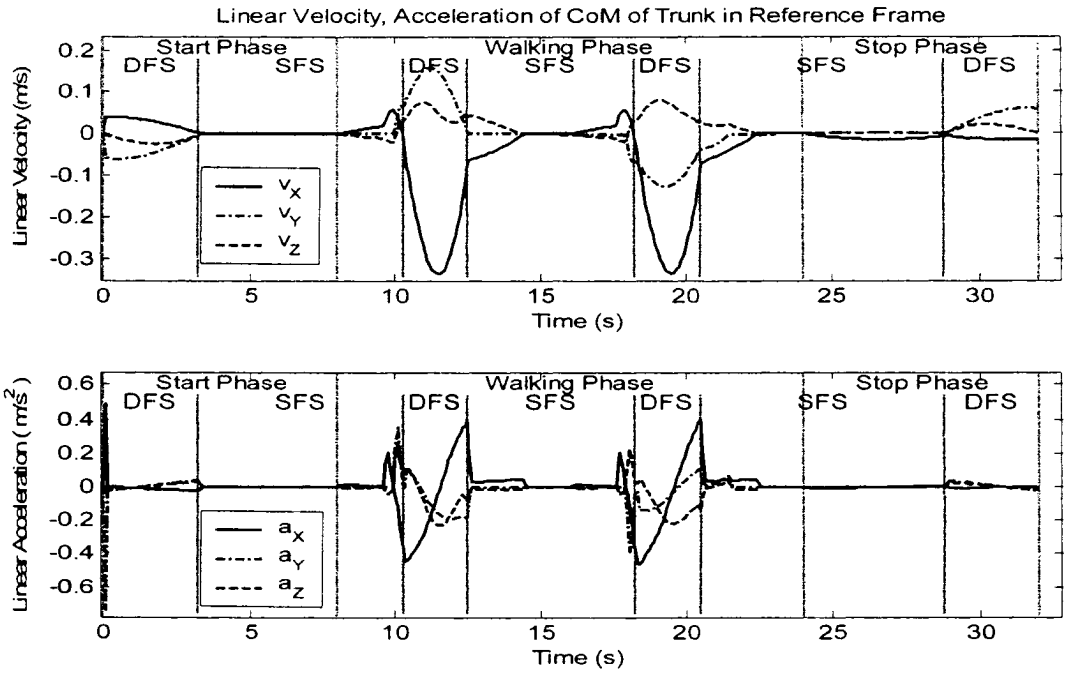

Figure 5-21 Linear Velocity and Acceleration of CoM of Trunk in Reference Frame

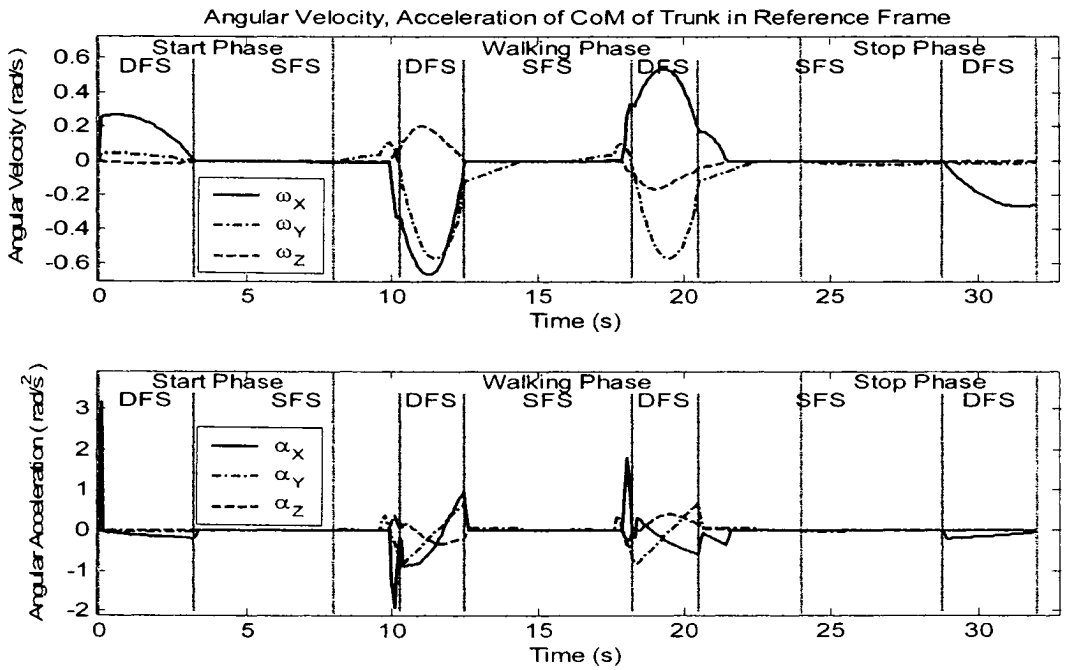

Figure 5-22 Angular Velocity and Acceleration of CoM of Trunk in Reference Frame

5.3 Simulation Results of Joint Torque and Power

In order to investigate the mechanical requirements for each joint, the simulation on the joint torque and power is carried on in this section. But the torque and power in double support phase are not calculated in this research due to unfinished dynamic modeling in this phase.

The joint torque is calculated by dynamic motion equations (3.2.5).

$$\sum_{j=1}^{n} d_{kj}(\mathbf{q})\ddot{q}_j + \sum_{i=1}^{n}\left(\sum_{j=1}^{n} c_{ijk}(\mathbf{q})\dot{q}_j\right)\dot{q}_i + \phi_k(\mathbf{q}) = \tau_k, \qquad k = 1,\cdots,n \quad \text{.....(3.2.5)}$$

The joint power can be calculated with equation (5.3.1)

$$P = \omega\tau \quad \text{.....(5.3.1)}$$

where the unit for P is Watt, the unit for ω is rad/s, and the unit for τ is N.m.

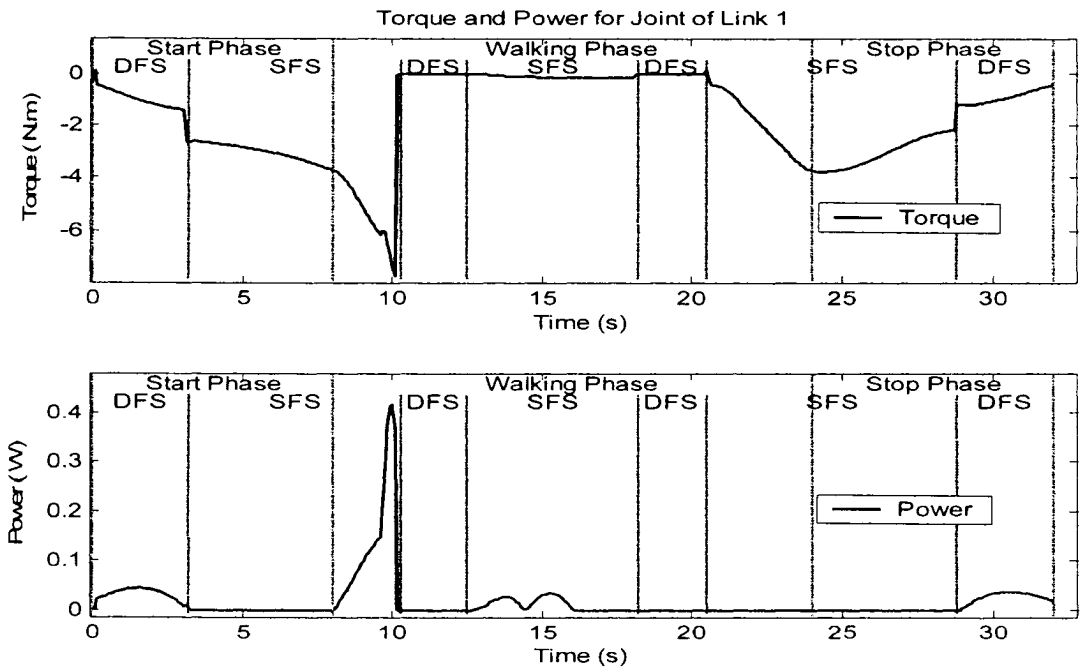

Figure 5-23 Torque and Power for Joint of Link 1

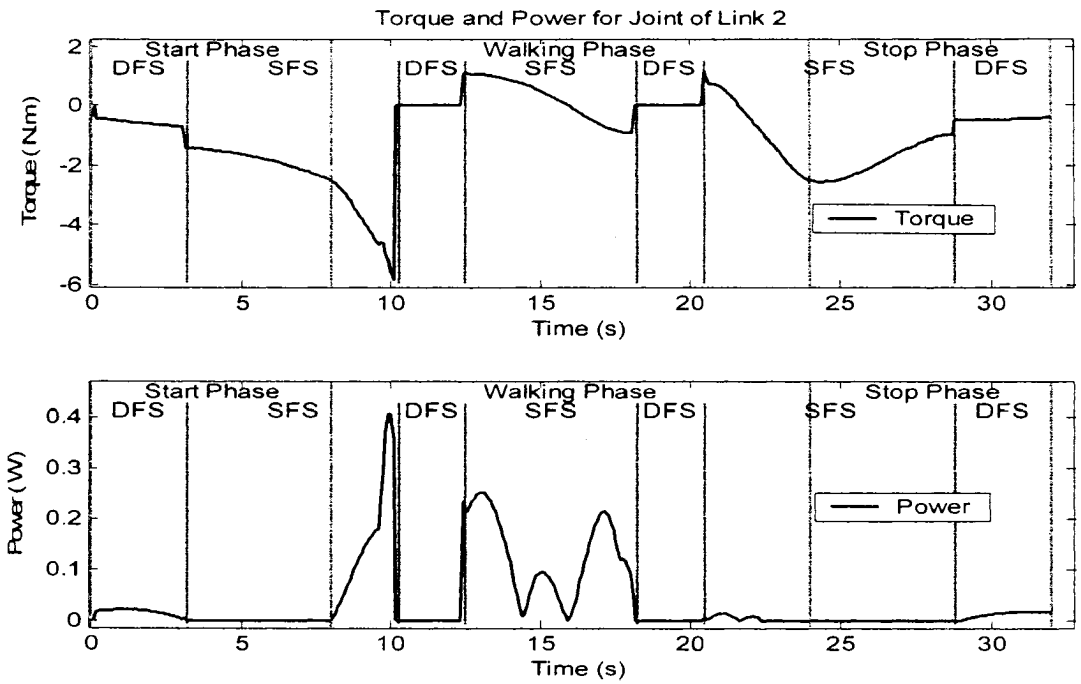

Figure 5-24 Torque and Power for Joint of Link 2

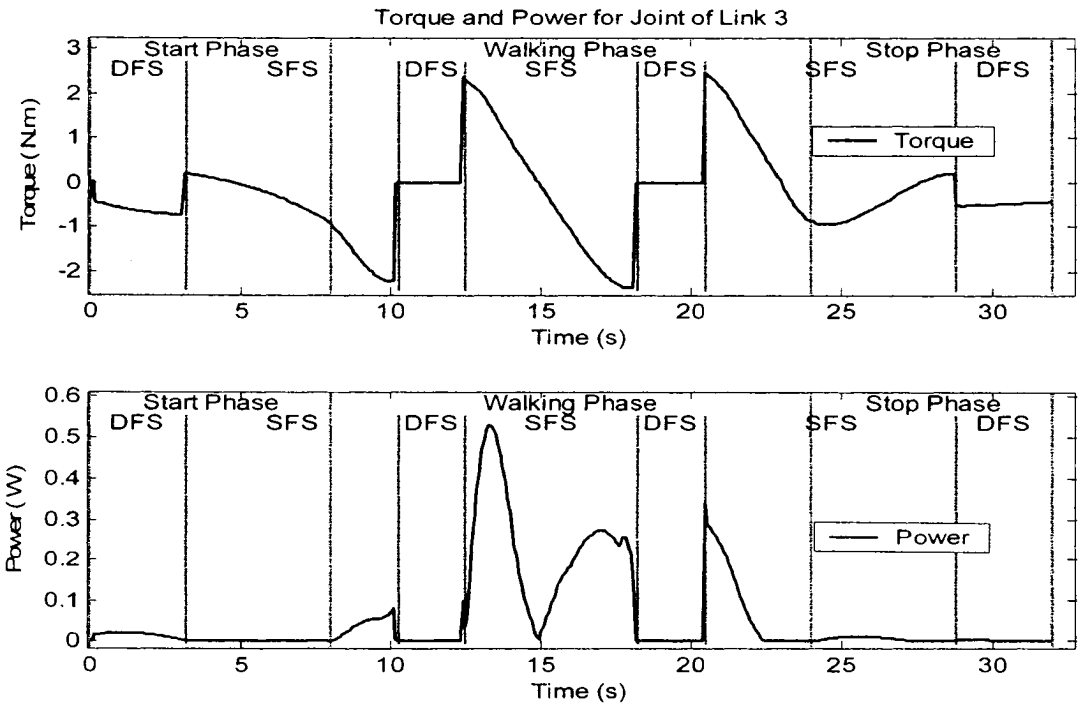

Figure 5-25 Torque and Power for Joint of Link 3

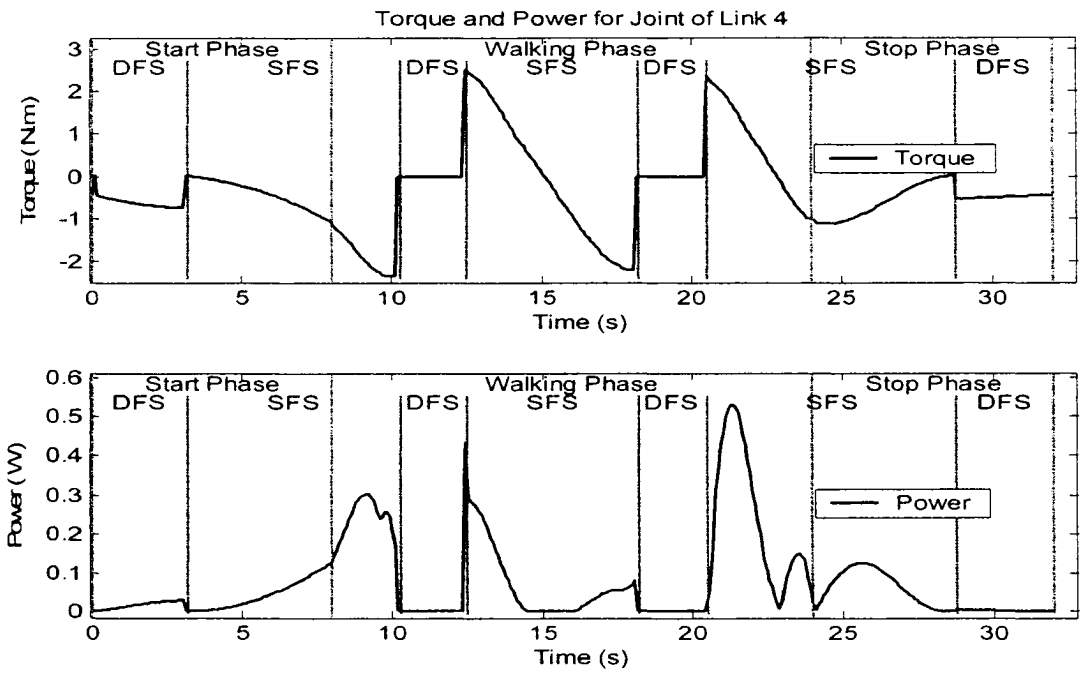

Figure 5-26 Torque and Power for Joint of Link 4

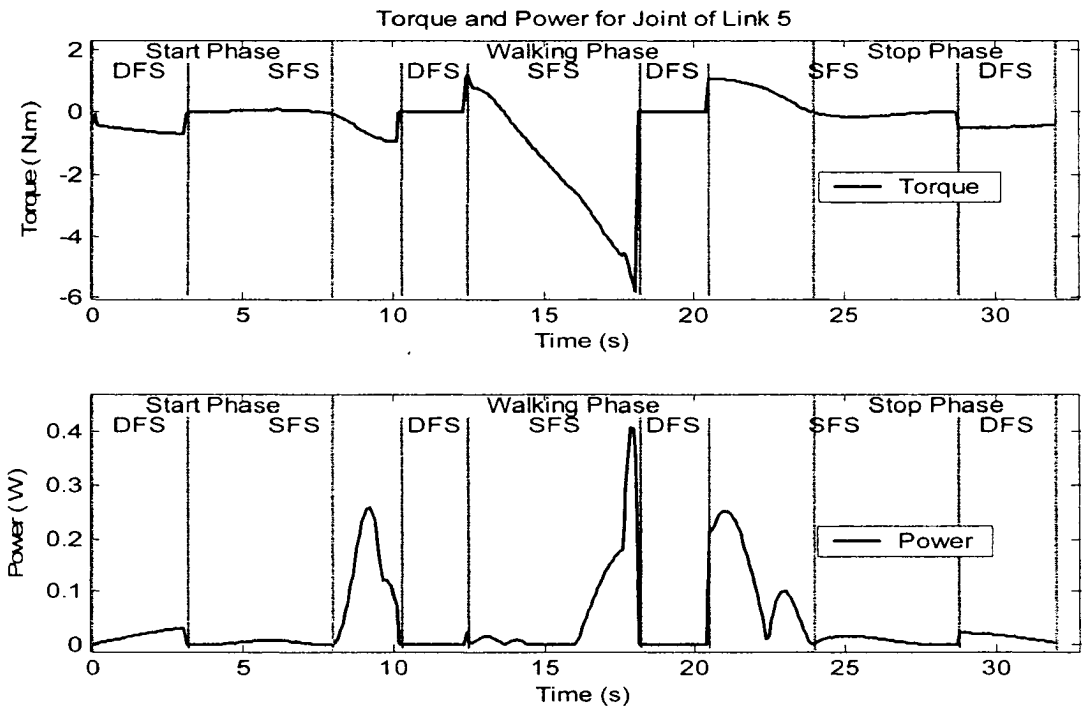

Figure 5-27 Torque and Power for Joint of Link 5

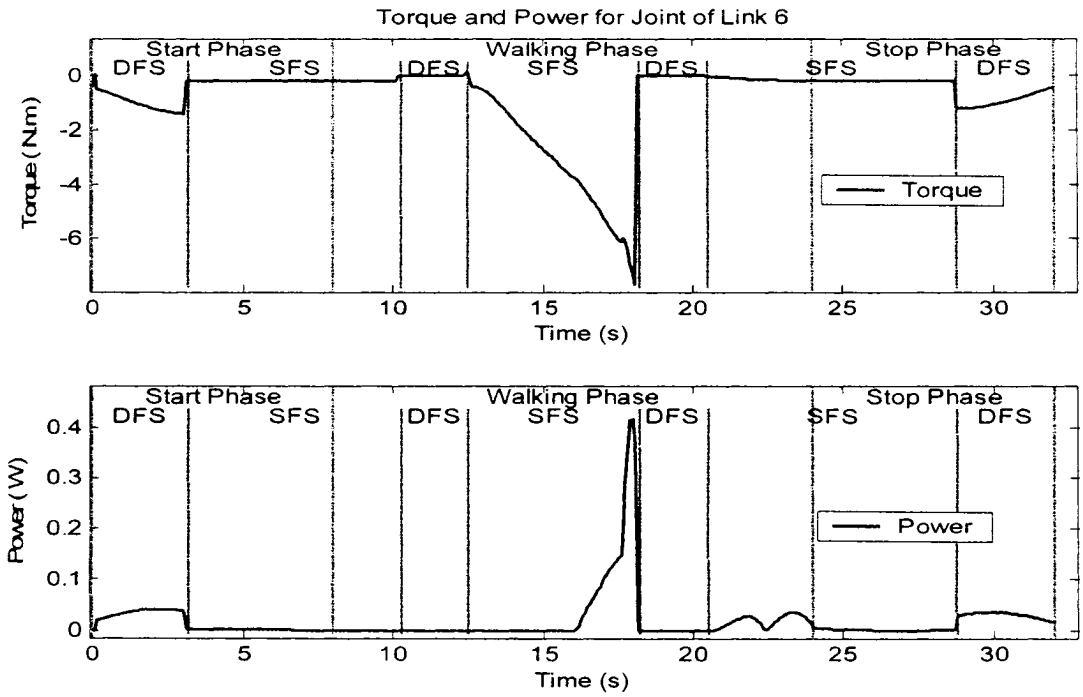

Figure 5-28 Torque and Power for Joint of Link 6

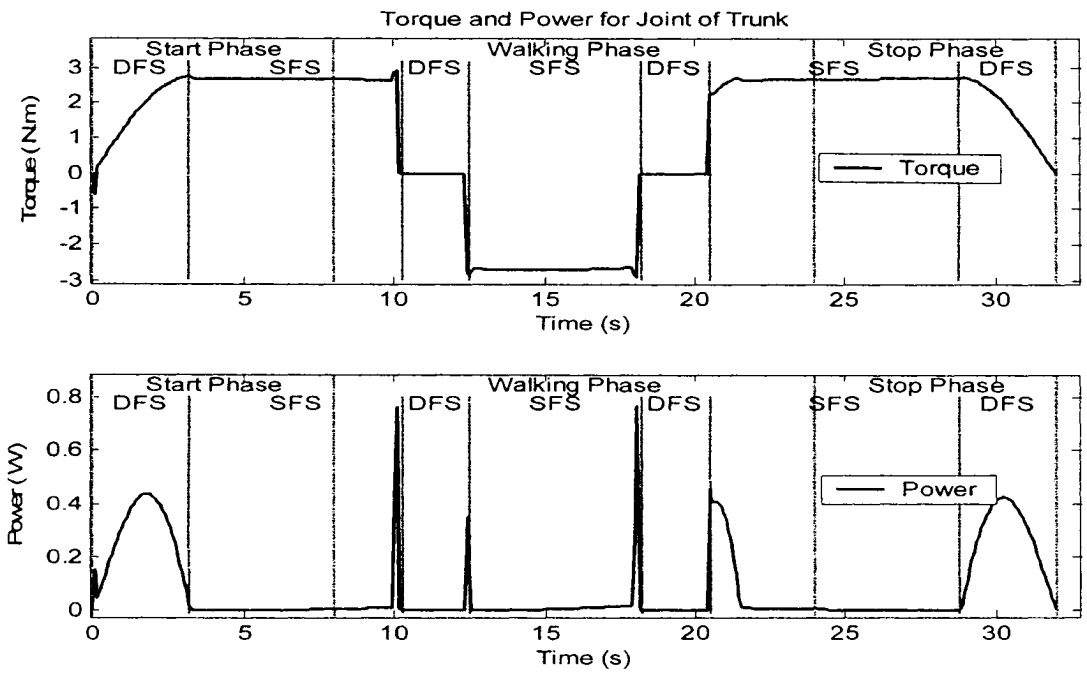

Figure 5-29 Torque and Power for Joint of Trunk

The simulation results show that torque for joint 1 to joint 6 reached the maximum values at the intersections between the DFS phase and the SFS phase. The trunk joint requires bigger torque in the single foot support phase than the double support phase. The torque for the ankle joint of the support leg requires the biggest torque among all 7 joints, about 8 N.m. The driven power for each joint varies in the walking period, and the value of the power reaches the maximum value close to the intersections between the DFS phase and the SFS phase. The trunk joint requires the biggest power about 0.8 Watts in this simulation. These simulation results of torque and power for each joint provide a guidance to choose proper link material and joint driven motor.

5.4 Simulation Results of ZMP and CoM

The simulation results are based on walking period equal to 16 seconds, the start and stop period equal to 8 seconds.

The ZMP is calculated with equations simplified from (3.4.1) and (3.4.2) by eliminating the angular acceleration part, as shown in (5.4.1) and (5.4.2).

$$x_{ZMP} = \frac{\sum_{i=1}^{n} m_i(\ddot{z}_i - g)x_i - \sum_{i=1}^{n} m_i \ddot{x}_i z_i}{\sum_{i=1}^{n} m_i(\ddot{z}_i - g)} \quad \text{.....(5.4.1)}$$

$$y_{ZMP} = \frac{\sum_{i=1}^{n} m_i(\ddot{z}_i - g)y_i - \sum_{i=1}^{n} m_i \ddot{y}_i z_i}{\sum_{i=1}^{n} m_i(\ddot{z}_i - g)} \quad \text{.....(5.4.2)}$$

The CoM is calculated with equations (5.4.3) and (5.4.4).

$$x_{CoM} = \frac{\sum_{i=1}^{n} m_i x_i}{\sum_{i=1}^{n} m_i} \quad \text{.....(5.4.3)}$$

$$y_{CoM} = \frac{\sum_{i=1}^{n} m_i y_i}{\sum_{i=1}^{n} m_i} \quad \text{.....(5.4.4)}$$

where m_i is the mass of link i . g is the gravitational acceleration, and (x_{ZMP}, y_{ZMP}, 0)

are the ZMP coordinates expressed in the reference frame. (x_i, y_i, z_i) are the coordinates of the center of mass of link i expressed in the reference frame.

Figure 5-30 shows the ZMP and CoM of the biped robot based on the proposed trajectory. In the figure, the closed area plotted with dash dot line is the stable region. Simulation results show the ZMP and CoM are very close with the proposed trajectory, which implies that the planning walking trajectory by placing the CoM of the biped within the stable region is acceptable if the acceleration of the robot is not big. The simulation results also indicate that the ZMP with the proposed trajectory is in the stable region during the whole walking period.

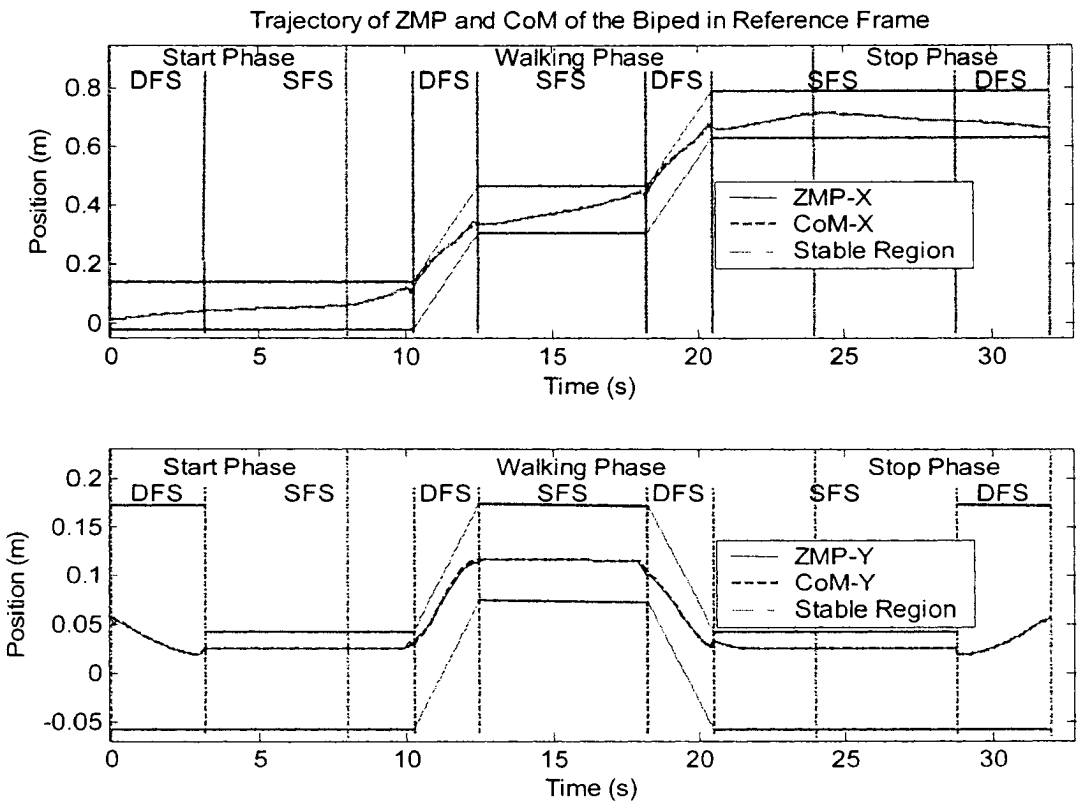

Figure 5-30 Zero Moment Point in Walking

Chapter 6 PID Control of the Single Joint

6.1 Setpoint Sampling Methods in Trajectory Tracking

In order to minimize both hardware and software consumption, it is necessary to choose proper sampling method and sampling rate for trajectory tracking control with acceptable tracking errors. In this section, the study is based on DC motor sinusoidal curve position tracking.

If f(t) is the continuous function of the trajectory, then the sampled function of this trajectory F(t) can be generated in 3 different ways.

$$F(t) = f(floor(t/Ts) \times Ts) \quad \text{.....(6.1.1)}$$

$$F(t) = f(ceil(t/Ts) \times Ts) \quad \text{.....(6.1.2)}$$

$$F(t) = f(round(t/Ts) \times Ts) \quad \text{.....(6.1.3)}$$

where Ts is the sampling time, floor, ceil and round are function to round the number towards minus infinity, plus infinity and nearest integers respectively.

Figure 6-1~Figure 6-3 show the results with three different setpoint sampling methods. Compared with the original function the first two methods have bigger errors at the same sampling rate and introduce time shift of +Ts/2 and –Ts/2. The third method has the least errors and no time shift, so it should be the best one among the three methods. But in this method, the first sample and last sample are taken in the middle of the sampling period. More cautious actions must be taken in application. In this research, the third method is used for setpoint sampling.

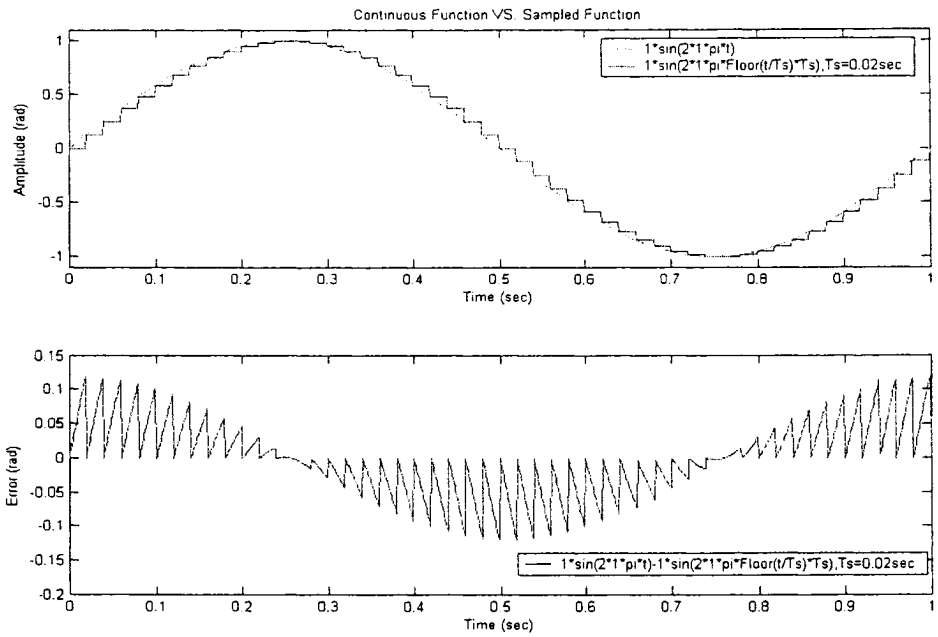

Figure 6-1 Setpoint Sampling Method 1

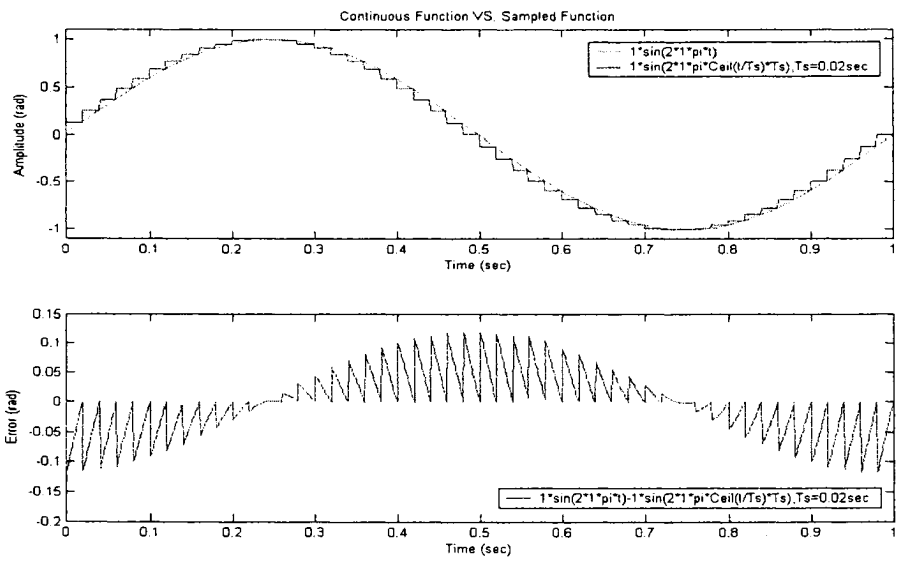

Figure 6-2 Setpoint Sampling Method 2

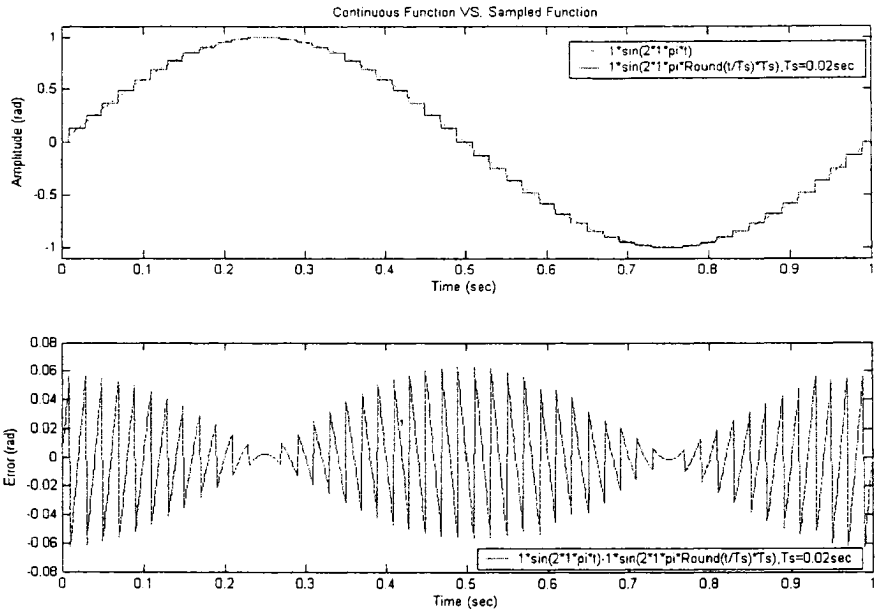

Figure 6-3 Setpoint Sampling Method 3

6.2 Setpoint Sampling Rate in Trajectory Tracking

According to the Nyquist–Shannon sampling theorem, the sampling frequency should be at least twice as the signal's frequency. But the twice frequency rate is not sufficient in practical application. Table 6-1 is the simulation results of different setpoint sampling rates for different signal frequencies. The simulations are based on a continuous time motor position controller with the following motor parameters:

$$k_\tau = 2.18 \times 10^{-2} N \cdot m / A \; k_e = 2.18 \times 10^{-2} rad / s / V; \; R_a = 4.33\Omega$$

$$L_a = 2.34 \times 10^{-3} H; \; I_m = 1.6 \times 10^{-6} kg \cdot m^2; \; B = 0.02 Nm \cdot s; \; \tau_L = 0; \; K_p = 250$$

From this table, the acceptable sampling frequency (tracking error <1% of the signal's amplitude) is at least 50 times the signal frequency.

Table 6-1 Simulation Results of Setpoint Sampling

	No saturation Control	Sin Wave =2*sin(1*pi*t) F= 0.5Hz System data:ip=0.1419	Sin Wave =2*sin(2*pi*t) F=1Hz System data:ip=0.1771	Sin Wave =2*sin(3*pi*t) F= 1.5Hz System data:ip=0.1771	Sin Wave =2*sin(4*pi*t) F= 2Hz System data: tp=0.1771	Sin Wave =2*sin(5*pi*t) F= 2.5Hz System data:ip=0.1771	Sin Wave =2*sin(6*pi*t) F= 3Hz System data:ip=0.1771	Sin Wave =2*sin(7*pi*t) F= 3.5Hz System data:ip=0.1771	Sin Wave =2*sin(8*pi*t) F= 4Hz System data:ip=0.1771
Max Error	Continuous	2.33E-03	9.24E-03	2.06E-02	3.62E-02	5.57E-02	7.89E-02	1.05E-01	1.34E-01
	Sampled Ts=0.01	3.44E-03	1.05E-02	2.26E-02	3.92E-02	5.99E-02	8.45E-02	1.13E-01	1.43E-01
Average Error	Continuous	1.53E-03	6.14E-03	1.39E-02	2.49E-02	3.85E-02	5.48E-02	7.30E-02	9.27E-02
	Sampled Ts=0.01	1.80E-03	6.56E-03	1.45E-02	2.58E-02	3.97E-02	5.66E-02	7.52E-02	9.56E-02
Average Error Norm	Continuous	2.80E-06	4.51E-06	2.29E-04	7.23E-04	1.73E-03	3.49E-03	6.20E-03	1.00E-02
	Sampled Ts=0.01	4.03E-06	5.21E-06	2.52E-04	7.82E-04	1.85E-03	3.74E-03	6.60E-03	1.07E-02
Delay	Continuous	1.60E-02	1.59E-02	1.59E-02	1.58E-02	1.56E-02	1.55E-02	1.53E-02	1.51E-02
Max Error	Continuous	2.32E-03	9.24E-03	2.06E-02	3.62E-02	5.57E-02	7.88E-02	1.05E-01	1.34E-01
	Sampled Ts=0.02	1.19E-02	2.47E-02	3.96E-02	5.74E-02	7.81E-02	1.07E-01	1.41E-01	1.75E-01
Average Error	Continuous	1.53E-03	6.15E-03	1.40E-02	2.49E-02	3.85E-02	5.47E-02	7.28E-02	9.24E-02
	Sampled Ts=0.02	3.94E-03	1.00E-02	1.90E-02	3.12E-02	4.67E-02	6.46E-02	8.57E-02	1.08E-01
Average Error Norm	Continuous	2.80E-06	4.51E-06	2.30E-04	7.22E-04	1.73E-03	3.48E-03	6.17E-03	9.99E-03
	Sampled Ts=0.02	2.27E-05	1.31E-04	4.52E-04	1.19E-03	2.63E-03	5.05E-03	8.78E-03	1.39E-02
Delay	Continuous	1.60E-02	1.59E-02	1.59E-02	1.58E-02	1.56E-02	1.55E-02	1.53E-02	1.51E-02
Max Error	Continuous	2.33E-03	9.24E-03	2.06E-02	3.62E-02	5.57E-02	7.89E-02	1.05E-01	1.35E-01
	Sampled Ts=0.03	2.69E-02	5.42E-02	8.22E-02	1.11E-01	1.40E-01	1.73E-01	2.00E-01	2.43E-01
Average Error	Continuous	1.53E-03	6.15E-03	1.38E-02	2.47E-02	3.85E-02	5.47E-02	7.26E-02	9.21E-02
	Sampled Ts=0.03	7.97E-03	1.73E-02	2.97E-02	4.51E-02	6.30E-02	8.56E-02	1.09E-01	1.36E-01
Average Error Norm	Continuous	2.80E-06	4.51E-05	2.29E-04	7.17E-04	1.74E-03	3.40E-03	6.14E-03	9.96E-03
	Sampled Ts=0.03	1.00E-04	4.40E-04	1.20E-03	2.66E-03	5.06E-03	9.15E-03	1.50E-02	2.31E-02
Delay	Continuous	1.60E-02	1.59E-02	1.59E-02	1.58E-02	1.56E-02	1.55E-02	1.53E-02	1.50E-02
Max Error	Continuous	2.33E-03	9.23E-03	2.06E-02	3.62E-02	5.57E-02	7.88E-02	1.05E-01	1.36E-01
	Sampled Ts=0.04	4.71E-02	9.37E-02	1.39E-01	1.83E-01	2.35E-01	2.78E-01	3.31E-01	3.75E-01
Average Error	Continuous	1.51E-03	6.13E-03	1.39E-02	2.48E-02	3.84E-02	5.48E-02	7.27E-02	9.19E-02
	Sampled Ts=0.04	1.34E-02	2.80E-02	4.53E-02	6.58E-02	9.02E-02	1.20E-01	1.53E-01	1.85E-01
Average Error Norm	Continuous	2.78E-06	4.50E-05	2.29E-04	7.19E-04	1.72E-03	3.47E-03	6.15E-03	9.92E-03
	Sampled Ts=0.04	2.92E-04	1.21E-03	3.00E-03	6.00E-03	1.10E-02	1.83E-02	2.99E-02	4.53E-02
Delay	Continuous	1.59E-02	1.59E-02	1.59E-02	1.58E-02	1.57E-02	1.55E-02	1.53E-02	1.50E-02
Max Error	Continuous	2.33E-03	9.24E-03	2.06E-02	3.62E-02	5.57E-02	7.88E-02	1.05E-01	1.35E-01
	Sampled Ts=0.05	7.04E-02	1.41E-01	2.10E-01	2.83E-01	3.54E-01	4.05E-01	4.95E-01	4.71E-01
Average Error	Continuous	1.53E-03	6.12E-03	1.39E-02	2.47E-02	3.85E-02	5.44E-02	7.26E-02	9.23E-02
	Sampled Ts=0.05	2.00E-02	4.16E-02	6.46E-02	9.34E-02	1.27E-01	1.64E-01	2.03E-01	2.53E-01
Average Error Norm	Continuous	2.80E-06	4.49E-05	2.29E-04	7.14E-04	1.72E-03	3.45E-03	6.14E-03	9.96E-03
	Sampled Ts=0.05	6.52E-04	2.74E-03	6.29E-03	1.27E-02	2.24E-02	3.64E-02	5.50E-02	8.24E-02
Delay	Continuous	1.60E-02	1.59E-02	1.58E-02	1.58E-02	1.57E-02	1.55E-02	1.53E-02	1.50E-02
Max Error	Continuous	2.33E-03	9.24E-03	2.06E-02	3.62E-02	5.57E-02	7.89E-02	1.05E-01	1.35E-01
	Sampled Ts=0.06	1.54E-01	3.09E-01	2.80E-01	6.18E-01	4.71E-01	5.53E-01	6.33E-01	1.02E+00
Average Error	Continuous	1.53E-03	6.10E-03	1.39E-02	2.48E-02	3.84E-02	5.44E-02	7.24E-02	9.18E-02
	Sampled Ts=0.06	4.44E-02	9.02E-02	8.70E-02	1.96E-01	1.64E-01	2.11E-01	2.56E-01	4.67E-01
Average Error Norm	Continuous	2.80E-06	4.48E-05	2.29E-04	7.19E-04	1.72E-03	3.45E-03	6.14E-03	9.89E-03
	Sampled Ts=0.06	3.16E-03	1.31E-02	1.16E-02	5.36E-02	3.89E-02	6.45E-02	9.02E-02	2.93E-01
Delay	Continuous	1.60E-02	1.59E-02	1.59E-02	1.58E-02	1.57E-02	1.55E-02	1.53E-02	1.50E-02
Max Error	Continuous	2.32E-03	9.24E-03	2.06E-02	3.62E-02	5.57E-02	7.88E-02	1.05E-01	1.35E-01
	Sampled Ts=0.07	1.25E-01	2.50E-01	3.65E-01	4.60E-01	6.02E-01	7.10E-01	8.77E-01	8.40E-01
Average Error	Continuous	1.52E-03	6.14E-03	1.39E-02	2.49E-02	3.84E-02	5.41E-02	7.29E-02	9.19E-02
	Sampled Ts=0.07	3.56E-02	7.16E-02	1.12E-01	1.58E-01	2.06E-01	2.59E-01	2.81E-01	3.67E-01
Average Error Norm	Continuous	2.79E-06	4.50E-05	2.29E-04	7.21E-04	1.71E-03	3.44E-03	6.19E-03	9.86E-03
	Sampled Ts=0.07	2.06E-03	8.03E-03	2.00E-02	3.64E-02	6.26E-02	9.76E-02	1.44E-01	2.06E-01
Delay	Continuous	1.60E-02	1.59E-02	1.59E-02	1.58E-02	1.56E-02	1.55E-02	1.53E-02	1.50E-02
Max Error	Continuous	2.33E-03	9.24E-03	2.06E-02	3.62E-02	5.57E-02	7.88E-02	1.05E-01	1.35E-01
	Sampled Ts=0.08	1.54E-01	3.09E-01	4.64E-01	6.18E-01	6.96E-01	9.26E-01	8.77E-01	1.02E+00
Average Error	Continuous	1.53E-03	6.10E-03	1.39E-02	2.48E-02	3.85E-02	5.47E-02	7.21E-02	9.18E-02
	Sampled Ts=0.08	4.44E-02	9.02E-02	1.33E-01	1.96E-01	2.56E-01	2.62E-01	3.68E-01	4.67E-01
Average Error Norm	Continuous	2.80E-06	4.48E-05	2.29E-04	7.19E-04	1.73E-03	3.48E-03	6.07E-03	9.89E-03
	Sampled Ts=0.08	3.16E-03	1.31E-02	2.84E-02	5.36E-02	9.45E-02	1.40E-01	2.11E-01	2.93E-01
Delay	Continuous	1.60E-02	1.59E-02	1.58E-02	1.58E-02	1.57E-02	1.54E-02	1.53E-02	1.50E-02

Figure 6-4 shows the simulation results of tracking a continuous sinusoidal curve and the sampled curve, while Figure 6-5 is the detail of the zoomed area of Figure 6-4.

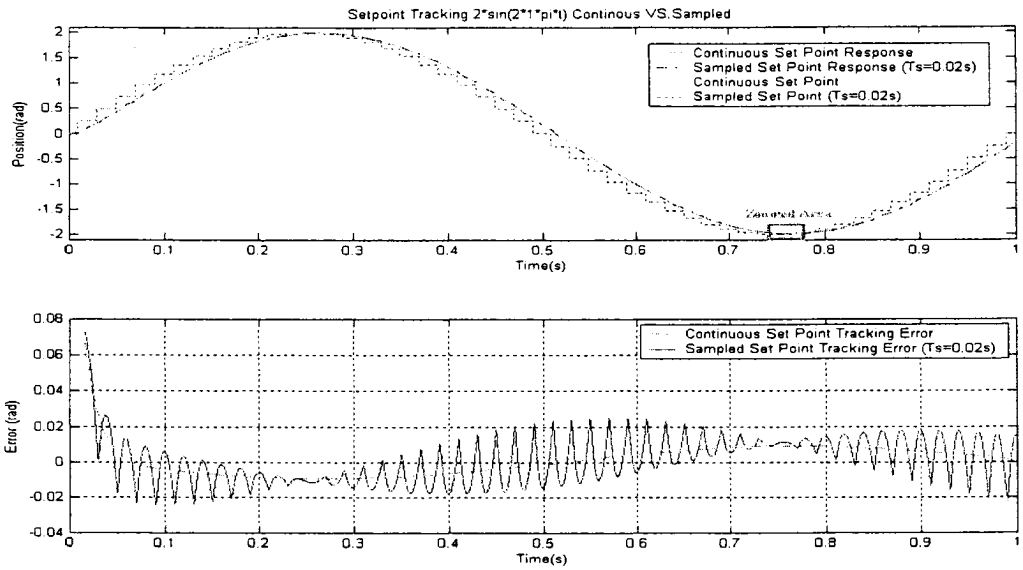

Figure 6-4 Setpoint Tracking

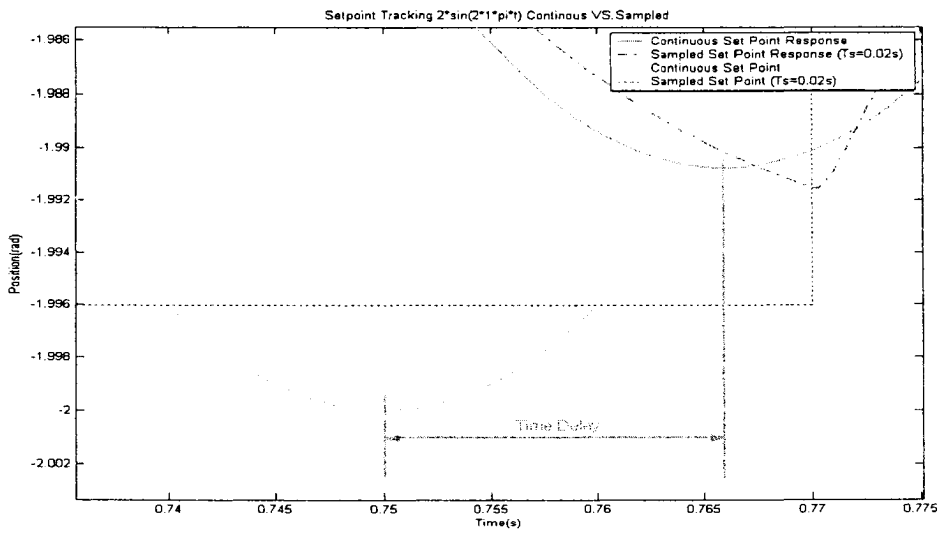

Figure 6-5 Setpoint Tracking (detailed)

6.3 Sampling Time for Digital Controllers

Theoretically the smaller the sampling time the better the system response. But for a specified digital control system, it is not necessary to choose a very small control sampling time. A proper control sampling time can be chosen according to the system configuration. Here two methods are given to calculate the control sampling time.

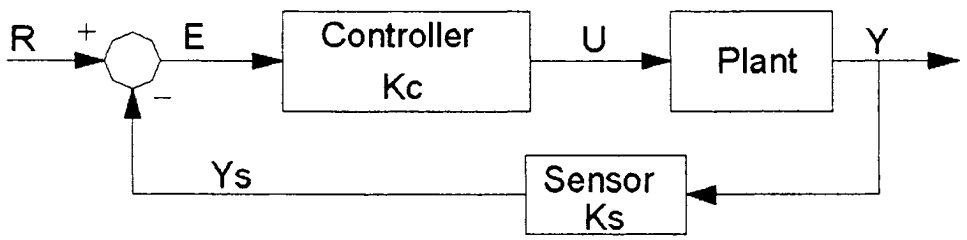

Figure 6-6 Digital Control System Model

In a digital control system (Figure 6-6), the controller and sensor have gains of Kc and Ks, respectively.

First method (control sampling time based on sensor):

$$T_s = (0.5 \sim 4)\frac{1LSB(Sensor)}{|\dot{Y}|(max)K_s} \quad \text{.....(6.3.1)}$$

where 1 least significant bit (LSB) of sensor represents one LSB of sensor's output; Ks is the sensor's gain; $|\dot{Y}_{d(max)}|$ is the maximum speed (absolute value) of the plant output.

Proof:

$$\left.\begin{array}{l} \because Y_s(k) = Y_s(k-1) \\ If\ R(k) = R(k-1) \end{array}\right\} \Rightarrow E(k) = E(k-1) \Rightarrow U(k) \approx U(k-1)$$

Second method (control sampling time based on controller):

$$T_s = (0.5 \sim 4)\frac{1LSB(Controller)}{K_C}\frac{1LSB(Sensor)}{|\dot{Y}|(max)K_s} \quad \text{.....(6.3.2)}$$

where 1LSB(Sensor) represents one LSB of sensor's output; 1LSB(Controller) denotes one LSB of controller's output; Ks is the sensor's gain; Kc is the controller's gain; $|\dot{Y}_{d(max)}|$ **is the maximum speed (absolute value) of the plant output.**

Then the bigger sampling time in these two methods can be considered proper.

Note: In these two methods the sensor sampling time should be smaller or equal to the control sampling time.

In this research, the maximum speed of the motor is 2.41 rad/s, Ks=1024/450 degree, the output of the controller has 8 bit resolution, and Kc=256/68. The control sampling time can be calculated as follows:

Control sampling time based on the sensor:

$$T_s = (0.5 \sim 4)\frac{1}{2.41 \times 180/\pi \times 1024/450} = (0.5 \sim 4) \times 0.00318 = 1.59 \sim 12.7ms$$

Control sampling time based on the controller:

$$T_s = (0.5 \sim 4) \times \frac{1}{256/68} \times \frac{1}{2.41 \times 180/\pi \times 1024/450} = 0.424 \sim 3.39ms$$

For the above system, the control sampling time based on sensor is proper. In this research, 1ms is chosen as the sampling period (it could be bigger) for the control system and the sampling time for the sensor (ADC) is 0.208 ms.

6.4 PID Controller Design

The ideal proportional, plus integral, plus derivative (PID) controller transfer function can be described in equation (6.4.1)

$$G_C(s) = K_P + \frac{K_I}{s} + K_D s \quad \text{.....(6.4.1)}$$

A practical PID controller with a low-pass filter in D controller has an expression in (6.4.2).

$$G_C(s) = K_P + \frac{K_I}{s} + \frac{K_D s}{1+\tau s} \quad \text{.....(6.4.2)}$$

Then the plant control input is:

$$U(s) = G_C(s)E(s) = K_P E(s) + \frac{K_I}{s}E(s) + \frac{K_D s}{1+\tau s}E(s) \quad \text{.....(6.4.3)}$$

Rewrite (6.4.3) in discrete time domain with the sampling time Ts,

$$u(k) = k_P e(k) + k_I I(k) + k_D Y(k) \quad \text{.....(6.4.4)}$$

where e(k) is the error at time k; I(k) is the integral part at time k; Y(k) is the derivative part at time k, which are calculated by

$$\begin{aligned} &e(k) = SetPoint(k) - FeedBack(k) \quad (k \geq 1) \\ &I(k) = I(k-1) + e(k)Ts \quad (k \geq 1, I(0) = 0) \\ &Y(k) = \frac{1}{\tau + Ts}\left(\tau Y(k-1) + e(k) - e(k-1)\right) \quad (k \geq 1, Y(0) = 0) \end{aligned} \quad \text{.....(6.4.5)}$$

Equations (6.4.5) are used in digital PID controller implementation in this research. For tracking control, only PD controller is used with k_I=0. For setpoint control, full PID controller is employed. The experimental parameters and results of PD and PID controllers in tracking and setpoint control are shown in Table 6-2 and Table 6-3.

6.5 Experiment Setup for the Single Joint Control System

The DC motor position control system is shown in Figure 6-7. The load in this setup is 2.613kg and the link length is 0.11 meter. The motor is horizontally installed, the load is vertically installed; therefore the load varies when the motor rotates. The nominal output power and speed of this system are 22 Watts and 2.41 rad/s, respectively.

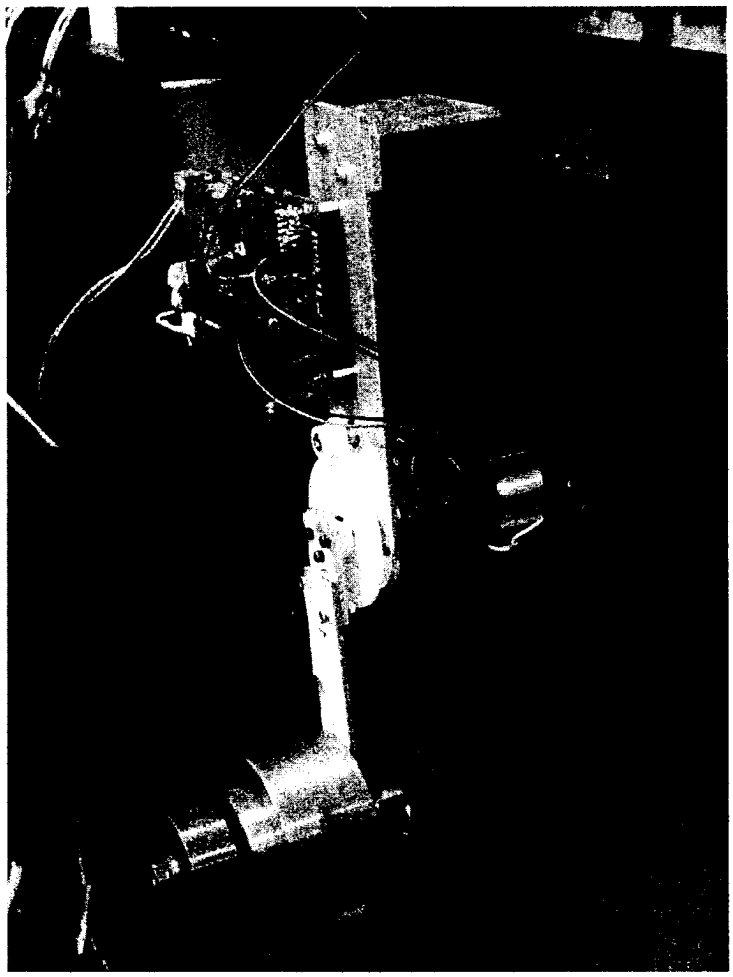

Figure 6-7 Experiment Set Up

6.6 Setpoint Control Results

Table 6-2 lists experiment parameters and steady-state errors. With proper parameters listed in this table, the system has robust performance with steady-state error minimized to 1 LSB of the system resolution, which is equivalent to 0.4395 degree in the link angle.

Table 6-2 Setpoint Control Experiment Parameters and Results

No.	Load Value (g)	Error (degree)	P Gain	I Gain	D Gain	Setpoint Amplitude (degree)
1	2613	-4.2	0.00618	0.00767	0.00183	40.87
2	2613	0.88	0.00801	0.00217	0.00183	40.87
3	46	-1.76	0.00801	0.00217	0.00183	40.87
4	46	-0.44	0.0191	0.00217	0.00183	40.87
5	2613	-0.44	0.0191	0.00217	0.00183	40.87

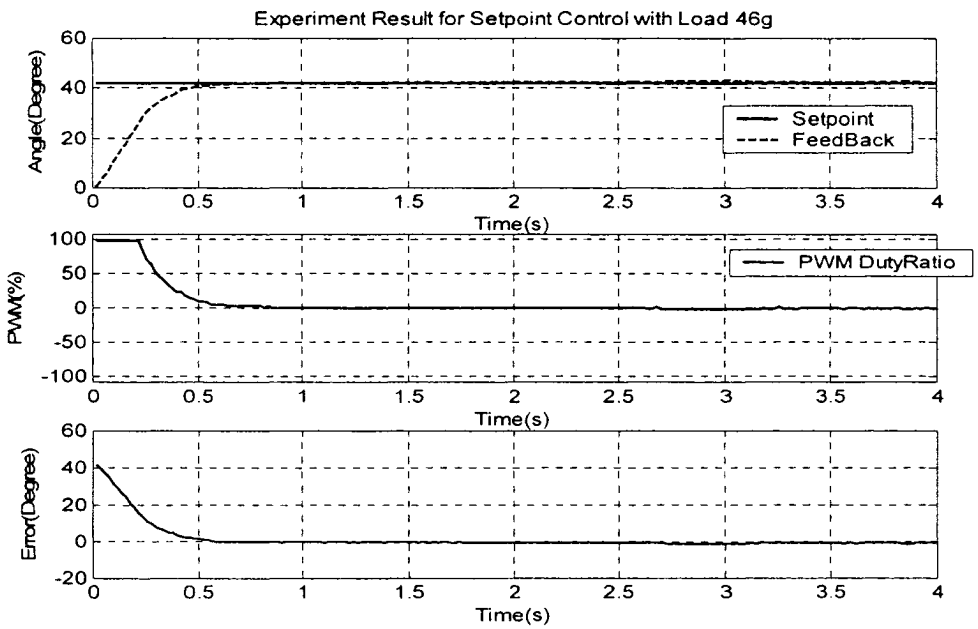

Figure 6-8 Setpoint Control Experiment Result (Load 46g)

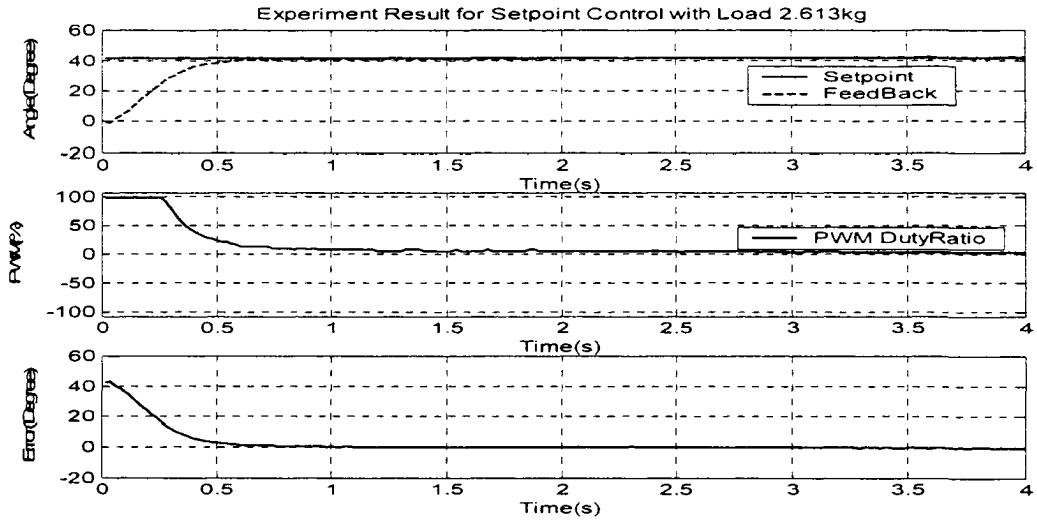

Figure 6-9 Setpoint Control Experiment Result (Load 2613g)

In the 4-th and 5-th rows of Table 6-2, PID parameters are the same, while the loads are much different. The system has good performance without overshoot and the steady state errors are minimized to 0.4395 degree in these different load configurations. So we can say, the system is robust in the setpoint control.

6.7 Sinusoidal Tracking Control Results

Table 6-3 gives system parameters and tracking errors. We can draw the following conclusions:

(1) The system can track the signal whose speed is not faster than the motor speed;

(2) To achieve an acceptable performance, tracking control requires bigger controller gains than setpoint control. The faster the speed of the signal to be tracked, the bigger the controller gains;

(3) With the same system configuration, the bigger the signal speed above the system speed, the longer the tracking delay.

In Figure 6-10 to Figure 6-15, the 'max speed' in the title means the maximum speed of the setpoint signal. The 'Time Delay' denotes the time shift between the trajectory curve and response curve, which is caused by the system time constant. The error is calculated by shifting the response curve back with the time delay.

Table 6-3 Sinusoidal Tracking Control Experiment Parameters and Errors

No.	Load Value (g)	Error RMS(d)	Error ABS(d)	P Gain	I Gain	D Gain	Time Delay	Setpoint Amplitude	Setpoint Period (s)	Setpoint Max Speed (rad/s)
1	46	0.9697	0.7302	0.03010	0	0.00446	0.09s	41.8	2	2.30
2	2613	2.5054	2.1290	0.03010	0	0.00446	0.1s	41.8	2	2.30
3	2613	1.6012	1.3504	0.03010	0	0.00629	0.08s	41.8	2	2.30
4	2613	0.9836	0.7830	0.03284	0	0.00721	0.07s	41.8	2	2.30
5	46	0.6221	0.5103	0.03284	0	0.00721	0.07s	41.8	2	2.30
6	46	0.6857	0.5059	0.03284	0	0.00813	0.07s	41.8	2	2.30
7	2613	1.0020	0.8138	0.03284	0	0.00813	0.07s	41.8	2	2.30
8	2613	0.9465	0.7522	0.03387	0	0.00721	0.07s	41.8	2	2.30
9	46	0.6613	0.5103	0.03387	0	0.00721	0.07s	41.8	2	2.30
10	46	10.6713	9.8710	0.03284	0	0.00721	0.16s	41.8	1	4.59
11	46	3.2867	2.7625	0.03284	0	0.00721	0.1s	41.8	1.5	3.06
12	2613	5.8516	5.2903	0.03284	0	0.00721	0.12s	41.8	1.5	3.06
13	46	1.1869	1.0088	0.03284	0	0.00721	0.08s	20.9	1.5	1.53
14	46	0.7343	0.6041	0.03376	0	0.00446	0.09s	20.9	1.5	1.53
15	2613	0.9171	0.7977	0.03376	0	0.00446	0.09s	20.9	1.5	1.53
16	2613	0.9966	0.8387	0.03559	0	0.00538	0.07s	20.9	1.5	1.53
17	2613	1.9613	1.6188	0.04108	0	0.00263	0.08s	24.2	1	2.65
18	2613	1.4335	1.2229	0.04108	0	0.00366	0.09s	24.2	1	2.65
19	2613	1.3771	0.9677	0.04108	0	0.00446	0.07s	24.2	1	2.65
20	2613	1.2550	0.9062	0.04108	0	0.00538	0.07s	24.2	1	2.65
21	46	0.8731	0.6950	0.04108	0	0.00538	0.07s	24.2	1	2.65

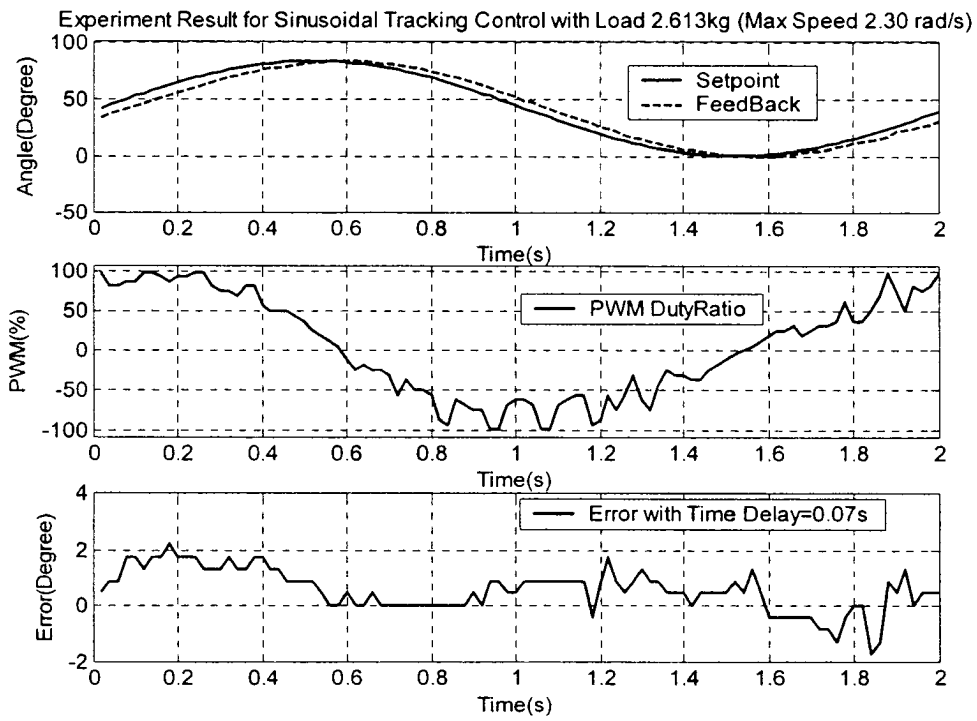

Figure 6-10 Sinusoidal Tracking Control Result 1 (Max Speed 2.3 rad/s, Load 2613g)

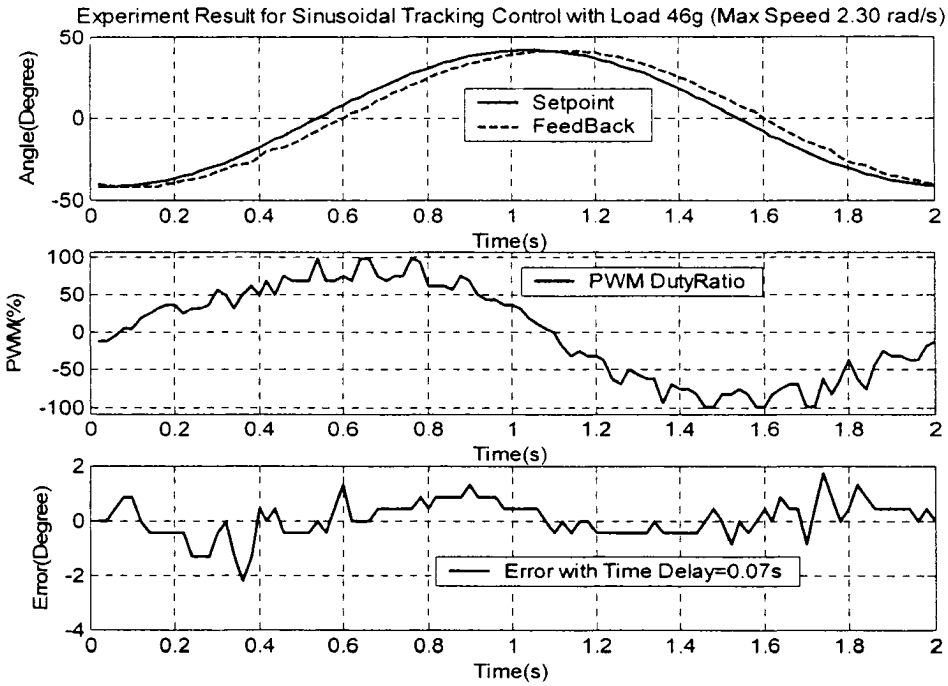

Figure 6-11 Sinusoidal Tracking Control Result 2 (Max Speed 2.3 rad/s, Load 46g)

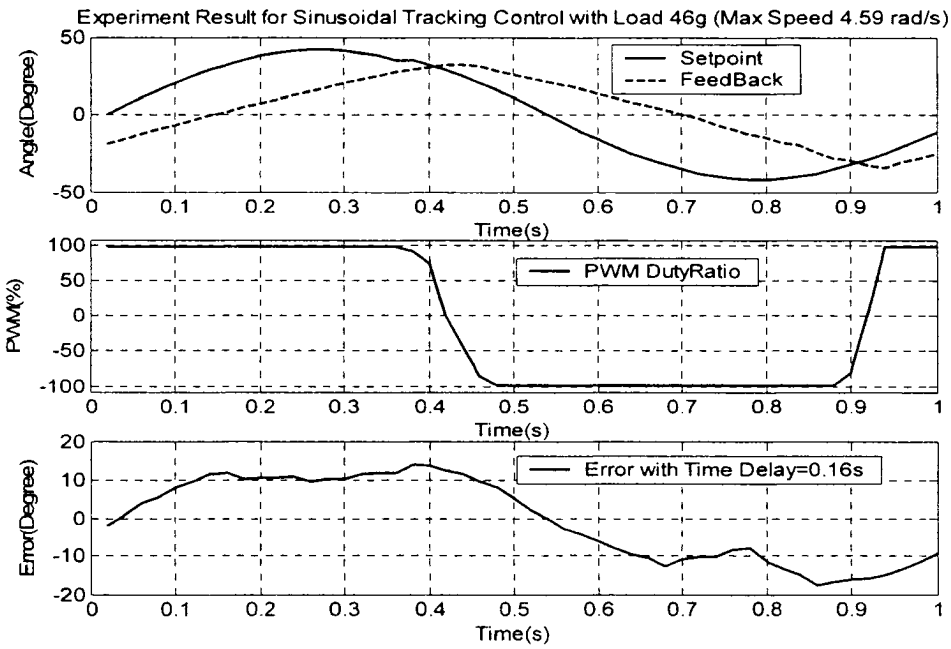

Figure 6-12 Sinusoidal Tracking Control Result 3 (Max Speed 4.59 rad/s, Load 46g)

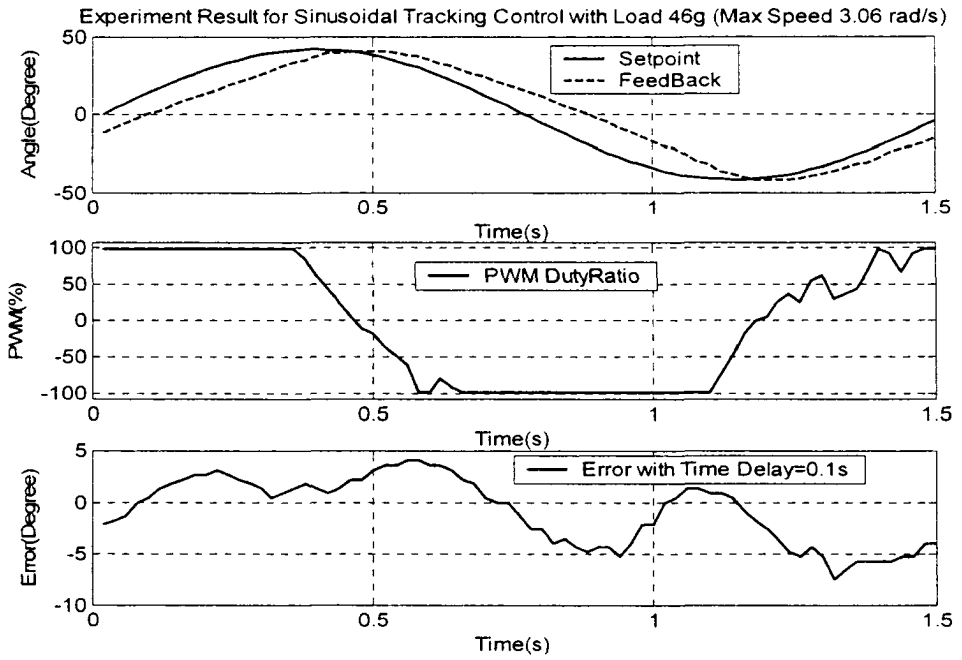

Figure 6-13 Sinusoidal Tracking Control Result 4 (Max Speed 3.06 rad/s, Load 46g)

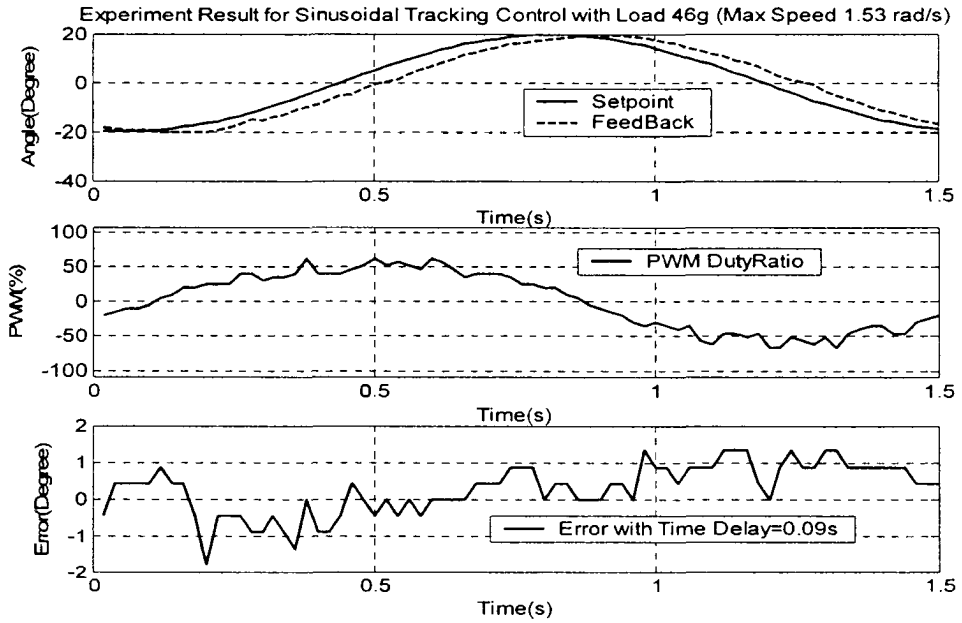

Figure 6-14 Sinusoidal Tracking Control Result 5 (Max Speed 1.53 rad/s, Load 46g)

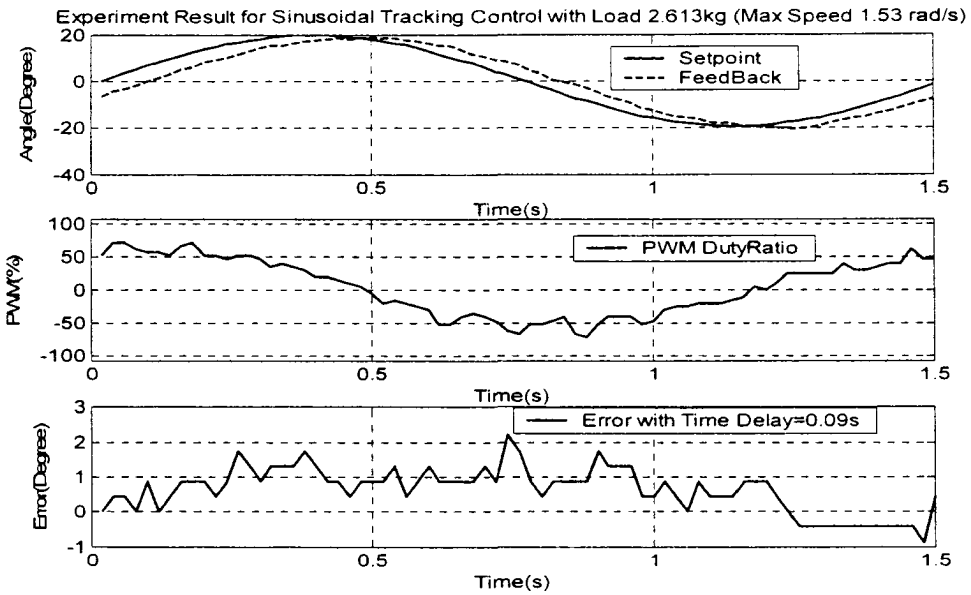

Figure 6-15 Sinusoidal Tracking Control Result 6 (Max Speed 1.53 rad/s, Load 2613g)

Chapter 7 Prototyping of the 7-DOF Biped

7.1 Mechanical Structure Design

The physical structure of the 7-DOF biped is designed according to the dimension listed in Table 5-1. The final prototype is shown in Figure 7-1. The biped is composed of 7 links: a trunk, upper right leg, upper left leg, lower right leg, lower left leg, right foot and left foot. All the joints are driven by DC motors with gear head. The trunk consists of a waist joint and heavy mass. The trunk is controlled to swing from side to side, therefore, the mass on the trunk is shifted accordingly to balance the robot. Because the waist joint drives the heavy mass, self-lock mechanism is necessary. Therefore a worm gear box is used for this joint.

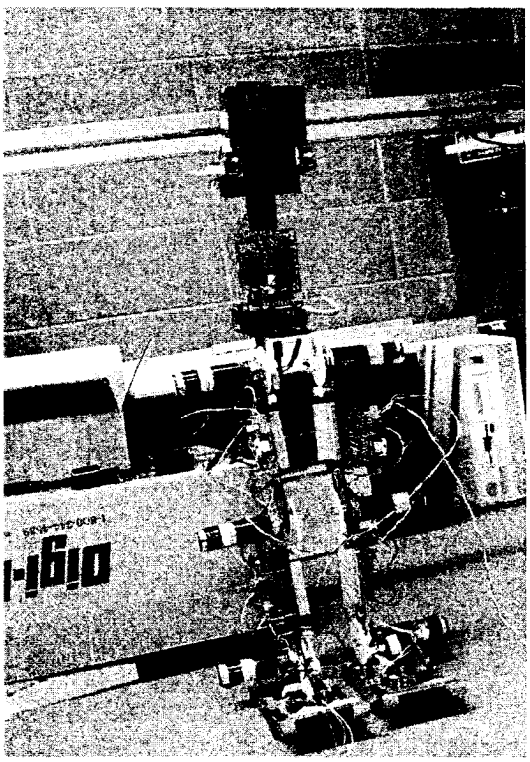

Figure 7-1 Whole Biped Structure

The position feedback devices for all the joints are chosen as multi-turn potentiometers driven by a 4 to 1 gear pair. Compared with encoders as feedback devices, this kind of structure has the following four advantages:

1). Directly reflecting the position of the output shaft;

2). Not necessary to set initial values for positions when power is turned on;

3). Eliminating the backlash effect of gear boxes;

4). Reducing the backlash effect of the potentiometer by factor of 0.2.

Each joint also has upper and lower position limit switches to limit the link motion when they are activated by accident. The detailed structure of limit switch structure is shown in Figure 7-4.

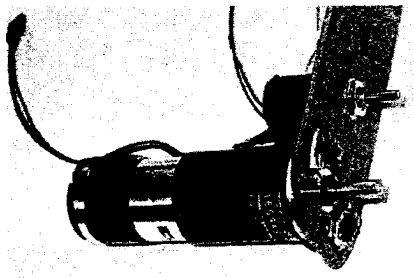

Figure 7-2 Leg Joint Structure

The structures of the leg joint and waist joint are shown in Figure 7-2 and Figure 7-3, respectively. Bumpers are installed on robot feet to absorb impacts when the feet contact the floor, as shown in Figure 7-6.

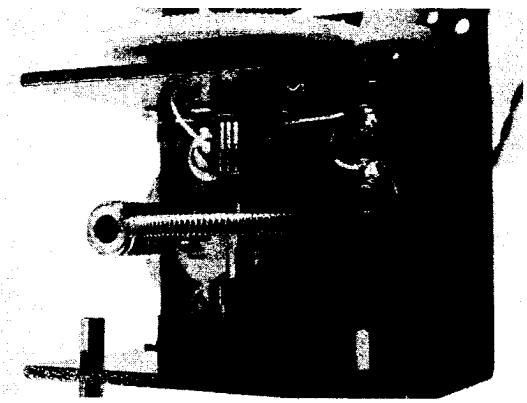

Figure 7-3 Waist Joint Structure

To reduce the weight, most of the structural materials are aluminum. Figure 7-6 shows the structure plates for the robot.

Figure 7-4 Limit Switch Structure

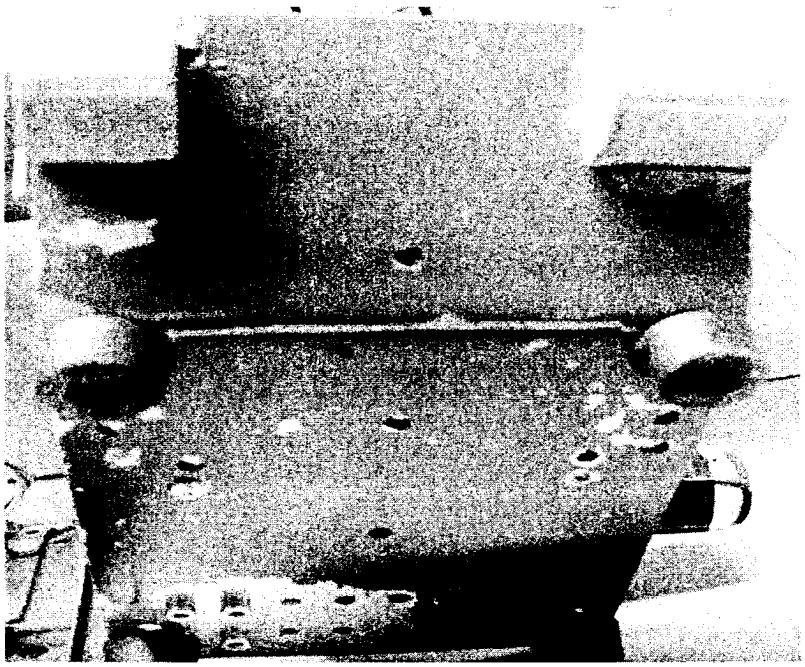

Figure 7-5 Foot Bumper Structure

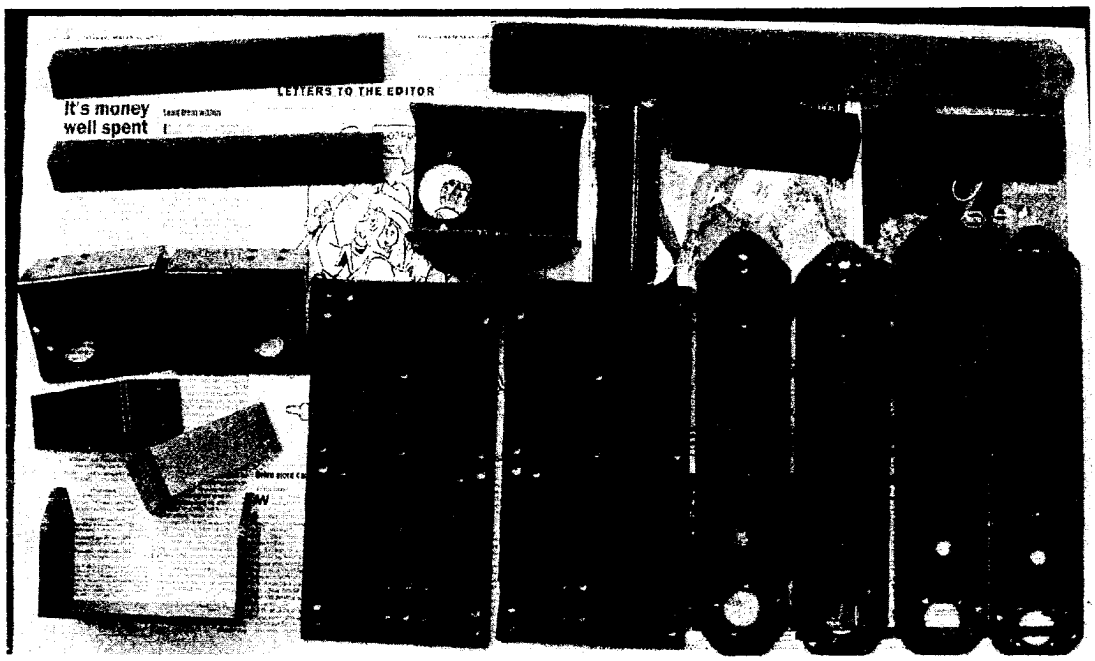

Figure 7-6 Biped Structure Plates

7.2 Electrical Hardware Design

Each joint of the biped is controlled by a micro-controller unit. All the joints are synchronized by the synchronization signal. Figure 7-7 is the whole system connection diagram. In this figure, ① - ⑥ denote joint 1-6 and ⑦ denotes trunk joint.

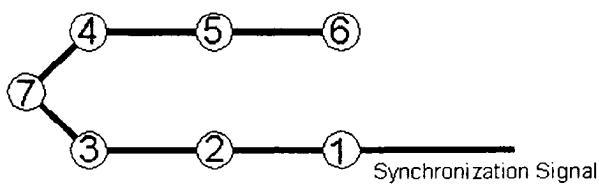

Figure 7-7 Joint Control System

The block diagram of the micro-controller unit is described in Figure 7-8. The heart of this unit is the micro controller-ATMEGA48 [1], which is in charge of A/D

conversion, PID controller computation, timers, interrupt handlers and PWM generation, etc. The H-bridge driver [3] in this unit is a LMD18200 integrated chip. The schematic diagram of this control board is shown in Appendix.

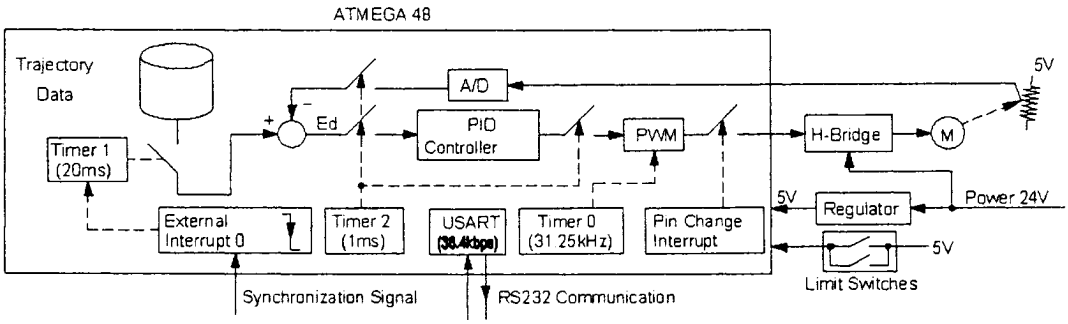

Figure 7-8 Joint Control Unit Block Diagram

The ADC in ATMEGA48 is 10 bit and the feedback device is a 5 turn potentiometer driven by a 4 to 1 gear pair. The position signal is adjusted by an operational amplifier [2] before entering ADC. The maximum resolution of this system is:

$$1LSB = \frac{1}{1024} \times \frac{5}{4} \times 360^{\circ} = 0.4395^{\circ} \quad \text{.....(7.2.1)}$$

The datasheets for the motor and gear head are listed in Appendix.

7.3 Electrical Software Design

In order to reduce the program executing time, assembly language is used in the micro controller programming. The whole program is composed of the following subroutines. The flowcharts of the program are shown in Figures 7-9~7-12

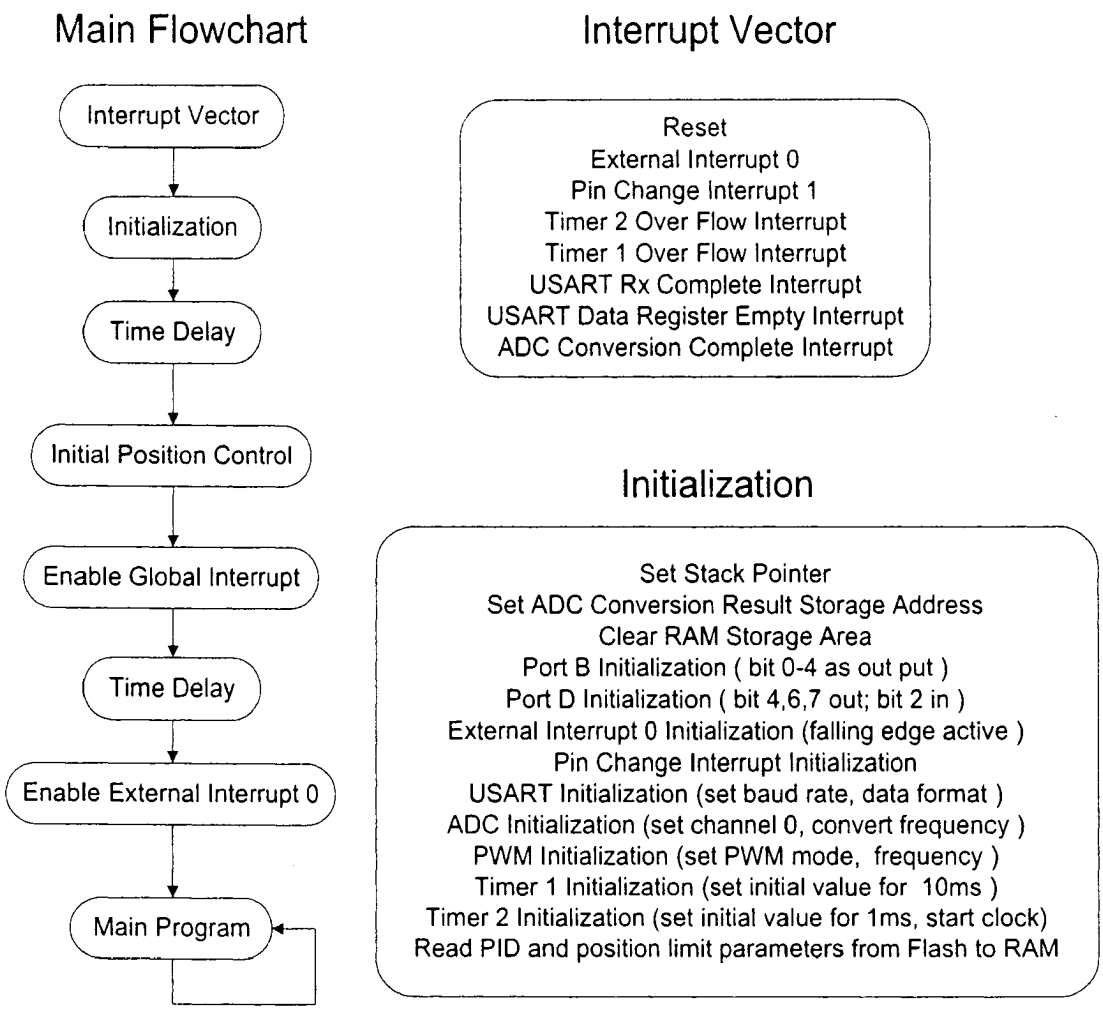

Figure 7-9 Main Flowchart

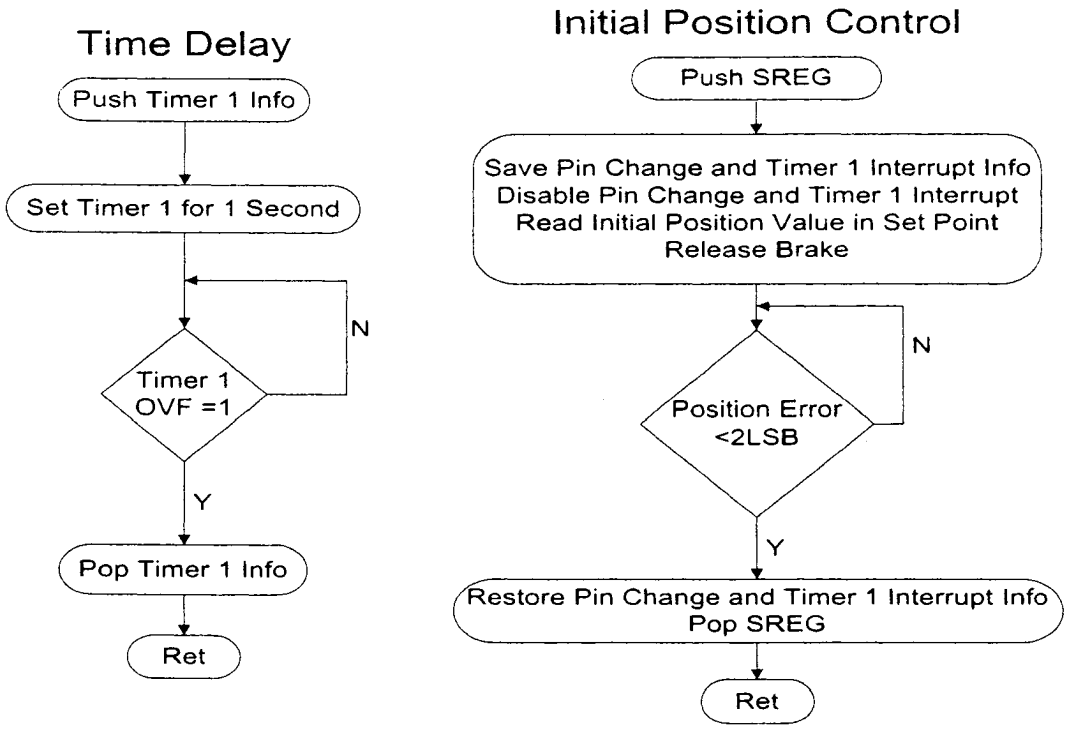

Figure 7-10 Flowchart for Time Delay and Initial Position Control

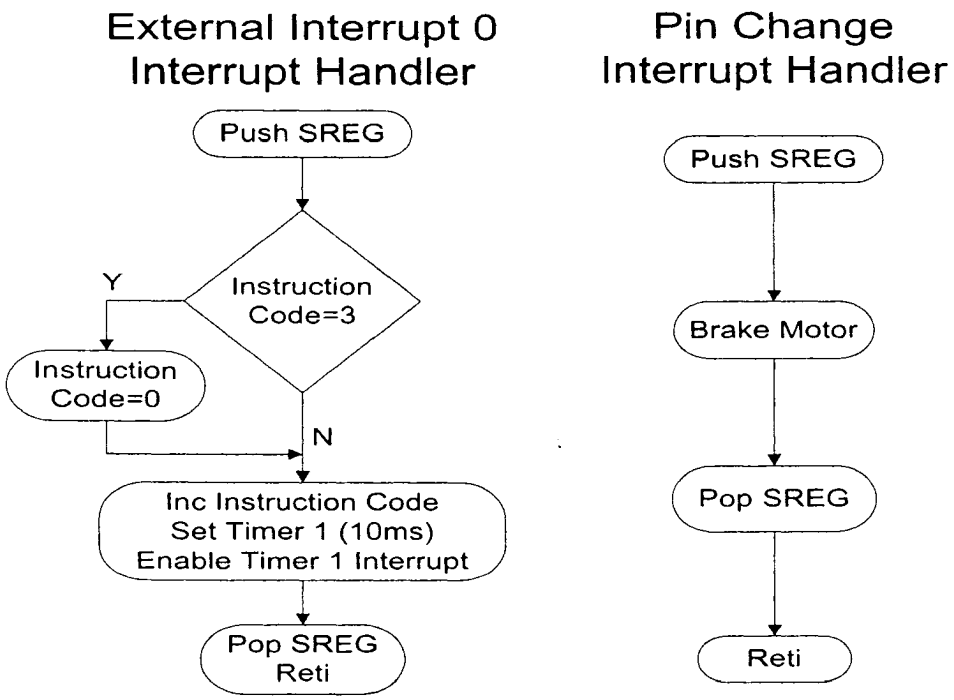

Figure 7-11 Flowchart for PIN Change and External Interrupt Handler

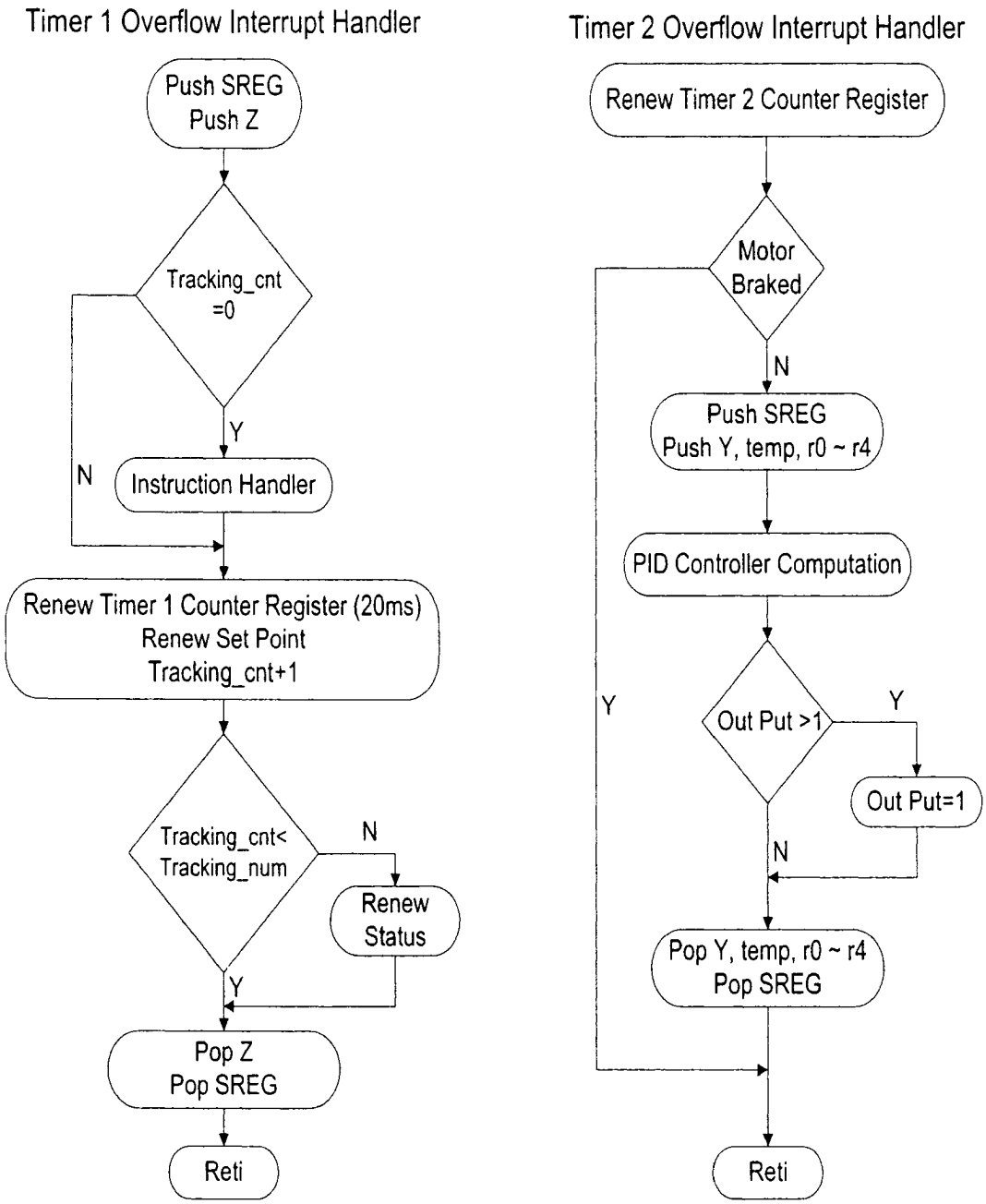

Figure 7-12 Flowchart for Timer 1 and Timer 2 Overflow Interrupt Handler

Chapter 8 Experiment Results on the Biped

Experiments of marching in place were done on the 7-DOF biped built for this project. The prototype of the biped is shown in Figure 7-1. The PD controller designed in Section 6-4 is used to control each link of the biped.

In this experiment, the biped is controlled to march in place on the ground. The desired trajectories for the biped joints are designed by using the method proposed in Section 4-3.

The whole process for marching in place is composed of lifting the right foot, landing the right foot, lifting the left foot, and landing the left foot. During this process, the trunk shifts the mass from side to side to maintain the balance of the robot. It takes 32 second to finish the whole process.

The experiment parameters and results for errors are listed in Table 8-1. The 'Time Delay' denotes the time shift between the trajectory curve and response curve, which is caused by the system time constant. The error is calculated by shifting the response curve back with the time delay. In this table, the 'Error ABS' is the average of the absolute value of the errors; the 'Max Error' presents the maximum of the absolute value of the errors.

Table 8-1 Biped Walking Experiment Parameters and Results

Joint No.	Error RMS(d)	Error ABS(d)	Max Error (d)	P Gain	I Gain	D Gain	Time Delay (s)
1	1.3162	1.0766	5.2785	0.02780	0	0.00721	0.08
2	0.7031	0.4971	2.6370	0.02780	0	0.00721	0.08
3	0.5311	0.4696	1.3185	0.02780	0	0.00721	0.08
4	0.8487	0.5092	4.8345	0.02780	0	0.00721	0.28
5	0.6818	0.5422	2.6370	0.02780	0	0.00721	0.08
6	0.6298	0.4531	2.1975	0.02780	0	0.00721	0.09
Trunk	1.9963	1.6760	3.9555	0.03387	0	0.00721	0.28

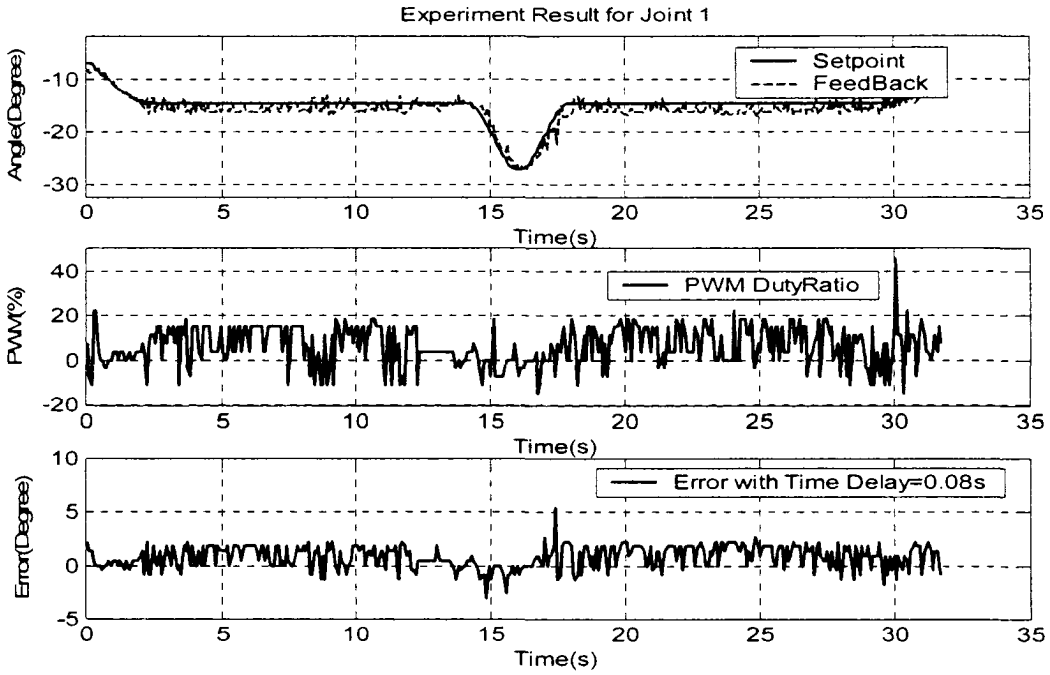

Figure 8-1 Experiment Result for Joint 1

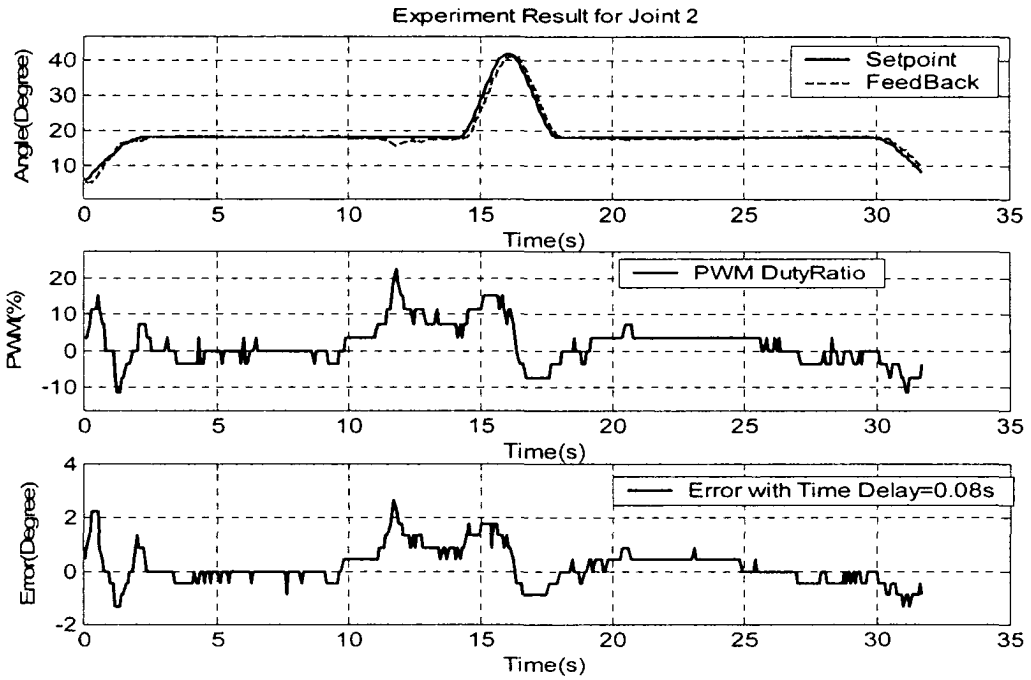

Figure 8-2 Experiment Result for Joint 2

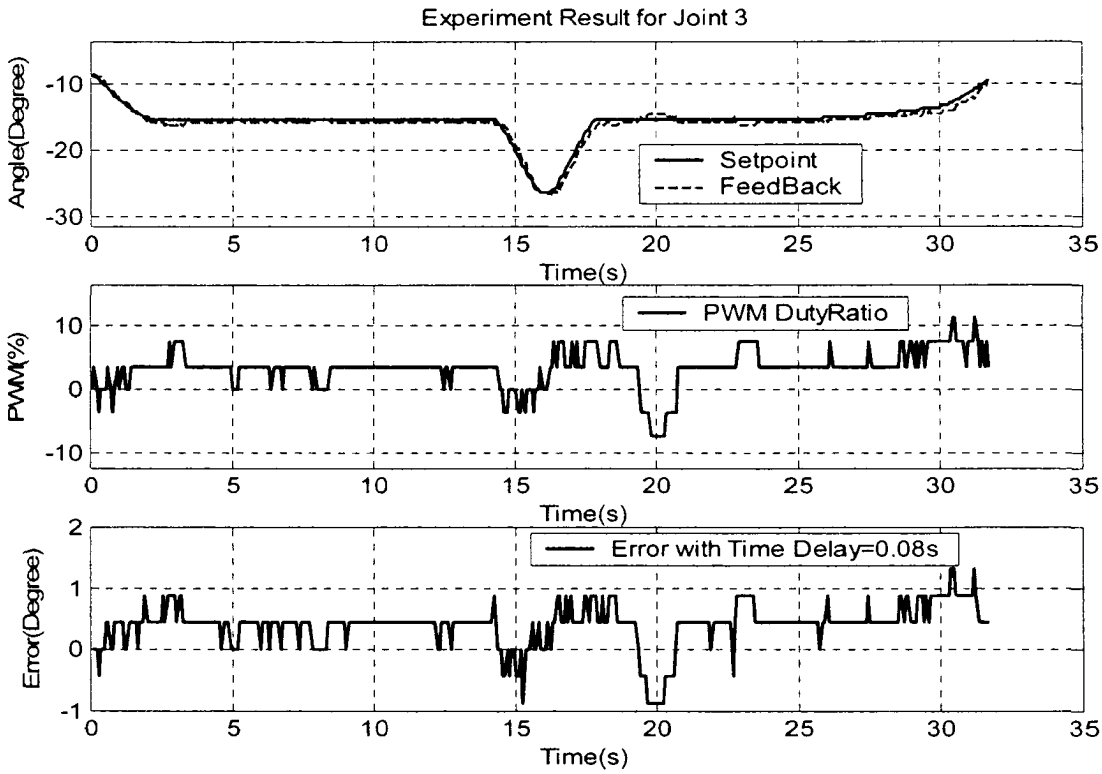

Figure 8-3 Experiment Result for Joint 3

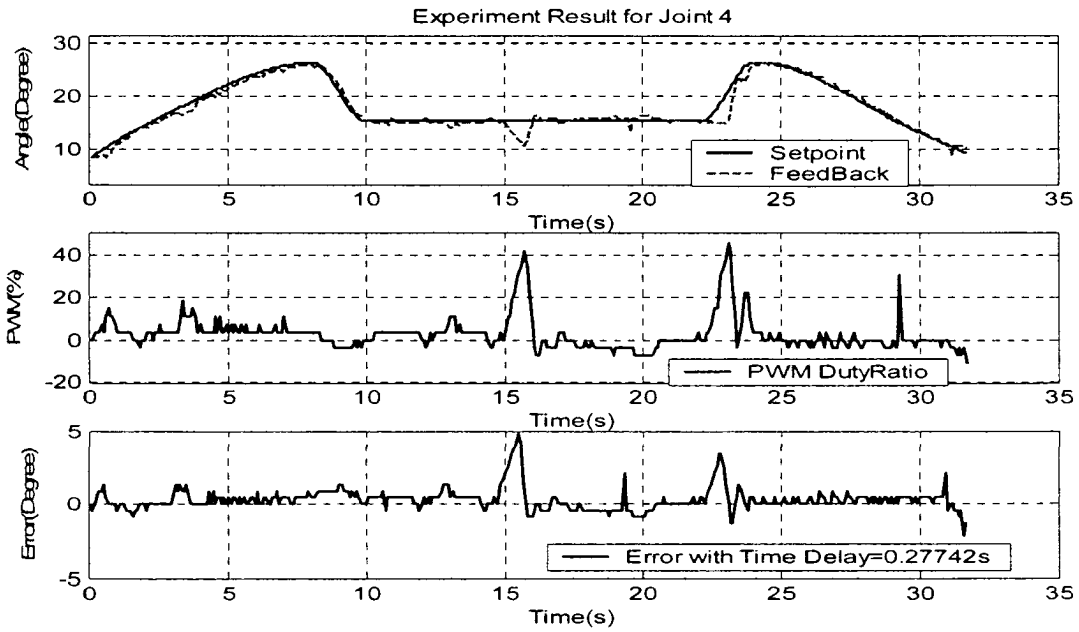

Figure 8-4 Experiment Result for Joint 4

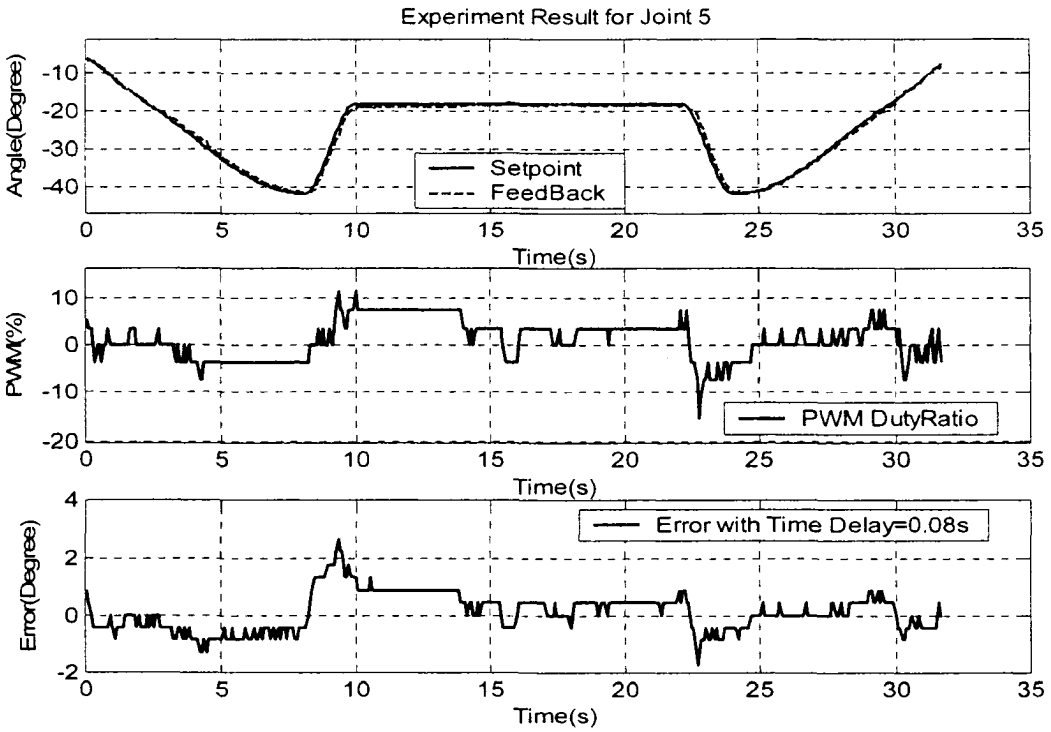

Figure 8-5 Experiment Result for Joint 5

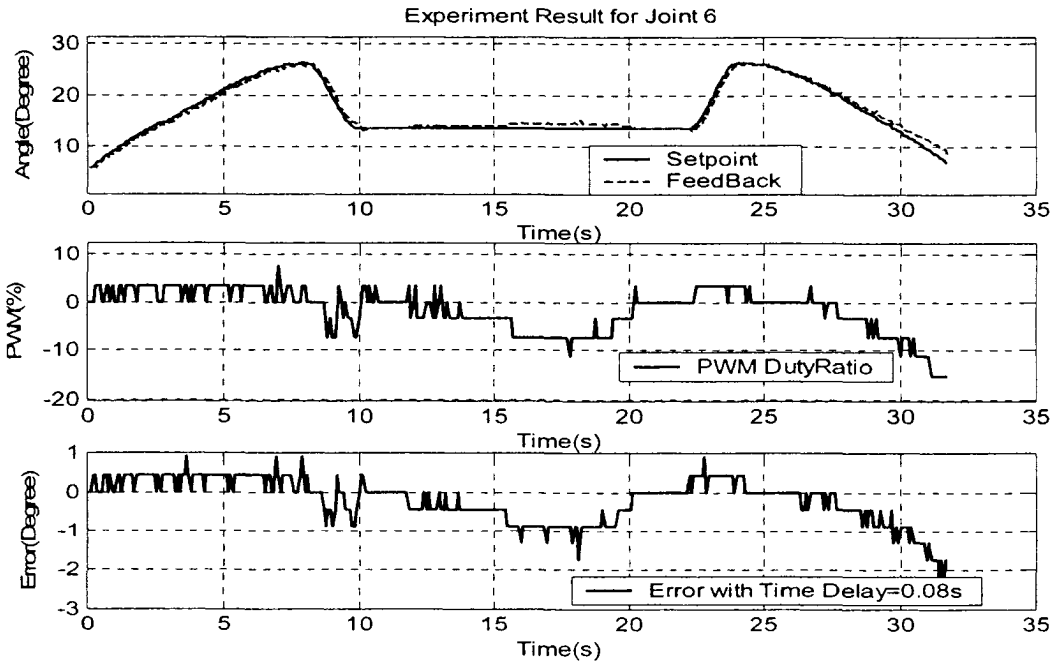

Figure 8-6 Experiment Result for Joint 6

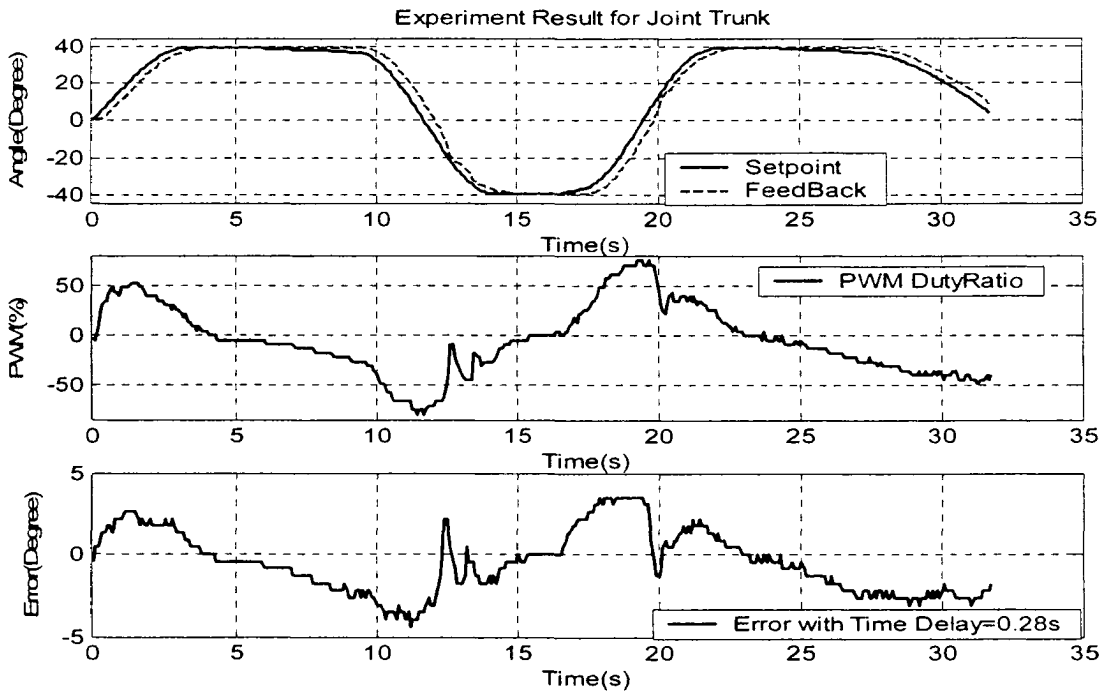

Figure 8-7 Experiment Result for Trunk Joint

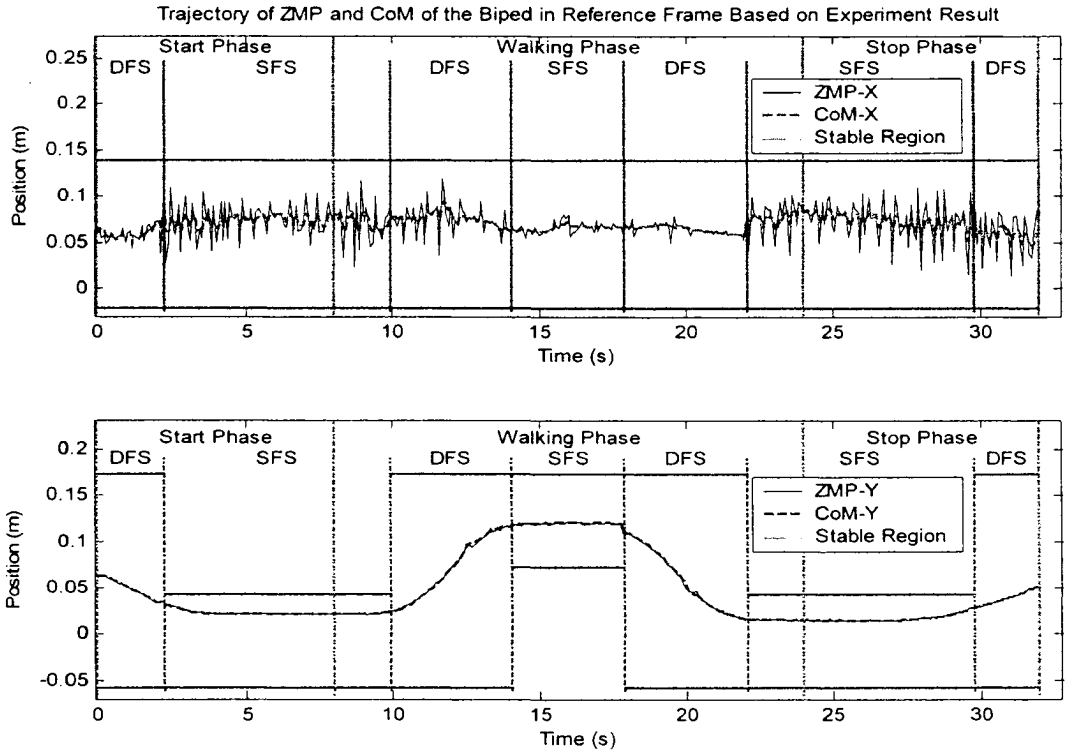

Figure 8-8 Trajectory of ZMP and CoM of the Biped Based on Experiment Result

The angles, PWM ratios and errors for all joints of the biped are shown in Figure 8-1 to Figure 8-7. It is observed from the error graphs that the robot joints can follow the desired trajectories with reasonable tracking errors. It is noticed that the errors are controlled within a range of 5.3 degrees. However, the errors are in the range of 2 degrees most of time. The graphs for the PWM ratios show that the motors are not saturated during the marching process. It is noted that the marching process takes 32 second, so the marching speed is low and acceleration is small. Therefore, the ZMP should be close to CoM, which is verified by the fact that the trajectories for CoM almost coincide with the trajectories of ZMP in both x- and y-directions, as shown in Figure 8-8. It can be also observed that ZMP is within the stable region, so the balance of the robot is maintained during the marching process.

Chapter 9 Conclusions and Future Work

9.1 Conclusions

The literature preparation is successfully achieved in this research. The experiment implementation is successful for marching in place with the planned walking trajectory. This research has the following major contributions:

1) A procedure to generate walking trajectories by extracting and modifying human walking data was proposed.

2) Kinematic and dynamic modeling for a 7-DOF biped were conducted. Joint's power and torque were also computed to analyze mechanical requirements.

3) A proper setpoint sampling method and sampling rate were studied for trajectory tracking and were proven to be effective by both the simulations and experiments.

4) Two control sampling time calculation methods were introduced and were proven to be effective in practical application.

5) An Atmel® microcontroller-based PID control system was designed and implemented for individual joint position control. This control system was proven to be robust to the load changes for both setpoint control and trajectory tracking.

6) A 7-DOF biped was designed and built with aluminum links. The mechanical-electrical structure design was proven to be able to provide stable and smooth position feedback and avoid accidental damages to the system.

9.2 The Problems Encountered

1) In the dynamic modeling for double support phase, it is difficult to solve the adjoint vector.

2) The communication between microcontrollers does not work properly. It could be caused by bad electrical connection or programming.

3) Worm gear structure is difficult to be made precisely with current equipment in our lab.

9.3 Future Work

The 7-DOF biped robot in this research can march in place, using passive balance method. The following is the future work for further improving the biped robot system.

1) Dynamic modeling for double support phase. This part is very important to compute the ZMP and impact forces on the robot, especially at the switching instant from the single support phase to double support phase.

2) Improvement of the mechanical structure. To improve the control performance, it is necessary to build the mechanical structure more rigidly. And 4 joints should be added to the hip and ankles to eliminate the heavy balance mass at the waist. Shock absorbers in each link will be added to absorb the impact forces, which may even damage the robot's structure, when the robot contacts objects or the support surface.

3) Many attempts to maintain the balance of the biped during walking were made, but all failed. The main reason for these unsuccessful experiments might be that the walking trajectories were not able to balance the biped. Therefore, further modification on the walking trajectories need to be done.

4) Dynamic balance of the robot. The passively balanced robot is not able to walk on uneven surface, or balance itself with any external disturbances. So, dynamic balance becomes important for practical biped robots.

5) Adding more functional features to the robot. To make this robot humanoid, upper body, arms, hands, head, visual system, hearing and speaking system should be put on the robot, so that the robot can sense and response to the external world.

References

[1] "ATmega48/V, ATmega88/V, ATmega168/V, Preliminary", Rev 2545G - AVR-06/06, ATMEL, Inc., 2006.

[2] "Dual/Quad Rail-to-Rail Operational Amplifiers OP295/OP495", Rev. C, Analog Devices, Inc., 2002.

[3] "LMD18200 3A,55V H-Bridge", National Semiconductor, Inc., April 2005

[4] M. Y. Zarrugh and C. W. Radcliffe, "Computer Generation of Human Gait Kinematics", J. Biomech., Vol. 12, pp. 99-111, 1979.

[5] M. Vukobratovic and D. Juricic, "Contribution to the synthesis of biped gait", IEEE Transaction on Bio-Medical Engineering Vol. BME-16, No.1, pp. 1-6, 1969.

[6] A.G. Bharatkumar, K.E. Daigle, M.G. Pandy, Q. Cai and J.K. Aggarwal, "Lower Limb Kinematics of Human Walking with the Medial Axis Transformation" , Proceedings of IEEE Workshop on Motion of Non-Rigid and Articulated Objects, pp.70-76, Austin, TX , November 1994.

[7] A. Goswami and V. Kallem, "Rate of Change of Angular Momentum and Balance Maintenance of Biped Robots", Proceedings of IEEE International Conference on Robotics & Automation, Vol.4, pp. 3785-3790, Mountain View, CA, April 2004.

[8] D. Cunado, M.S. Nixon and J.N. Carter, "Extracting a Human Gait Model for Use as a Biometric", Proceedings of IEE Colloquium on Computer Vision for Virtual Human Modelling, pp. 11-1~11-4, Savoy Place, London, UK, July 1998.

[9] D. Hanselman and B. Littlefield, "Mastering MATLAB® 6", Prentice Hall Inc., 2001.

[10] D.J. Todd, "Fundamentals of Robot Technology", Halsted Press Inc. , 1986

[11] J. Wendlandt, "A Recursive Balancing Controller for a 3D Multibody Model of a Biped", Proceedings of 36th IEEE Conference on Decision and Control, Vol.5, pp. 4838-4843, San Diego, CA, USA, December 1997.

[12] http://www.mel.go.jp/soshiki/robot/undo/kajita/bipedsite-e.html

[13] http://www.sony.net/SonyInfo/QRIO/technology/index_nf.html

[14] http://www.bostondynamics.com/

[15] J. J. Cathey, "Electronic Devices and Circuits", 2nd Edition, McGraw-Hill Companies, 2002.

[16] J. Lo and D. Metaxas, "Recursive Dynamics and Optimal Control Techniques for Human Motion Planning", Proceedings of Computer Animation, pp. 220-234, Geneva, May 1999.

[17] M. Vukobratovic, B. Borovac and D. Surdilovic, "Zero Moment Point—Proper Interpretation and New Applications", Proceedings of IEEE International Conference on Humanoid Robots, pp. 237-244, Tokyo, Japan, 2001

[18] M. W. Spong and M. Vidyasaga, "Robot Dynamics and Control", John Wiley & Sons, Inc. 1989.

[19] J.Baltes, S.McGrath and J.Anderson, "The Use of Gyroscope Feedback in the Control of the Walking Gaits for a Small Humanoid Robot", Proceedings of 2nd International Conference on Autonomous Robots and Agents, pp. 470-475, Palmerston North, New Zealand, December 2004.

[20] M. H. Railbert , "Legged Robots That Balance", MIT Press, Cambridge, Massachusetts, 1986.

[21] M. Vukobratovic, V. Potkonjak, V. Matijevic, "Dynamics of Robots with Contact Tasks", Kluwer Academic Publishers, Inc., Netherlands, 2003.

[22] P. Sardain and G. Bessonnet, "Forces Acting on a Biped Robot. Center of Pressure—Zero Moment Point", IEEE Transaction on Systems, Man and Cybernetics—Part A: System and Humans, Vol. 34, No.5, pp. 630-637, Sept. 2004.

[23] Q. Huang, K. Yokoi, S. Kajita, K. Kaneko, H. Arai, N. Koyachi and K. Tanie "Planning Walking Patterns for a Biped Robot", IEEE Transaction on Robotics and Automation, Vol. 17, No. 3, pp. 280-289, June 2001.

[24] Q. L, A. Takanish and I. Kato, "Learning Control of Compensative Trunk Motion for Biped Walking Robot Based on ZMP Stability Criterion", Proceedings of IEEE International Conference on Intelligent Robots and Systems, Vol. 1, pp. 597-603, July 1992.

[25] F.M.Silva and J.A.T. Machado, "Energy Analysis During Biped Walking" Proceedings of IEEE International Conference on Robotics and Automation, Vol.1, pp. 59-64, Detroit, MI, USA, May 1999.

[26] R. L. Norton, "Machine Design, an Integrated Approach", 3rd Edition, Prentice Hall, Inc., 2006.

[27] R.C. Hibbeler, "Engineering Mechanics Dynamics", 10th Edition, Pearson Prentice Hall, Inc., 2004.

[28] P. Djoudi, C.Chevallereau and Y.Aoustin, "Optimal Reference Motion for Walking of a Biped Robot", Proceedings of IEEE International Conference on Robotics and Automation, pp. 2002-2007, Barcelona, Spain, April 2005

[29] M.Rostami and G.Bessnnet, "Impactless Sagittal Gait of a Biped Robot During the Single Support Phase", Proceedings of IEEE International Conference on Robotics and Automation, Vol. 2, pp. 1385-1391, Leuven, May 1998

[30] L.Roussel, C.Canudas-de-Wit and A.Goswami, "Generation of Energy Optimal Complete Gait Cycles for Biped Robots", Proceedings of IEEE International Conference on Robotics and Automation, Vol.3, pp 2036-2041, Leuven, May 1998.

[31] Z.Tang, C. Zhou and Z.Sun, "Trajectory Planning for Smooth Transition of a Biped Robot", Proceedings of IEEE International Conference on Robotics and Automation, Vol.2, pp 2455-2460, Taipei, Taiwan, September 2003.

[32] S.Kajita, F.Kanehiro, K.Kaneko, K.Fujiwara, K.Harada, K.Yokoi and H.Hirukawa, "Biped Walking Pattern Generation by Using Preview Control of Zero Moment Point", Proceedings of IEEE International Conference on Robotics and Automation, Vol.2, pp 1620-1626, Taipei, Taiwan, September 2003.

[33] O.Bebek and K. Erbatur, "A Fuzzy System for Gait Adaptation of Biped Walking Robots", Proceedings of IEEE International Conference on Control Applications, Vol.1, pp 669-673, June 2003.

[34] P. Sardain and G.Bessonnet, " Zero Moment Point—Measurements from a Human Walker Wearing Robot Feet as Shoes", IEEE Transaction on Systems, Man and Cybernetics—Part A: System and Humans, Vol. 34, No.5, pp. 638-648, September 2004

[35] C.Shih and W.Gruver, " Control of a Biped Robot in the Double Support Phase", IEEE Transaction on Systems, Man and Cybernetics, Vol. 22, No.4, pp. 729-735, July/August 1992

[36] J.Kanniah, Z.Lwin, D.Kumar and N.Fatt, "A 'ZMP' Management Scheme for Trajectory Control of Biped Robots Using a Three Mass Model", Proceedings of 2nd International Conference on Autonomous Robots and Agents, pp. 458-463, Palmerston North, New Zealand, December 2004

[37] C.Zhou and Q. Meng, "Dynamic Balance of a Biped Robot Using Fuzzy Reinforcement Learning Agents", Fuzzy Sets and Systems, Vol.134, No.1, pp. 169-187, February 2003

[38] E.Celaya and J.Pota, "Control of a Six-Legged Robot Walking on Abrupt Terrain", Proceedings of IEEE International Conference on Robotics and Automation, Vol.3, pp 2731-2736, Minneapolis, MN, USA, April 1996.

[39] D.Pongas, M.Mistry and S.Schaal, "A Robust Quadruped Walking Gait for Traversing Rough Terrain" , Proceedings of IEEE International Conference on Robotics and Automation, pp. 1474-1479, Roma, Italy, April 2007.

Appendix

A. Structure Design

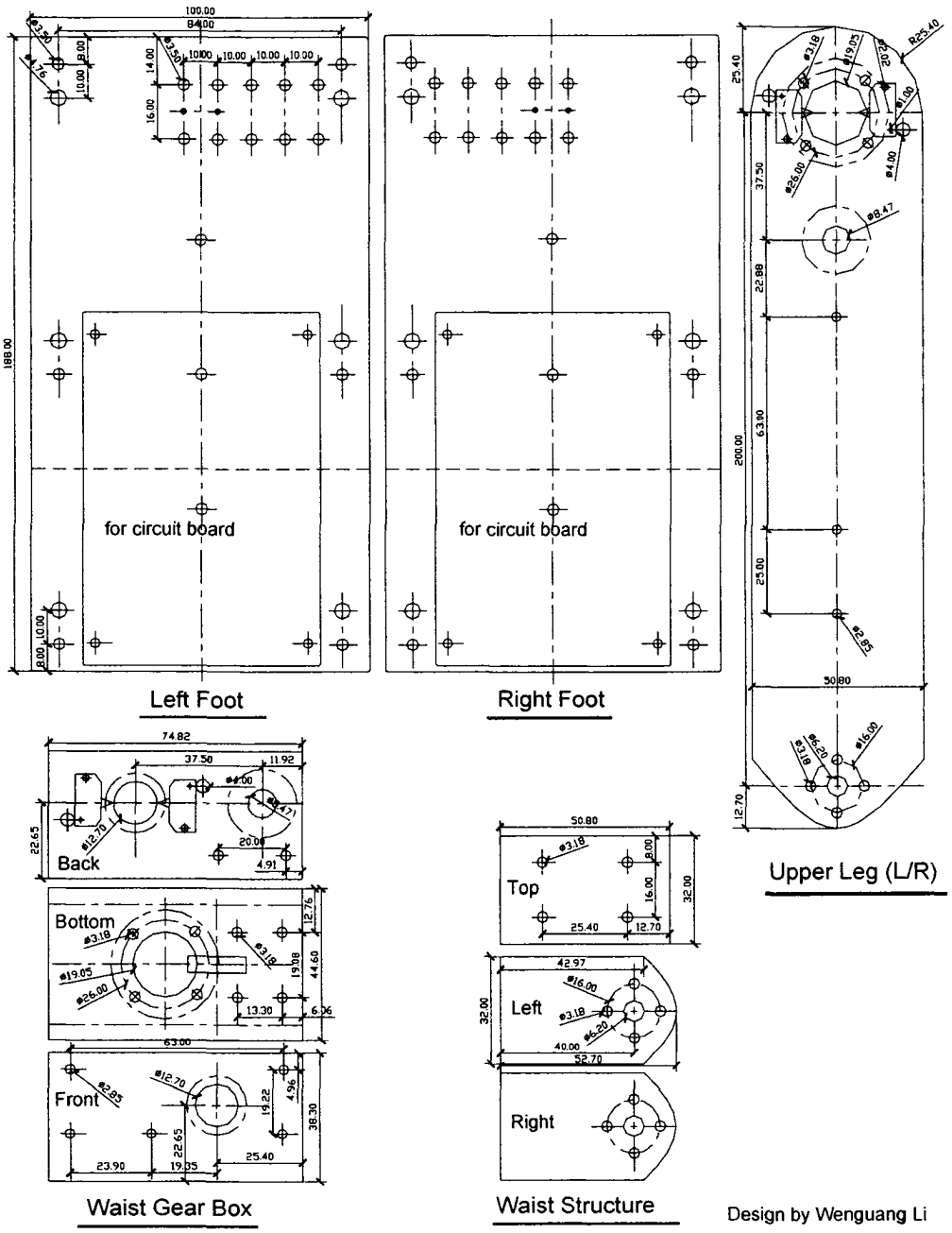

Design by Wenguang Li

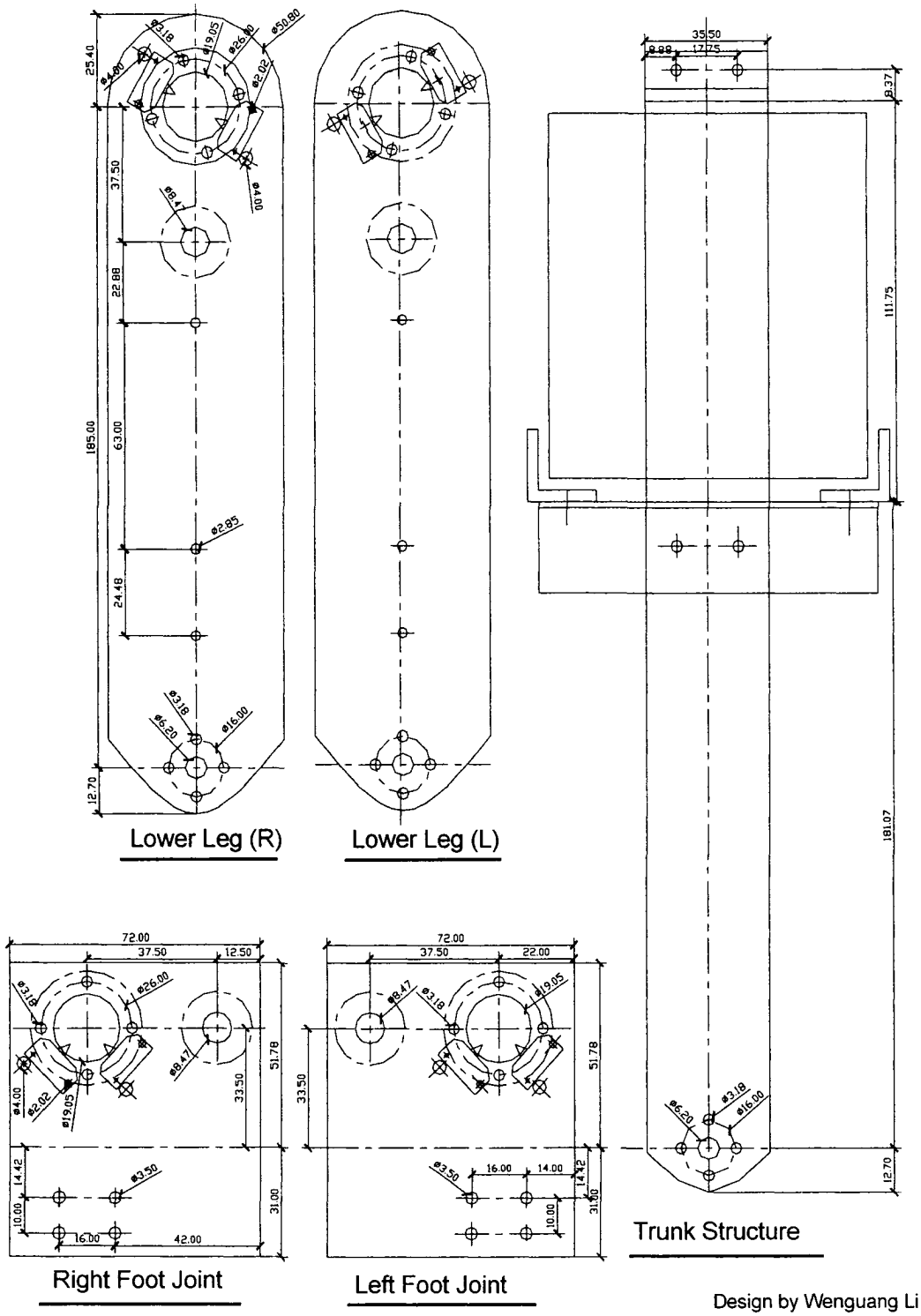

B. Electrical Schematic Design

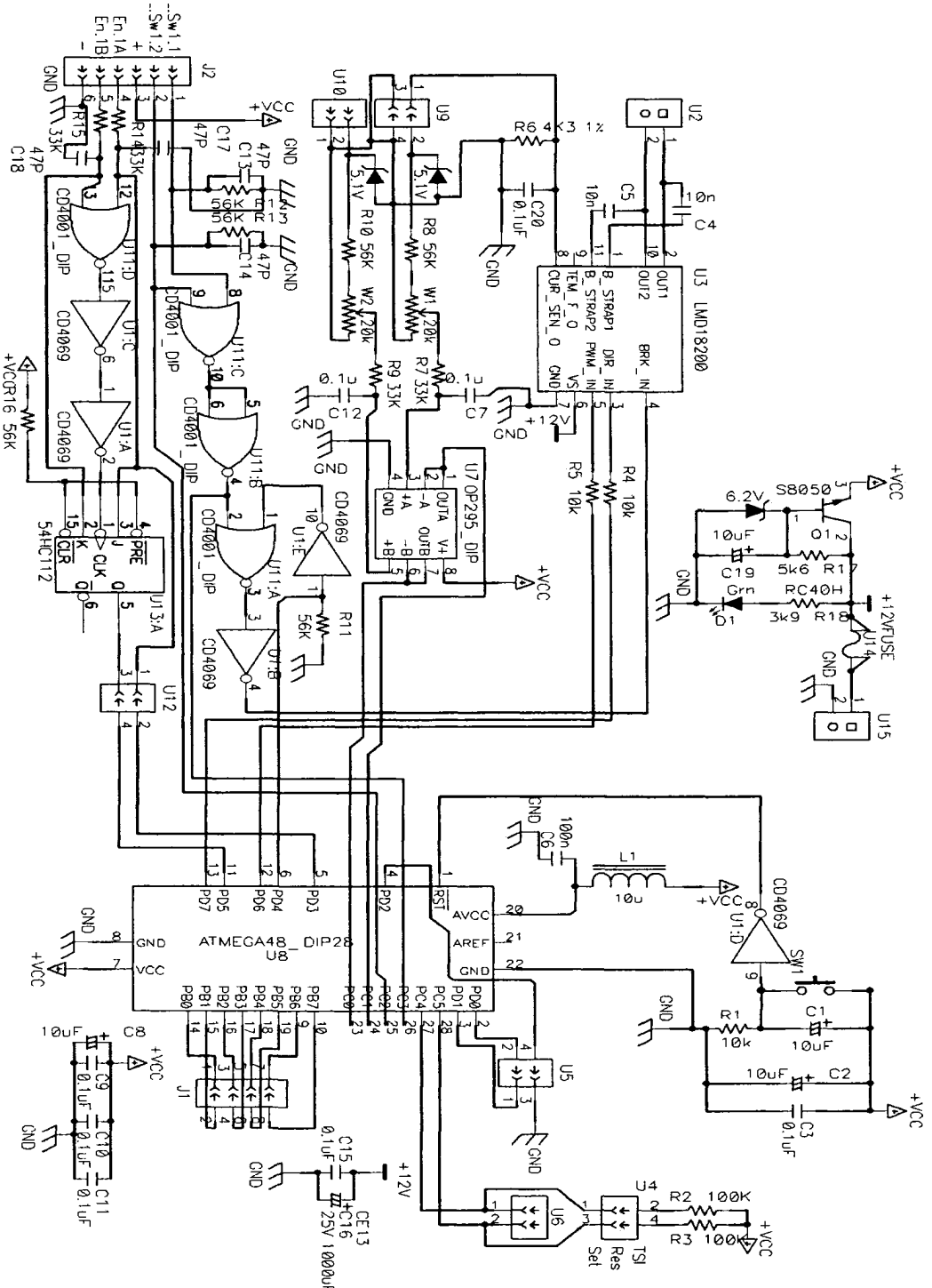

C. Gear Head Data Sheet (Gear Ratio 246:1)

Planetary Gearhead GP 32 C ∅32 mm, 1.0 - 6.0 Nm

Ceramic Version

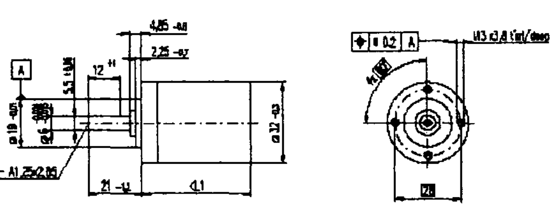

Technical Data	
Planetary Gearhead	straight teeth
Output shaft	stainless steel
Shaft diameter as option	8 mm
Bearing at output	ball bearing
Radial play, 5 mm from flange	max. 0.14 mm
Axial play	max. 0.4 mm
Max. radial load, 12 mm from flange	140 N
Max. permissible axial load	120 N
Max. permissible force for press fits	120 N
Sense of rotation, drive to output	=
Recommended input speed	< 8000 rpm
Recommended temperature range	-20 ... +100°C
Extended area as option	-35 ... +100°C

M 1:2

Option: Low-noise version

Stock program
Standard program
Special program (on request)

Order Number		166930	166933	166938	166939	166944	166949	166954	166959	166962	166967	166972	166977
Gearhead Data													
1 Reduction		3.7 : 1	14 : 1	33 : 1	51 : 1	111 : 1	246 : 1	492 : 1	762 : 1	1181 : 1	1972 : 1	2829 : 1	4380 : 1
2 Reduction absolute		26/7	676/49	529/16	17576/343	13824/125	421824/1715	86112/175	19044/25	10123776/8575	8626176/4375	495144/175	109503/25
3 Max. motor shaft diameter	mm	6	6	3	6	4	4	3	3	4	4	3	3
Order Number		166931	166934		166940	166945	166950	166955	166960	166963	166968	166973	166978
1 Reduction		4.8 : 1	18 : 1		66 : 1	123 : 1	295 : 1	531 : 1	913 : 1	1414 : 1	2189 : 1	3052 : 1	5247 : 1
2 Reduction absolute		24/5	624/35		16224/245	6877/56	101062/343	331776/625	36501/40	2425488/1715	536406/245	1907712/625	839523/160
3 Max. motor shaft diameter	mm	4	4		4	3	3	4	3	3	3	3	3
Order Number		166932	166935		166941	166946	166951	166956	166961	166964	166969	166974	166979
1 Reduction		5.8 : 1	21 : 1		79 : 1	132 : 1	318 : 1	589 : 1	1093 : 1	1526 : 1	2362 : 1	3389 : 1	6285 : 1
2 Reduction absolute		23/4	299/14		3157/40	3312/25	389376/1225	20631/35	279841/256	[illegible]	2066688/875	474513/140	[illegible]
3 Max. motor shaft diameter	mm	3	3		3	3	4	3	3	4	3	3	3
Order Number			166936		166942	166947	166952	166957		166965	166970	166975	
1 Reduction			23 : 1		86 : 1	159 : 1	411 : 1	636 : 1		1694 : 1	2548 : 1	3656 : 1	
2 Reduction absolute			575/25		14976/175	1587/10	359424/875	79488/125		[illegible]	[illegible]	457056/125	
3 Max. motor shaft diameter	mm		4		4	3	4	3		3	4	3	
Order Number			166937		166943	166948	166953	166958		166966	166971	166976	
1 Reduction			26 : 1		103 : 1	190 : 1	456 : 1	706 : 1		1828 : 1	2623 : 1	4060 : 1	
2 Reduction absolute			[illegible]		3588/35	12167/64	89401/196	158171/224		[illegible]	[illegible]	[illegible]	
3 Max. motor shaft diameter	mm		3		3	3	3	3		3	3	3	
4 Number of stages		1	2	2	3	3	4	4	4	5	5	5	5
5 Max. continuous torque	Nm	1	3	3	6	6	6	6	6	6	6	6	6
6 Intermittently permissible torque at gear output	Nm	1.25	3.75	3.75	7.5	7.5	7.5	7.5	7.5	7.5	7.5	7.5	7.5
7 Max. efficiency	%	80	75	75	70	70	60	60	60	50	50	50	50
8 Weight	g	118	162	162	194	194	226	226	226	258	258	258	258
9 Average backlash no load		1.4	1.6	1.6	2.0	2.0	2.0	2.0	2.0	2.0	2.0	2.0	2.0
10 Mass inertia	gcm²	1.5	0.8	0.8	0.7	0.7	0.7	0.7	0.7	0.7	0.7	0.7	0.7
11 Gearhead length L1	mm	26.4	36.3	36.3	43.0	43.0	49.7	49.7	49.7	56.4	56.4	56.4	56.4

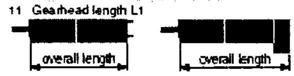

Combination

+ Motor	Page	+ Tacho / Brake	Page	Overall length [mm] = Motor length + gearhead length + (tacho / brake) + assembly parts											
RE 25, 10 W	77			81.0	90.9	90.9	97.6	97.6	104.3	104.3	104.3	111.0	111.0	111.0	111.0
RE 25, 10 W	77	MR	246	92.0	101.9	101.9	108.6	108.6	115.3	115.3	115.3	122.0	122.0	122.0	122.0
RE 25, 10 W	77	Enc 22	248	95.1	105.0	105.0	111.7	111.7	118.4	118.4	118.4	125.1	125.1	125.1	125.1
RE 25, 10 W	77	HED_ 5540	250/252	101.8	111.7	111.7	118.4	118.4	125.1	125.1	125.1	131.8	131.8	131.8	131.8
RE 25, 10 W	77	DCT 22	259	103.3	113.2	113.2	119.9	119.9	126.6	126.6	126.6	133.3	133.3	133.3	133.3
RE 25, 20 W	78			81.0	90.9	90.9	97.6	97.6	104.3	104.3	104.3	111.0	111.0	111.0	111.0
RE 25, 20 W	78	MR	246	92.0	101.9	101.9	108.6	108.6	115.3	115.3	115.3	122.0	122.0	122.0	122.0
RE 25, 20 W	78	Enc 22	248	95.1	105.0	105.0	111.7	111.7	118.4	118.4	118.4	125.1	125.1	125.1	125.1
RE 25, 20 W	78	HED_ 5540	250/252	101.8	111.7	111.7	118.4	118.4	125.1	125.1	125.1	131.8	131.8	131.8	131.8
RE 25, 20 W	78	DCT 22	259	103.3	113.2	113.2	119.9	119.9	126.6	126.6	126.6	133.3	133.3	133.3	133.3
RE 25, 20 W	78	AB 40	289	115.1	125.0	125.0	131.7	131.7	138.4	138.4	138.4	145.1	145.1	145.1	145.1
RE 25, 20 W	78	HED_ 5540/AB 40	250/289	132.2	142.1	142.1	148.8	148.8	155.5	155.5	155.5	162.2	162.2	162.2	162.2
RE 26, 18 W	79			85.3	95.2	95.2	101.9	101.9	108.6	108.6	108.6	115.3	115.3	115.3	115.3
RE 26, 18 W	79	MR	246	96.3	106.2	106.2	112.9	112.9	119.6	119.6	119.6	126.3	126.3	126.3	126.3
RE 26, 18 W	79	Enc 22	248	102.7	112.6	112.6	119.3	119.3	126.0	126.0	126.0	132.7	132.7	132.7	132.7
RE 26, 18 W	79	HED_ 5540	250/252	103.7	113.6	113.6	120.3	120.3	127.0	127.0	127.0	133.7	133.7	133.7	133.7
RE 26, 18 W	79	DCT 22	259	106.3	116.2	116.2	122.9	122.9	129.6	129.6	129.6	136.3	136.3	136.3	136.3
RE 30, 60 W	80			94.5	104.4	104.4	111.1	111.1	117.8	117.8	117.8	124.5	124.5	124.5	124.5
RE 30, 60 W	80	MR	247	105.9	115.8	115.8	122.5	122.5	129.2	129.2	129.2	135.9	135.9	135.9	136.9
RE 35, 90 W	81			97.4	107.3	107.3	114.0	114.0	120.7	120.7	120.7	127.4	127.4	127.4	127.4
RE 35, 90 W	81	MR	247	108.8	118.7	118.7	125.4	125.4	132.1	132.1	132.1	138.8	138.8	138.8	138.8
RE 35, 90 W	81	HED_ 5540	250/252	118.4	128.3	128.3	135.0	135.0	141.7	141.7	141.7	148.4	148.4	148.4	148.4
RE 35, 90 W	81	DCT 22	259	115.5	125.4	125.4	132.1	132.1	138.8	138.8	138.8	145.5	145.5	145.5	145.5
RE 35, 90 W	81	AB 40	289	133.5	143.4	143.4	150.1	150.1	156.8	156.8	156.8	163.5	163.5	163.5	163.5
RE 35, 90 W	81	HEDS 5540 / AB 40	250/289	150.6	160.5	160.5	167.2	167.2	173.9	173.9	173.9	180.6	180.6	180.6	180.6
RE 36, 70 W	82			97.7	107.6	107.6	114.3	114.3	121.0	121.0	121.0	127.7	127.7	127.7	127.7
RE 36, 70 W	82	MR	247	109.1	119.0	119.0	125.7	125.7	132.4	132.4	132.4	139.1	139.1	139.1	139.1
RE 36, 70 W	82	HED_ 5540	250/252	118.7	128.6	128.6	135.3	135.3	142.0	142.0	142.0	148.7	148.7	148.7	148.7
RE 36, 70 W	82	DCT 22	259	115.8	125.7	125.7	132.4	132.4	139.1	139.1	139.1	145.8	145.8	145.8	145.8

April 2006 edition / subject to change

maxon gear 229

D. DC Motor Data Sheet (Rated Voltage 24V)

RE-max 29 ∅29 mm, Graphite Brushes, 22 Watt

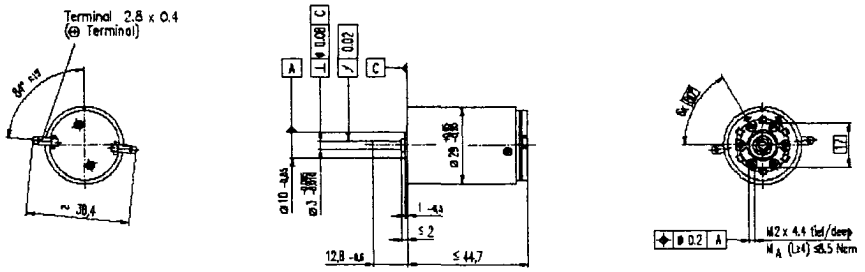

M 1:2

Stock program
Standard program
Special program (on request)

Order Number	226784	226785	226787	226788	226789	226790	226791	226792	226793	226795	226796	226797	226798	226799	226800
Motor Data															
Values at nominal voltage															
1 Nominal voltage V	9.0	12.0	18.0	24.0	30.0	36.0	42.0	48.0	48.0	48.0	48.0	48.0	48.0	48.0	48.0
2 No load speed rpm	7630	9130	8860	8780	9090	8660	8380	8600	7450	6100	5240	4860	4030	3250	2700
3 No load current mA	77.4	73.1	46.6	34.2	28.6	22.3	18.3	16.5	13.7	10.5	8.70	7.93	6.33	4.90	3.96
4 Nominal speed rpm	6690	8170	7760	7690	8020	7630	7360	7590	6580	5060	4200	3810	2970	2180	1610
5 Nominal torque (max. continuous torque) mNm	10.9	12.3	19.7	26.8	27.4	28.5	28.9	29.0	28.2	29.8	30.3	30.4	30.3	30.5	30.3
6 Nominal current (max. continuous current) A	1.08	1.08	1.08	1.07	0.903	0.745	0.625	0.563	0.475	0.409	0.357	0.332	0.275	0.222	0.184
7 Stall torque mNm	171	207	202	262	273	268	257	265	208	182	157	146	118	94.1	76.5
8 Starting current A	15.8	16.9	10.6	10.2	8.73	6.80	5.41	4.99	3.40	2.43	1.81	1.56	1.04	0.672	0.465
9 Max. efficiency %	79	82	84	87	87	89	89	88	87	87	86	86	85	83	82
Characteristics															
10 Terminal resistance Ω	0.571	0.708	1.69	2.36	3.44	5.29	7.76	9.61	14.1	19.7	26.5	30.9	46.1	71.4	106
11 Terminal inductance mH	0.0353	0.0447	0.108	0.199	0.292	0.464	0.676	0.839	1.12	1.67	2.26	2.63	3.81	5.86	8.46
12 Torque constant mNm / A	10.9	12.2	19	25.8	31.2	39.4	47.5	53	61.1	74.7	86.9	93.7	113	140	168
13 Speed constant rpm / V	879	781	502	370	306	242	201	180	156	128	110	102	84.6	68.2	56.8
14 Speed / torque gradient rpm / mNm	46.2	45.3	44.7	33.9	33.6	32.6	32.8	32.7	36.1	33.8	33.5	33.5	34.5	34.8	35.6
15 Mechanical time constant ms	6.04	6.08	5.10	4.78	4.63	4.52	4.46	4.42	4.44	4.41	4.39	4.38	4.38	4.38	4.38
16 Rotor inertia gcm²	14.3	12.8	10.9	13.5	13.1	13.2	13.0	12.9	11.7	12.5	12.5	12.5	12.1	12.0	11.7

Specifications

	Thermal data	
17	Thermal resistance housing-ambient	15.8 K / W
18	Thermal resistance winding-housing	4.6 K / W
19	Thermal time constant winding	13.8 s
20	Thermal time constant motor	1260 s
21	Ambient temperature	-30 ... +85 °C
22	Max. permissible winding temperature	+125 °C
	Mechanical data (ball bearings)	
23	Max. permissible speed	10400 rpm
24	Axial play	0.1 - 0.2 mm
25	Radial play	0.025 mm
26	Max. axial load (dynamic)	5.9 N
27	Max. force for press fits (static)	75 N
28	Max. radial loading, 5 mm from flange	29.5 N
	Mechanical data (sleeve bearings)	
23	Max. permissible speed	10400 rpm
24	Axial play	0.1 - 0.2 mm
25	Radial play	0.012 mm
26	Max. axial load (dynamic)	1.7 N
27	Max. force for press fits (static)	80 N
28	Max. radial loading, 5 mm from flange	12.3 N
	Other specifications	
29	Number of pole pairs	1
30	Number of commutator segments	13
31	Weight of motor	159 g

Values listed in the table are nominal.
Explanation of the figures on page 43.

Option
Sleeve bearings in place of ball bearings
Pigtails in place of terminals

Operating Range

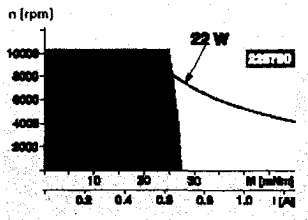

Comments

Continuous operation
In observation of above listed thermal resistance (lines 17 and 18) the maximum permissible winding temperature will be reached during continuous operation at 25 °C ambient.
= Thermal limit.

Short term operation
The motor may be briefly overloaded (recurring).

Assigned power rating

maxon Modular System Overview on page 17 - 21

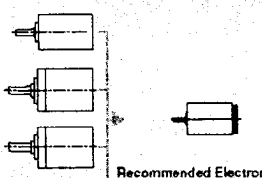

Planetary Gearhead
Ø26 mm
0.5 - 2.0 Nm
Page 224

Planetary Gearhead
Ø32 mm
0.75 - 4.5 Nm
Page 227

Planetary Gearhead
Ø32 mm
1.0 - 6.0 Nm
Page 230

Recommended Electronics:

LSC 30/2	Page 264
ADS 50/5	264
ADS_E 50/5	265
Notes	17

E. Denavit-Hartenberg Representation Convention Procedures

Step 1: Locate and label the joint axes: $z_0, z_1, \ldots, z_{n-1}$. z_i is the axis of revolution of joint $i+1$ if joint $i+1$ is revolute and is the axis of translation of joint $i+1$ if joint $i+1$ is prismatic.

Step 2: Establish the base frame. Set the origin anywhere on the z_0 -axis. The x_0 and y_0 axes are chosen conveniently to form a right-hand frame.

For $i=1, \ldots, n-1$, perform Steps 3 to 5.

Step 3: Locate the origin o_i where the common normal to z_i and z_{i-1} intersects z_i. If z_i intersects z_{i-1}, locate o_i at this intersection. If z_i and z_{i-1} are in parallel, locate o_i at joint i.

Step 4: Establish x_i along the common normal between z_{i-1} and z_i through o_i, or in the direction that is normal to the z_{i-1}-z_i plane if z_{i-1} and z_i intersect.

Step 5: Establish y_i to complete a right-hand frame.

Step 6: Establish the end-effector frame $o_n x_n y_n z_n$. Assuming the n-th joint is revolute, set the axis z_n parallel to the axis z_{n-1}. Establish o_n conveniently along axis z_n, preferably at the center of the gripper or at the tip of any tool that the manipulator may be carrying. Establish x_n along the common normal between z_{n-1} and z_n through o_n. Establish y_n to complete a right-hand frame.

Step 7: Create a table of link parameters $\theta_i, a_i, d_i, \alpha_i$.

a_i = distance along x_i from o_i to the intersection of x_i and z_{i-1} axes.

d_i = distance along z_{i-1} from o_{i-1} to the intersection of x_i and z_{i-1} axes. d_i is variable if joint i is prismatic. (d_i has sign, the direction from o_{i-1} to the intersection of x_i and z_{i-1} axes is the positive direction)

α_i = the angle between z_{i-1} and z_i measured about x_i (direction according to the right-hand rule, thumb pointing to the direction of axis x_i)

θ_i = the angle between x_{i-1} and x_i measured about z_{i-1} . θ_i is variable if joint i is revolute. (direction according to the right-hand rule, thumb pointing to the direction of axis z_{i-1})

Step 8: Form the homogeneous matrices A_i by substituting the joint parameters $\theta_i, a_i, d_i, \alpha_i$ into equation (2.2.4).